

University of Alberta

**Fabrication of Multi-component Surface Energy Gradients of Different Shapes
and Lengths**

by

Saravanan Meyyappan 

A thesis submitted to the Faculty of Graduate Studies and Research
in partial fulfillment of the requirements for the degree of Master of Science

Department of Mechanical Engineering

Edmonton, Alberta
Spring 2008



Library and
Archives Canada

Bibliothèque et
Archives Canada

Published Heritage
Branch

Direction du
Patrimoine de l'édition

395 Wellington Street
Ottawa ON K1A 0N4
Canada

395, rue Wellington
Ottawa ON K1A 0N4
Canada

Your file *Votre référence*
ISBN: 978-0-494-45857-0
Our file *Notre référence*
ISBN: 978-0-494-45857-0

NOTICE:

The author has granted a non-exclusive license allowing Library and Archives Canada to reproduce, publish, archive, preserve, conserve, communicate to the public by telecommunication or on the Internet, loan, distribute and sell theses worldwide, for commercial or non-commercial purposes, in microform, paper, electronic and/or any other formats.

The author retains copyright ownership and moral rights in this thesis. Neither the thesis nor substantial extracts from it may be printed or otherwise reproduced without the author's permission.

AVIS:

L'auteur a accordé une licence non exclusive permettant à la Bibliothèque et Archives Canada de reproduire, publier, archiver, sauvegarder, conserver, transmettre au public par télécommunication ou par l'Internet, prêter, distribuer et vendre des thèses partout dans le monde, à des fins commerciales ou autres, sur support microforme, papier, électronique et/ou autres formats.

L'auteur conserve la propriété du droit d'auteur et des droits moraux qui protègent cette thèse. Ni la thèse ni des extraits substantiels de celle-ci ne doivent être imprimés ou autrement reproduits sans son autorisation.

In compliance with the Canadian Privacy Act some supporting forms may have been removed from this thesis.

Conformément à la loi canadienne sur la protection de la vie privée, quelques formulaires secondaires ont été enlevés de cette thèse.

While these forms may be included in the document page count, their removal does not represent any loss of content from the thesis.

Bien que ces formulaires aient inclus dans la pagination, il n'y aura aucun contenu manquant.


Canada

Abstract

Laser patterning surface energy gradients of different shapes and lengths has been demonstrated using alkanethiols on gold. A gradient in desorption of the 1-hexadecanethiol Self Assembled Monolayer (SAM) has been achieved by continuous variation of laser intensity along the scanned path. The incident laser intensity has been varied by continuous manipulation of either the laser beam radius or the laser power. The desorption gradient was then backfilled with mercaptohexadecanoic acid (MHA) SAM to fabricate two component gradient features. Gradient line features were fabricated using both the methodologies. Secondary Ion Mass Spectroscopy was used to capture the rate of MHA concentration variation along the length. The trend in variation was found to be non-linear for the laser beam radius manipulation approach whereas approximately linear for the other. The experimental trend observed in both the cases was followed by the corresponding theoretical trend function derived for each case. As demonstration of capabilities, a 'UofA' shaped gradient and three SAM species gradient have been fabricated.

Acknowledgement

I take this opportunity to thank all the people who made this thesis possible. Firstly, I would like to express my deep and sincere gratitude to my supervisor Dr. Alidad Amirfazli for his inspiration, kind advice and great efforts to explain things clearly. The credits for making this masters work, a fun learning experience for me, in all fronts, also goes to him. I would like to thank Dr. Jillian Buriak for fruitful discussions with regard to analysis of the sample. I thank Andrew J. Milne for useful suggestions with regard to alignment of sample. I also thank Jesse Bacque for assisting in programming of stages. This work was financially supported by Natural Sciences and Engineering Research Council of Canada (NSERC) - Discovery Grant and Canada Research Chair program.

Table of Contents

Chapter 1 - Introduction	1
1.1 Background	1
1.2 Objectives and Scope	8
1.3 Fabrication of Gradient Line Features	8
1.4 Reference	12
Chapter 2 - Fabrication of Surface Energy/Chemical Gradients Using Self Assembled Monolayer Surfaces	14
2.1 Introduction.....	14
2.2 Methodology	18
2.2.1 Sample preparation	18
2.2.2 Experimental Set up.....	18
2.2.3 Experimental Methodology	19
2.2.4 Characterization	21
2.3 Results and Discussion	23
2.4 Summary	33
2.5 References.....	46
Chapter 3 - Fabrication of Multi-Component Chemical/ Surface Energy Gradients of Different Shapes and Lengths	48
3.1 Introduction.....	48
3.2 Methodology	54
3.2.1 Sample preparation	54
3.2.2 Experimental Setup.....	55

3.2.3 Experimental Methodology	56
3.3 Results and Discussion	59
3.4 Conclusions.....	69
3.5 References.....	84
Chapter 4 – Summary, Conclusions and Future Work	86
4.1 Summary and Conclusions	86
4.2 Future Work.....	88
4.3 Reference	90
Appendix 1 – Details of Experimental Procedures	91
A1-1 Cleaning of Glassware.....	91
A1-2 Calibration of Laser Power.....	91
A1-3 Focusing of the laser beam	92
A1-4 Keeping the sample inclined using the tilt stage	94
A1-4 Programming of the stages	95
A1-5 Measuring pattern width.....	97
A1-5 References.....	109
Appendix 2 – Other Experimental Results.....	110

List of Tables

Table 1-1: Prevailing methods for fabrication of surface energy gradients.....	3
Table A1- 1: Laser power calibration data.....	99

List of Figures

Fig. 2-1: Application of DLP to produce surface energy gradients.....	34
Fig. 2-2: Schematic of the experimental setup for laser patterning of gradients.....	35
Fig. 2-3: Working principle of ‘out of focus’ method, used to fabricate gradients.....	36
Fig.2-4: SIMS oxygen ion image at start of base and gradient lines.....	37
Fig. 2-5: Pixel intensity plots from the oxygen ion images at start, middle and end of base and gradient lines.....	38
Fig. 2-6: Calculation method of pixel intensity per unit area from oxygen ion images...39	
Fig. 2-7: High resolution SIMS oxygen ion images along the base and gradient line.....	40
Fig. 2-8: Condensation image of base and gradient line.....	41
Fig. 2-9: Condensation images along the length of the gradient and base line.....	42
Fig. 2-10: Juxtaposed SIMS oxygen ion images along the base and gradient lines.....	43
Fig. 2-11: Oxygen concentration variation as a function of out of focus distance.....	44
Fig. 2-12: Comparison of theoretical trend function with the SIMS experimental data...45	
Fig. 3-1: Schematic of single, double and triple component SAM gradients.....	71
Fig. 3-2: The three steps involved in laser patterning of surface energy gradients.....	72
Fig. 3-3: Block diagram of the experimental set up for laser patterning of gradients.....	73
Fig. 3-4: SEM image of lines patterned at different laser powers.....	74
Fig. 3-5: SEM image of 3, 6 and 12 mm long gradient lines.....	75
Fig. 3-6: SEM images along the 6mm long gradient line.....	76
Fig. 3-7: Schematic of the different gradients in the patterned gradient lines.....	77
Fig. 3-8: Pattern width variation plot along the 3, 6 and 12mm long gradients.....	78
Fig. 3-9: SIMS oxygen count variation along the gradient lines.....	79

Fig. 3-10: Parametric model as best fit to experimental data of the gradient lines.....	80
Fig. 3-11: Trend of theoretical model fitted to experimental data of the gradient lines....	81
Fig. 3-12: SEM and condensation image of ‘UofA’ shaped gradient.....	82
Fig. 3-13: SIMS oxygen and bromine ion images of three component gradient.....	83
Fig. A1-1: Schematic of the experimental setup for laser power calibration.....	100
Fig. A1-2: Schematic of the experimental setup for focusing the objective lens.....	101
Fig. A1-3: Schematic explaining the method to keep the sample flat or inclined.....	102
Fig. A1-4: Knife edge data and Gaussian fit to the laser beam intensity profile.....	103
Fig. A1-5: Hyperbolic fit to the beam radii measured along the propagation direction..	104
Fig. A1-6: Front panel of the gradient maker program.....	105
Fig. A1-7: Flow chart of gradient maker program.....	106
Fig. A1-8: Front panel of the gradient shapes program.....	107
Fig. A1-9: Measurement of width of the patterned gradient lines from SEM image.....	108
Fig. A2-1: Sequential images taken while condensation of water drops	111
Fig. A2-2: Parametric model fitted to the SIMS data for second set of gradient lines	112

List of Acronyms and Symbols

BUD	Bromoundecanethiol
CW	Continuous wave
DLP	Direct laser patterning
HDT	Hexadecanethiol
HWP	Half wave plate
MEMS	Microelectromechanical systems
MHA	Mercaptohexadecanoic acid
OTS	Octdecyltrichlorosilane
PDMS	Poly dimethyl siloxane
RF	Radio frequency
SAM	Self assembled monolayer
SIMS	Secondary ion mass spectroscopy
SIMS-TOF	Secondary ion mass spectroscopy – time of flight
SLAB	Submerged laser ablation
STM	Scanning tunnel microscopy
TEM	Transverse electromagnetic mode
UV	Ultraviolet
A	Absorptivity of the sample
ΔG	Gibbs free energy for activation
K_B	Boltzmann constant
P	Laser power

R	Universal gas constant
T	Temperature
T_0	Room temperature
c	Concentration of SAM at a point
c_0	Initial concentration at a given point
h	Planck's constant
k	Thermal conductivity of glass
r	Beam radius at 2e-folding
t	Time
θ	Azimuth angle of half wave plate
ψ	Fraction of Hexadecanethiol desorbed

Chapter 1 - Introduction

1.1 Background

Fabrication of surfaces having gradually varying properties, such as in wetting, surface charge etc. is important for applications in emerging fields like tissue engineering, lab-on-chip devices and microelectromechanical systems (MEMS). Surfaces exhibiting a spectrum in surface properties also serve as combinatorial tools to study biological interactions and are further useful for fundamental studies in surface sciences (e.g. a wettability spectrum). The main objective of this thesis is to develop a novel methodology to fabricate surface energy gradients using Self Assembled Monolayers (SAM).

A SAM provides excellent means of systematically manipulating surface properties in a predictive manner. A typical example is alkanethiols ($\text{HS}-(\text{CH}_2)_n\text{-X}$) on gold. Alkanethiols spontaneously bond (covalently) to metallic surfaces such as gold, silver and copper and form a densely packed single layer of molecules. The layer of alkanethiol molecules mask the surface properties of the substrate and exhibit surfaces characteristics as a function of the tail group. For example, if the tail group (X) is CH_3 then the surface is hydrophobic whereas if it is COOH then the surface is hydrophilic. So by selective removal or replacement of the SAM molecules in a binary fashion, the surfaces can be patterned to exhibit different surface properties (locally). However, for a surface energy gradient, it is required to have a continuous variation of surface properties (along a length). This can be achieved by creating a gradient in removal of the SAM molecules. Such a surface would exhibit gradual variation in surface properties/energy and is called

a single component surface energy gradient. After removal, if the bare and partially bare regions of the substrate are backfilled with a secondary alkanethiol, i.e. alkanethiol with a different tail group, then a two component gradient is fabricated. If the patterning process is repeated and more than two different SAMs are utilized, then a three or multi-component gradient is produced. Single and double component SAM gradients are found useful in a number of applications such as: chemotaxis¹, cell migration studies^{2,3} propelling and directing liquid drops⁴⁻⁷. A three component or multi-species gradient (as detailed above), if possible to fabricate, can serve as a useful tool in applications requiring, different parts of a cell to be separated or different types of cells to be migrated in different directions etc. Further, a multi-species gradient exhibiting a range in spectrum of different surface properties, can be used as a multi-combinatorial tool to study biological interactions.

SAMs can also be patterned so as to exhibit different surface properties over surface area of a required shape such as trapezium, triangle etc. Such patterns would constitute shape gradients, similar to what has been demonstrated in ref 7 and can be used for applications such as propulsion of liquids both on a horizontal and upward on an inclined plane⁷.

Surface energy gradients ranging from a few nanometers to centimeters in width have been previously produced using SAMs⁸⁻²¹. Several methods and their characteristics have been tabulated in Table 1-1, for comparison.

Table 1-1: Lists the prevailing methods for fabrication of surface energy gradients and their characteristics.

Width Scale	Method	Different Shapes and Lengths	Other factors	Reference
Millimeter to Centimeter	Liquid or gas phase molecular diffusion of alkylsilanes	Different shapes not possible, length/steepness tunable	Process is slow	[8], [9] and [10]
	Cross diffusion of alkanethiols using glass filters	Not possible to alter shapes and length		[11]
	Computer controlled slow immersion into alkanethiol solution	Not possible to alter shapes and length	Specific control of surface chemistry not possible	[13]
	Applying spatial voltage to alkanethiol SAM	Not possible to alter shapes and length		[14]
	Mechanical manipulation of self assembly	Possible		[15]
Micrometer	Micro-contact printing based methods	Possible	Requires different stamps for varying parameters	[16] and [17]
	Lithography based methods	Possible, but see 'other factors'	Requires different masks for varying length or shape	[18], [19] and [20]
Nanometer	Scanning Tunnel Microscopy (STM) based methods	Possible	Expensive Infrastructure required	[21]

Surface energy gradients, a few centimeters to millimeters in width has been produced using diffusion based methods such as liquid and vapor phase diffusion of alkylsilanes, cross diffusion of alkanethiols and computer controlled immersion of the substrate into dilute alkanethiol solution. Also other methods such as applying a spatial variable voltage over an alkanethiol monolayer and mechanical manipulation of self assembly of molecules have been used to produce energy gradients in similar scale. However, it was not possible to fabricate surface energy gradients of finer resolutions such as a few micrometers or nanometers in width which was required for certain applications. The rising demand aided by the availability of technologically advanced tools, gave rise to methods based on: micro-contact printing, lithography and Scanning Tunnel Microscopy (STM). Micrometer scaled energy gradients of different shapes and lengths were fabricated using methods based on micro-contact printing and lithography. However, it was difficult to fabricate nanometer scale gradients. So a STM based method, capable of producing nanometer scale gradients was developed. The method had precise control over the shapes and length of the gradients. However, it was not possible to fabricate multi-species gradient. So a method capable of producing multi-component gradients and surface energy gradients of different shapes and lengths was required. This need has been re-stressed in the following paragraphs by comparing and explaining in detail all of the available methods (listed in the Table 1-1).

The earliest methods developed were mainly based on diffusion. Energy gradients on silicon were fabricated by controlled diffusion of alkylsilanes in liquid^{8,9} or gas¹⁰ phase. Also, a method based on controlled diffusion of alkanethiols was developed to create two

component gradients on gold¹¹ (see ref 12 for complete account on diffusion based methods). The gradients fabricated using these methods (based on diffusion) were a few centimeters in width and there was little or no control over the rate of surface property variation or steepness of the gradient. Also, the length of the gradients produced was limited to the maximum length over which diffusion could occur. While other techniques developed later such as: computer controlled slow immersion of a bare gold substrate in a dilute alkanethiol solution¹³, applying a spatially variable (linear) electrochemical potential across a mercaptoundecanol coated gold film¹⁴ and mechanical manipulation of self assembly of n-octyl trichlorosilane (on silicon) using variably stretched PDMS stamps¹⁵ had better control over the steepness of the gradients, they were primarily aimed at producing energy gradients of the order of few millimeters in width and could not be used for smaller scales and there was also not precise control over the surface chemistry.

Recent advancements in fabrication technology has helped partly address outstanding issues through methods based on micro-contact printing^{16,17}, lithography¹⁸⁻²⁰ and Scanning Tunnel Microscopy (STM)²¹. The simplest of them is based on micro-contact printing. A variable thickness PDMS stamp has used to print hexadecanethiol (HDT) gradients on gold¹⁶. Also, octadecyltrichlorosilane (OTS) gradients on silicon have been fabricated by varying the time and contact area during printing¹⁷. These methods were simple, two component and gradients of different shapes were also possible. However, since the method was largely based on diffusion, precise control of surface chemistry was not possible and further the need for new stamps, each time, for varying the geometry and steepness of gradient surfaces made it cumbersome. In lithography based methods, UV

radiation through the mask was manipulated so as to create a gradient in oxidation/photo-degradation of SAMs. The gradient in UV exposure was achieved through use of a graded photo mask i.e. a grayscale mask^{18,19} or customized variable density filters²⁰. These methods (based on lithography) can produce different types and shapes of gradients in micrometer scale. However, the need for expensive infrastructure (e.g. mask maker, lithography equipment) and different masks, each time, to vary the parameters of the gradient such as size, shape and steepness made the methods inflexible, cumbersome or expensive. Energy gradients, a few nanometers in scale, have also been produced using STM based replacement method²¹. In this method a bias voltage was applied between the STM tip and the dodecanethiolate monolayer to desorb the monolayer selectively (in the presence of Ferrocenyl-undecanethiolate SAM solution). A gradient in desorption was achieved by varying the voltage and the scan rate. The desorbed gradient was subsequently backfilled by the secondary SAM i.e. ferrocenyl-undecanethiolate. This method has the flexibility of producing gradients of different shapes and simultaneously has precise control over both the surface chemistry and steepness of the gradient. However, multi-component gradient was not possible and expensive infrastructure was required. So a simple technique, capable of producing multi-component gradients and gradients of different shapes and length is required. The aim of the presented work is to develop a method with such capabilities to produce micrometer scale gradients.

Alkanethiols on gold are stable, widely characterized and studied and are available with a wide variety of tail groups²². As such in this research, patterning energy gradients using SAM surfaces has been studied in the context of Direct Laser Patterning (DLP) of

alkanethiols on gold²³. It has been established in DLP that the temperature induced due to localized heating of the sample (by an incident laser beam), results in the Au-S bond breakage and hence local desorption of the monolayer^{23,24}. So it is expected that a continuous variation in incident laser intensity (along the scanned path) would create a variation in the induced surface temperature which would result in a gradient in desorption of the alkanethiol. The bare and partially bare regions of this desorption/single-component gradient can then be backfilled to create a two component gradient. The process can be repeated to place more than two different SAM gradients on the substrate to create multi-component gradients. Also, the steepness of the gradient can be controlled by varying the rate of laser intensity variation along the scanned path. Further, desired shapes of gradients can be fabricated by appropriately moving the sample, relative to the laser beam. The continuous variation in laser intensity along the scan direction can be achieved by continuous manipulation of either the beam spot area or the laser power. Both of these methodologies have been examined in this thesis.

As an outcome, two simple methods (based on DLP) have been developed for fabrication of microscopic energy gradients on alkanethiol surfaces. Both these methods, based on different approaches for varying the incident laser intensity i.e. through continuous manipulation of either beam area or laser power (holding the other constant), have common advantages like being fast and non-contact, capable of producing multi-component gradients and gradient lines of different lengths. The developed methods also eliminate the need for lithography and STM. Also for the first time, we have produced, a three SAM species gradient. Further, by modification of the laser patterning method for

alkylsilanes developed in ref 25 (which is similar to DLP), the proposed methods can be extended to produce surface energy gradients on silicon as well.

1.2 Objectives and Scope

The objectives of this research are to: (1) Develop means of continuously varying the beam area/laser power along a scanned path and show feasibility of the proposed methodologies to produce surface energy gradients on alkanethiol surfaces at experimental level; (2) Characterize the gradients produced using applicable tools, to better understand the mechanism and also provide information on the rate of surface property variation in the gradients; (3) Demonstrate multi-component gradients and gradients of different lengths and shapes, experimentally.

1.3 Fabrication of Gradient Line Features

Surface energy gradients along straight lines were produced, using two methods to vary laser intensity i.e. varying the laser beam spot area or the laser power. In the first method, the continuous variation in laser beam area was achieved, by taking advantage of the divergence phenomenon of the laser beam. The sample was kept inclined to the scanning laser beam so as that the focused beam diverged and became more and more out of focus along the scanned path. As a result, the laser beam radius increased and correspondingly laser intensity decreased from a maximum to the threshold for desorption, along the scanned path. Hence a gradient was created. Gradients of different steepness could be fabricated by changing the angle of inclination of the sample (to the focal plane). However, fabrication of gradients of different shapes using this method i.e. the 'out of

focus' method was not easy, as complicated tilting of the surface was required. The second method for laser intensity variation i.e. the 'laser power method' is used to demonstrate gradients of different shapes. The laser power method involves computer controlled laser power manipulation, along the scanned path, to fabricate gradients. Also, using three SAMs, a multi-component gradient along different shapes was created, using this method. This laser power method was very flexible to vary the steepness (of the gradient) as well as producing arbitrary shapes. However, computerized control of laser power was required. As a contrast, the first method was simple and can be used to produce straight line gradients. Further, the trend in surface property variation, along the gradient lines fabricated using the two methods, was found to be different for each method. The different methodologies for producing gradients (i.e. the out of focus and the laser power method) have been explained and discussed in detail in two papers produced (submitted work) which has been included as Chapters 2 and 3 in this thesis.

In Chapter 2, the explained methodology has been demonstrated using 1-Hexadecanethiol (HDT) and Mercaptohexadecanoic acid (MHA) as primary and secondary SAMs to produce wettability gradients on gold. The sample (homogenous HDT monolayer on gold film supported by a glass substrate) is kept inclined at an angle of $1^{\circ}6'47''$ to the focal plane of the laser beam (CW Ar-ion laser at 488nm) and scanned at a constant speed of $200\mu\text{m}/\text{sec}$. As a result, the incident laser intensity reduces to the threshold of $1.9\text{ kW}/\text{cm}^2$, along the line scan, to produce a gradient in desorption of HDT. The bare and partially bare regions are then backfilled with MHA to create wettability line gradients ($\sim 15\mu\text{m}$ wide). Secondary Ion Mass Spectroscopy (SIMS) imaging was used to show the

gradient in chemical concentration along the scan direction and the gradient in wettability was revealed, by condensation imaging. The functional behavior of the governing equations was considered to derive the theoretical trend for variation of HDT desorption along the gradient. The trend obtained was found to represent the experimental data. This method is suitable for producing gradient lines of different lengths. It is fast and simple. However, gradients of different shapes were not possible easily. So an alternative method capable of producing gradients of different shapes was required.

In Chapter 3, gradients of different shapes and lengths and three component gradients have been demonstrated. The incident laser power on the sample (HDT SAM on a gold film supported by a glass substrate) was varied from 40mW to 9mW along a straight line (holding the beam radius constant), using computer controlled rotation of the Half Wave Plate i.e. HWP (placed before a Glan polarizer). As a result, a gradient in desorption of HDT SAM was created. Also, the speed of the half wave plate rotation and hence the rate of laser power variation, was changed (for each scan) to produce 3, 6 and 12 millimeter long gradient lines. The created desorption gradient was then backfilled at the bare regions of the substrate with mercaptohexadecanoic acid (MHA) SAM, to create two component gradients. SEM images were used to reveal the patterned gradient lines and SIMS spectral analysis was carried out, along the length, to capture the trend in MHA concentration variation. The theoretical trend function for the amount of HDT desorbed, along the gradient line, was derived by considering the functional dependence of the thermo-kinetic model. Also, the theoretical function included the power variation trend and the velocity of HWP rotation. The function hence obtained was fitted to the SIMS

experimental data obtained for the three different gradient lines, with close agreement (R^2 value close to unity). Also, a “U of A” shaped energy gradient (high to low) in the directions: top to bottom and left to right, was fabricated by varying the laser power along each character’s path (in the required direction). Further a three component gradient was fabricated along an arbitrary shape. Firstly, a two component gradient was created along a circle, using HDT and MHA as primary and secondary SAMs. After that, patterning of HDT was continued to create a gradient in desorption along a line crossing the circle. This pattern was then backfilled with 1, bromoundecanethiol SAM. Hence a three component gradient, first of its kind, was demonstrated.

In Chapter 4, the major conclusions drawn have been summarized. Also, the directions of future work have been discussed. In the appendices the experimental protocols followed have been explained in detail.

1.4 Reference

- (1) Dekker, L. V.; Segal, A. W. *Science* **2000**, *287*, 982-985.
- (2) Gunawan, R. C.; Silvestre, J.; Gaskins, H. R.; Kenis, P. J. A.; Leckband, D. E. *Langmuir* **2006**, *22*, 4250-4258.
- (3) Kumar, G.; Ho, C.; Co, C. In *In Geometric control of directional cell migration*; 05AICHE: 2005 AIChE Annual Meeting and Fall Showcase; NY, United States: Cincinnati, OH, United States, 2005; p 4268.
- (4) Chaudhury, M. K.; Whitesides, G. M. *Science* **1992**, *256*, 1539-1541.
- (5) Zhang, J.; Han, Y. *Langmuir* **2007**, *23*, 6136-6141.
- (6) Daniel, S.; Chaudhury, M.; Chen, J. *Science* **2001**, *291*, 633-636.
- (7) Ito Y; Heydari M.; Hashimoto A.; Konno T.; Hirasawa A.; Hori S.; Kurita K.; Nakajima A. *Langmuir* **2007**, *23*, 1845-1850.
- (8) Elwing, H.; Askendal, A.; Lundstrom, I. *J. Biomed. Mater. Res.* **1987**, *21*, 1023-1028.
- (9) Golander, C. G.; Caldwell, K.; Lin, Y. S.; *Coll. Surf.* **1989**, *42*, 165-172.
- (10) Daniel, S.; Chaudhury, M.; Chen, J. *Science* **2001**, *291*, 633-636.
- (11) Liedberg, B.; Tengvall, P. *Langmuir* **1995**, *11*, 3821-3827.
- (12) Ruardy, T. G.; Schakenraad, J. M.; van der Mei, H.C.; Busscher, H. J. *Surface Science Report* **1997**, *29*, 1-30.
- (13) Morgenthaler, S.; Lee, S.; Zurcher, S.; Spencer, N. D. *Langmuir* **2003**, *19*, 10459-10462.
- (14) Plummer, S. T.; Wang, Q.; Bohn, P. W.; Stockton, R.; Schwartz, M. A. *Langmuir* **2003**, *19*, 7528-7536.
- (15) Efimenko, K.; Genzer, J. *Adv Mater* **2001**, *13*, 1560-1563.
- (16) Kraus, T.; Stutz, R.; Balmer, T. E.; Schmid, H.; Malaquin, L.; Spencer, N. D.; Wolf, H. *Langmuir* **2005**, *21*, 7796-7804.

- (17) Song, F.; Cai, Y.; Newby, B. Z. *Appl. Surf. Sci.* **2006**, *253*, 2393-2398.
- (18) Blondiaux, N.; Zurcher, S.; Liley, M.; Spencer, N. D. *Langmuir* **2007**, *23*, 3489-3494.
- (19) Ito, Y.; Heydari, M.; Hashimoto, A.; Konno, T.; Hirasawa, A.; Hori, S.; Kurita, K.; Nakajima, A. *Langmuir* **2007**, *23*, 1845-1850.
- (20) Roberson, S. V.; Fahey, A. J.; Sehgal, A.; Karim, A. *App. Surace Sci.*, *200*, 150-164.
- (21) Fuierer, R. R.; Carroll, R. L.; Feldheim, D. L.; Gorman, C. B. *Adv Mater* **2002**, *14*, 154-157.
- (22) Yang, Z.; Wolfgang, F.; Oliver, T.; Chilkoti, A. *Langmuir* **2000**, *16*, 1751-1758.
- (23) Shadnam, M. R.; Kirkwood, S. E.; Fedosejevs, R.; Amirfazli, A. *Langmuir* **2004**, *20*, 2667-2676.
- (24) Shadnam, M. R.; Kirkwood, S. E.; Fedosejevs, R.; Amirfazli, A. *J. Phys. Chem. B* **2005**, *109*, 11996-12002.
- (25) Hartmann, N.; Balgar, T.; Bautista, R.; Franzka, S. *Surface Sci.* **2006**, *600*, 4034-4038

Chapter 2 - Fabrication of Surface Energy/Chemical Gradients Using Self Assembled Monolayer Surfaces*

2.1 Introduction

A surface having a gradual variation in surface energy/property in nano, micro or millimeter scale is termed as a surface with an energy gradient. Surface energy gradient based self-propulsion of liquids has been of interest to researchers for directing drop movements^{1,2}. They are also of interest for their biological applications such as cell migration³ and protein adsorption studies⁴. The main objective of this chapter is to demonstrate a novel method to fabricate surface energy gradient features using Self Assembled Monolayers (SAM) of thiol on gold.

A SAM is a thin organic film on a substrate, formed by spontaneous adsorption of molecules from the corresponding solutions. SAM surfaces exhibit properties as a function of the tail group of the adsorbed molecules. A typical example is alkanethiol SAM ($\text{HS}(\text{CH}_2)_n\text{X}$), where X can be any of CH_3 , COOH and NH_2 , etc. on gold. The SAMs are of widespread interest when surface properties/energy needs to be manipulated. For example, by replacing the homogenous alkanethiol SAM molecules having a CH_3 tail group (hydrophobic) with SAM molecules having a different tail group COOH (hydrophilic), the surface properties/energy can be manipulated. If the replacement of the second SAM molecule is as shown in Fig. 2-1c, then the resulting surface would exhibit a gradient in surface energy/property.

* A version of this chapter has been accepted for publication in *Langmuir*

Surface energy gradients using SAMs have been produced as early as 1987 by Elwing et al⁵. In the earliest method and subsequent refinements⁶⁻⁹ the gradients were produced by molecular diffusion of chlorosilanes in gas/liquid phase on a silicon or silicon dioxide substrate. The diffusion of the chlorosilane molecules (hydrophobic) on silicon or silicon dioxide (hydrophilic) was controlled such that the resulting surface had a gradient in wettability. Although surface energy gradients having a continuously changing wetting (120-10 degree water contact angle) were produced using molecular diffusion based methods, gradients of different shapes were not possible and the length of the gradient was restricted by the maximum distance over which diffusion could occur. Furthermore, there was little control over the surface energy variation rate or steepness of the gradient. Also, since the gradient was produced by the controlled diffusion of the hydrophobic chlorosilane molecules on the hydrophilic substrate, the surfaces exhibited a gradient in wetting alone. So there were restrictions on the types of gradients produced i.e. different types of gradients like gradients in surface charge, polarity or biocompatibility were not possible. However, in 1995, Liedberg and Tengvall¹⁰ reported a method based on cross diffusion of molecules. In this technique, different alkanethiol SAM molecules are cross diffused from opposite ends of a polysaccharide matrix placed on gold. Although this method has the flexibility of using different chemical combinations (using two SAM species) to produce different types of gradients, the other issues discussed above remain largely unaddressed.

Gradients have also been produced by oxidation of silanes¹¹. The alkylchlorosilane monolayer (hydrophobic) chemisorbed on silicon (hydrophilic) was selectively oxidized

and removed to produce wettability gradients. The graded oxidation of the silane monolayer was achieved by UV exposure through variable density filters¹¹. Techniques based on oxidation have also been used to produce gradients on polymeric substrates¹¹. The variation in the degree of oxidation is achieved either by a scanning radio frequency (RF) discharge¹² or Scanning corona RF discharge¹³. Two very recent methods are (1) Photo-degradation of alkylsilane monolayer in which the octadecyltrimethoxysilane monolayer (hydrophobic) was photo degraded under vacuum with ultra violet radiation at 172nm through mesh filters to produce wettability gradients¹⁴. (2) A photocatalytic lithography method¹⁵ in which a thiol monolayer on gold is exposed to a UV light that passes through a graded photomask and a TiO₂ covered glass (the thin TiO₂ film acts as a catalyst to oxidize the thiol). Using these techniques based on oxidation and photo-degradation, in combination with different masks, gradients of different shapes and lengths could be produced. However, all such methods directly or indirectly need to use photolithography, which requires expensive infrastructure and once the mask is produced, it is difficult to make changes; some also require long processing times of the order of one hour¹⁵. These factors make such methods cumbersome, inflexible and/or expensive. So a technique capable of producing gradients of different types, using two or more SAM species, and that was also flexible to produce gradients of different shape, length and steepness is required.

This chapter discusses a novel technique based on Direct Laser Patterning (DLP)^{16,17}, to produce surface energy gradient features. The proposed method can be used to produce different types of gradients using contrasting SAM molecules (even more than two

species). Further, the method has capabilities to produce gradients of different shapes, lengths, steepness and widths, without the need of photolithography either directly or indirectly. The application of DLP to produce gradients is shown in Fig. 2-1; it is a three step process similar to Scanning Tunnel Microscopy (STM) base replacement method of Fuierrer et al.¹⁸, but it is much faster and complementary to the nanometer-sized gradients produced in the STM method (i.e. it can produce gradients in the orders of micro to centimeter scale). The steps are: formation of a homogenous SAM on a substrate by solution deposition, followed by the selective desorption of the SAM molecules on the substrate using a laser beam. DLP works by thermally desorbing the SAM, which is controlled by laser intensity^{16,17}. So in the proposed method to produce surface energy gradients using DLP, the laser intensity is continuously varied along the scan path to produce a gradient in desorption as shown in Fig. 2-1b. This desorption gradient is then backfilled with the second SAM molecule (with a different tail group) in the final step, to produce a line pattern having a gradient in surface energy/property (see Fig. 2-1c). In principle, this method can be repeated more than once to produce multi-species surfaces (see Chapter 3). The feasibility of the proposed method is demonstrated by producing wettability gradient features using hexadecanethiol (HDT) and mercaptohexadecanoic acid (MHA) as the contrasting SAMs. The method can also be used for producing gradients using alkylsilane monolayer on silicon, by modifying the DLP technique used in ref 19.

2.2 Methodology

2.2.1 Sample preparation

The samples were made using 1mm thick “premium microscopic slides” (Fisher Scientific Co.) as the substrate. A 50Å titanium adhesion layer was sputtered on the microscopic slides at a rate of 0.30 Å/sec followed by a 300Å gold layer at a rate of 0.98 Å/sec, on top of it. After completion of sputtering with gold, the sample was immersed in a 1mM ethanolic solution of hexadecanethiol (HDT) (Fluka) for 48 hours to form the primary SAM. Note that all the glassware used for the experiments were cleaned as per the procedure detailed in section A1-1.

2.2.2 Experimental Set up

The schematic of the set up used is shown in Fig. 2-2. A continuous wave (CW) Argon ion laser (Melles Griot - 543-BS-A03) at 488nm was used as the laser source. The half wave plate combined with the glan polarizer was used to control the laser power through the optical train. The wedge in the optical set up was used for sampling the beam (~4%) for online power measurement. The quarter wave plate was used to avert the destructive interference of the incident and reflected laser beam (from the sample). The mirrors were used for steering the laser onto the sample. The apertures were used for aligning the laser beam before patterning. An automated beam blocker was employed for the purpose of blocking the laser beam temporarily i.e. when patterning needs to be paused or there was a need to have a break in a pattern design. The microscopic objective (10X) used for focusing the laser beam was mounted on a micrometer driven translational stage. The sample holder was attached to a tilt stage on a computer controlled two-axis translational

stage. The focal distance of the objective was determined by forming an image of the sample in the CCD camera using a white light source, as shown in Fig. 2-2. The focal distance obtained needed to be corrected by an offset to obtain the focal distance for the laser beam due to the difference in wavelength of the laser and the light source used. This correction factor was determined to be +131 μm for this setup as configured (note that the objective used has multiple proprietary lenses packed within the 10X casing; hence the correction factor needed to be determined experimentally).

2.2.3 Experimental Methodology

To fabricate surface energy gradients using DLP, the incident laser intensity needs to be continually varied along the length of the scan. This is achieved by scanning the sample, kept inclined at a suitable angle to the focal plane of the laser beam (see Fig. 2-3, Note: a detailed explanation on how to keep the sample inclined to the focal plane can be found in section A1-4). The incident beam spot radius increases from an initial value at the focused end to a larger value at the out of focus end, due to the divergence of the laser beam (see Fig. 2-3). Hence the incident laser intensity varies from a maximum to a minimum. The minimum is determined by the threshold laser intensity for which there is no desorption of the HDT SAM. The resulting gradient in desorption of the primary SAM molecules is then backfilled with the second SAM molecule to produce a gradient in surface energy/property. This process can be repeated multiple times for various species to be used, but here for simplicity only a two species sample is shown.

The laser power used for patterning was carefully selected to be well below the damage (to gold) threshold, after conducting a series of experiments in which the laser power was progressively decreased and the substrate checked for damage under an optical microscope (50X). The damage results were compared with previous results¹⁶. In the final experiments, laser with a power of 16.26 mW was focused using a 10X (Olympus UPLAN FI) objective onto the substrate (hydrophobic HDT SAM on gold). The incident laser intensity was 204.7 kW/cm² corresponding to a 2e-folding beam radius of 1.59µm (measured). The sample was kept inclined at an angle of 1°6' 47" to the focal plane, so that laser intensity reduces to the desorption threshold, determined to be ~1.9 kW/cm² at the end of the line scanned (~8mm long). The sample was scanned at a constant velocity of 200µm/sec to create the desorption gradient in primary SAM (i.e. HDT). Also, as a base line, a line was scanned by keeping the substrate perfectly perpendicular to the scanning laser beam. The base line is used as an internal reference, while characterizing the gradient using secondary ion mass spectroscopy (SIMS) or condensation imaging. The patterned sample was then rinsed with ethanol and dried in a stream of nitrogen before immersion into a 1mM solution of 16-mercaptohexadecanoic acid (MHA) (Sigma Aldrich) for 2 minutes to backfill the bare or partially bare gold regions. The second SAM (MHA) having a carboxylic tail is hydrophilic, hence will create a gradient in wettability. The processed samples were stored in a chamber filled with nitrogen until further analysis was conducted. A series of gradient and base lines were produced on a sample and characterized, to verify repeatability of the process.

2.2.4 Characterization

The gradient line features were characterized by Secondary Ion Mass Spectroscopy – Time of Flight analysis (SIMS-TOF) to show the gradient in chemical concentration of the second SAM molecule (MHA) by analyzing the oxygen signal. Also, the gradient in surface energy (wetting) has been captured by condensation imaging. The SIMS-TOF is an analytical method used to determine the chemical composition in the top few nanometers of a sample. In particular case of this study, as oxygen is expected to be concentrated along the gradient and base lines (corresponding to the MHA SAM), the sample was bombarded with a 15 KeV focused Gallium ion beam spot (300nm) to produce the oxygen distribution image at various locations along the patterns produced on the sample. The mass resolved secondary ion image for oxygen (see Fig. 2-4) with a lateral resolution of 0.78 μm was formed, by rastering the ion beam over a 200 μm x 200 μm area (256 x 256 pixels) and allotting each pixel, a value corresponding to the counts of oxygen ions collected over 100 shots of the ion beam (done by ion-tof software). Also, to further investigate the mechanism of patterning, SIMS imaging at a higher lateral resolution (0.34 μm) was carried out at various positions along the lines using a 25 KeV Gallium ion beam.

The oxygen ion image at each position was then analyzed using ion-image software. Transverse line scans were done as shown in Fig. 2-4, to obtain pixel intensity plots along any given point on the patterns imaged (see Fig. 2-5). The distinguishable peaks in the pixel intensity plots represent the patterned lines. The background (i.e. HDT) in the oxygen ion image, is not represented by a single value; it is rather represented by a range

of pixel intensities scattered within a range. This is probably due to the noise inherent in this type of instrument due to its channel plate sensitivity differences. Fig. 2-5 (a, b and c) clearly shows that the pixel intensity peak/oxygen signal for the gradient line decreases from a large value at the beginning (a) to a smaller value at the middle (b) and fades into the background signal at the end (c). In order to capture the relative quantitative reduction in oxygen concentration, it was required to assign a characteristic value proportional to the oxygen ions based on the pixel intensity, as SIMS does not provide absolute quantities of elements. The pixel intensity per unit area was deemed suitable, as it corresponds to the oxygen concentration at the analyzed position in the pattern and can be determined from the pixel intensity plots.

A curve described by two Gaussian components and a constant was fitted (using 'Trust-Region' algorithm in Matlab) as shown in Figs. 2-5 and 2-6. The two Gaussian components in Fig. 2-6 determine the fit for the pixel intensity/oxygen concentration peaks; the constant component, fitting a straight line to the scattered pixel intensities represents the background. A Gaussian shape was selected for the oxygen concentration peaks, as it corresponds to the incident laser beam intensity profile (TEM_{00} mode). The pixel intensity per unit area was determined by calculating the area under the fitted curve (shaded areas under the curves in Fig. 2-6) and dividing by a circular area corresponding to the thermal foot print of the laser beam (hatched contour areas in Fig. 2-6). The circular area/thermal foot print of laser beam corresponds to the full pattern width and hence can be calculated based on the Gaussian fit. Hence, the pixel intensity per unit area (pixel intensity concentration) was determined for various positions along the patterns

and was used to characterize the gradient in chemical concentration. In order to take into account the uncertainties associated with the data, five line scans at $\sim 50\mu\text{m}$ intervals were done for each position ($200\mu\text{m} \times 200\mu\text{m}$) and the corresponding pixel intensity concentrations calculated. The reported pixel intensity concentration for each position (middle of the scanned area/image) is the average of the values found from five line scans and the error bars correspond to $\pm 1\text{SD}$.

The gradients were also analyzed using condensation imaging, which involved imaging the condensation of water drops on the sample. The samples were cooled down using a Peltier cell in an enclosure with an atmosphere of high humidity. Pictures were taken along the length of the gradient line to reveal the gradient in wetting. A sequence of images taken, by the above explained procedure, while condensation was occurring can be found in Appendix-2.

2.3 Results and Discussion

The mechanism of the technique i.e. the effect of reducing the laser intensity along the scanning direction requires to be understood before interpreting the results. This is explained in detail with reference to the SIMS images in the following paragraphs. At the initial portion of the scanned line, when the intensity is well above the threshold for desorption, a central region with complete desorption, flanked by very narrow regions of partial desorption that is ultimately delimited by areas where there is no desorption (i.e. background) is observed. The reduction in laser intensity along the scan direction leads to rapid disappearance of the central full desorption region, leaving only partially desorbed

areas. Hence the lateral gradient present initially (due to transition from the full desorption to the background) disappears. Longitudinally, the steady decrease in the amount of partial desorption continues until the threshold for desorption is reached, where patterning ceases. Hence a longitudinal chemical gradient is created along the length of the scanned line.

The mechanism as explained above was revealed by the high resolution (0.34 μm) SIMS oxygen ion images. The oxygen ion images (see Fig. 2-7) revealed the MHA SAM has filled the bare or partially bare regions. It can be seen from the leftmost frame in Fig. 2-7 that at the beginning of the laser scan, the patterned base and gradient lines (top and bottom) are represented by: high concentration of oxygen at the center, lower at the edges and nil in the background, as mentioned earlier. However, further along the length of the gradient line (see frame 3), the high oxygen concentration/full desorption region is seen to vanish, leaving only a uniform weaker signal for oxygen, meaning partially desorbed HDT, backfilled with MHA. Also, it can be noted that the sharp lateral gradient (in the oxygen concentration/MHA molecules) present initially transverse to the direction of the scanned line, has vanished. Following this, there is a constant decrease in oxygen signal for the gradient line, along the length, as can be seen in subsequent frames. This means that, lesser and lesser MHA has been backfilled (HDT has been desorbed), along the scan, before the oxygen signal finally fades into the background, where there is no patterning. Hence a longitudinal gradient is created. Further, the base line is found to be consistent at the all the positions along the laser scan.

In order to verify whether the central high oxygen concentration region seen in the SIMS oxygen ion images of the base line and the gradient line (at the beginning) corresponds to full desorption, a control experiment was performed. A bare gold sample (gold film thickness of 30nm) was coated with MHA. Subsequently, a SIMS analysis (with parameters same as high resolution SIMS images) was performed to obtain the oxygen ion image for fully covered MHA. The average pixel intensity along with the 95% confidence level was found to be 168 ± 6 . This was very comparable to the average signal value for the central region seen in Fig. 2-7, i.e. 163 ± 42 . Therefore, to sum up, it has been shown that the central high concentration of oxygen in the SIMS image indeed corresponds to the full desorption region, but there is no full desorption region past the initial stages of scanning; in fact most of the scanned length is experiencing a partial desorption. The gradient surfaces produced was also characterized by condensation imaging and the variation of oxygen concentration in the gradient line was quantified by analyzing SIMS images at various positions along the scan direction.

While cooling the substrate, condensation was first observed to occur along the most hydrophilic regions (the base and gradient lines) of the substrate. This is due to higher surface energy of the hydrophilic lines compared to the background. Within few minutes, condensation was also observed in the primary monolayer/background (similar behavior has been observed previously²⁰). Apart from differentiating the patterned lines from the background, the condensation patterns also distinguished the base and gradient lines. The differences can be understood by considering the insights, provided by the high resolution SIMS images. From the SIMS images, it is seen that at the beginning of the

scan, there is a sharp lateral gradient. When the surface is cooled, condensation occurs in the full desorption areas and grow due to two reasons: (1) due to their higher surface energy²⁰ (compared to the background) and (2) due to drops in the partially desorbed areas on either side of the fully desorbed region coalescing with the central ones²¹ (due to the lateral gradient). This explains the large drops on the centre line and a clearing around it in the base line (see Fig. 2-8). Further along the scanning direction, when the full desorption area vanishes and only partially desorbed areas are present; there is no sharp lateral gradient and correspondingly no clearing in the lateral direction (see Fig. 2-8 - Note that the image was taken approximately at three quarter length of the gradient).

In order to capture this difference in wetting along the gradient line, condensation images of the base and gradient lines were taken at four positions along the scanned lines as shown in Fig. 2-9. It can be seen that at the beginning of the scan (1st picture in Fig. 2-9), the condensed drops on the base and gradient line are consistent in size and shape. Also, it can be noticed that the condensed drops are oval in shape, align along the centre line and have a clear surrounding (as explained earlier). At the mid-length of the scan, the drops in the gradient line are found to be smaller and circular compared to the drops in the base line (the top line feature in each of the panels). Further, it can be noticed that there is no clearing around the drops in the gradient line indicative of relatively homogenous desorption or no lateral gradient. Finally in frame 4, it can be seen that the drops (on gradient line) merge with the drops in the background, thus revealing the gradient in surface energy/wettability has ended. Ideally, there should not be any condensation on the hydrophobic background and the hydrophobic end of the gradient

pattern as well. However, this was not the case. The reason for the observation can be understood by following the sequential time frames of condensation shown in Fig. A2-1. It can be seen that initially condensation occurred only in the hydrophilic regions, but with time condensation also occurred in hydrophobic background. So the droplets on the gradient pattern not differentiating themselves from the the background ones indicates the end of the wettability gradient.

The SIMS oxygen ion image taken at various positions along the length of the gradient and base lines are shown in Fig. 2-10. The patterned lines are shown as brighter areas in the image, corresponding to higher oxygen ion counts than the background (HDT). The higher oxygen ion counts in the patterned lines are due to the presence of the second SAM molecules (MHA) having COOH tail group. It can also be seen from Fig. 2-10 that the gradient line is brighter at the start and gradually fades into the background representative of the reducing oxygen concentration (similar to the condensation imaging). The gradient line totally fades at ~8mm of the scanned length at which point, the sample is calculated to be ~160 μm out of focus. At this point there is no desorption of the primary SAM (HDT) and the corresponding laser intensity provides the threshold for desorption. Based on three replications it was found that the desorption threshold ranges between 1.79 and 1.95 kW/cm^2 . This range is found to agree with previously determined range of 1.9 and 2.1 kW/cm^2 from ref 16, using a +10 cm lens. Further it can be seen that the base line is consistently bright at the various positions along the scanned length and hence has constant oxygen concentration (again similar to the high resolution SIMS images condensation imaging results).

The oxygen ion signal fading into the background along the gradient line signifies the chemical concentration gradient. However, the relative reduction in oxygen concentration (proportional to the relative reduction in the second SAM population) along the length needs to be quantified, so that the trend of surface energy/property variation in the resulting gradient can be found. In order to quantify the relative reduction in oxygen concentration, the SIMS images obtained at various positions were processed as mentioned in Section 2.4 to determine the pixel intensity per unit area. This quantity, when plotted as a function of the substrate's out of focus distance, will allow one to know how to vary the laser intensity in order to vary the steepness of the gradient. Such a plot generated for the three gradient lines produced is shown in Fig. 2-11. It can be seen that the pixel intensity per unit area proportional to the oxygen concentration, decreases with increasing out of focus distance or decreasing laser intensity. The oxygen concentration is found to be a slowly varying function of the out of focus distance up to the point where the sample is 40 μm out of focus. The trend is followed by a sharp decrease in oxygen concentration until when the sample is $\sim 90\mu\text{m}$ out of focus. For out of focus values larger than 90 μm , the oxygen concentration is found to be a slowly varying function of the out of focus distance before it finally fades into the background (when the sample is $\sim 160\mu\text{m}$ out of focus). As such, the largest variation in oxygen concentration takes place when the sample is 40-90 μm out of focus. This means that the SAM desorption is the most sensitive to the laser intensity changes, for the range between 29.15 and 6.5 kW/cm² and, as such, useable to produce gradients; this range is named as the partial desorption regime. Also, it can be noted that the pixel intensity concentration varies from a value

4.8-4.56 to 2.17-2.09 in the partial desorption regime, with limiting values of 5.5-7, when the sample is at the focus of the laser beam (start of gradient) and 1-1.6 when the sample is 145-150 μm out of focus (just before the gradient line fades into the background). This again shows the majority of the variation occurs in the partial desorption regime and also gives an idea of the range of chemical concentration variation in the gradient line.

The general trend in oxygen concentration variation observed in the experiments can be explained theoretically by considering the thermo-kinetic model¹⁷, used to predict SAM desorption at a point:

$$c(x, y) = c_0(x, y) \exp\left(-\int_{t_0}^{t_1} \frac{K_B T(x, y, t)}{h} \exp\left(-\frac{\Delta G}{RT(x, y, t)}\right) dt\right) \quad (1)$$

where, c – concentration of SAM at a point, c_0 – initial concentration at a given point, K_B is Boltzmann constant, h – Planck's constant, ΔG – Gibbs free energy for activation, R – universal gas constant, T – temperature and t – time. Based on our previous study i.e. ref [16], the temperature induced (i.e. T in Eq. (1)) by the laser beam can be determined by solving the heat diffusion equation. However, it should be noted that there are inherent simplifying assumptions such as constant thermal diffusivity with temperature and a linearizing Kirchoff's transformation for considering the temperature dependent thermal conductivity. The solution of the heat diffusion equation hence given by Moody and Hendel²², in the form of Eq. (2), can be used to determine the temperature profile induced by a laser beam at a point.

$$T = T_0 + \frac{PA\sqrt{2}}{kr\pi^{\frac{3}{2}}} \int_0^{\infty} \frac{1}{(U^2 + 1)} \exp\left\{-2\left(\frac{(X + VU^2)^2 + Y^2}{(U^2 + 1)}\right)\right\} dU \quad (2)$$

where, T_0 – room temperature, k – thermal conductivity of glass, A – absorptivity of the sample, r – 2e-folding beam radius and X , Y , V and U are dimensionless numbers. They are defined as $X = 2x/r$, $Y = 2y/r$, $V = vr/8D$ and $U = (8Dt/r^2)^{1/2}$, where, v – velocity of patterning, D – thermal diffusivity, t is time and x , y are co-ordinates with x being the scanning direction.

For the given case i.e. varying beam radius along the scan direction a straight forward approach would be to use equations (1) and (2) to determine the theoretical desorption profiles at several positions along the scan direction and compare it with the experimental data. However, one needs to realize the limitations linked with such an approach to produce accurate absolute values. First Eqs. (1) and (2) are primarily to describe a quasi-static process for a constant beam spot, so using it to describe a dynamic process i.e. a continuously varying beam spot diameter would add another level of complexity to the temperature model on top of the inherent assumptions (as mentioned earlier). Hence a more conservative approach of considering the functional behavior of the governing equations was adopted rather than solving the equations to determine absolute values.

Considering the thermo-kinetic model, it can be seen that temperature is the only variable in the integrand of equation (1). Hence the integral in the equation is the time integral of the temperature at a particular point. Taking the initial concentration of the HDT SAM (c_0) as 1 (corresponding to 100% coverage), from equation (1), it can be seen that the

SAM concentration after irradiation (c) varies as exponential function of the negative of the temperature induced. So, the fraction of HDT (ψ) desorbed at a point can be calculated by subtracting the SAM concentration after irradiation (c) from the initial SAM concentration (c_0) and is given as:

$$\psi \propto (1 - \exp(-T)) \quad (3)$$

So, to be able to plot the variation of SAM concentration as a function of laser intensity or out of focus distance, the knowledge of the functional variation of temperature induced along the scan direction is required. Now considering Eq. (2), it can be seen that the integrand in equation is dimensionless. The term outside the integral has terms such as the power (p), thermal conductivity (k) and absorptivity (A) which are all constants. This quasi-static equation can be used to predict the temperature profile induced at a position. Thus for the case studied, considering the temperature induced at a series of points along the gradient, the beam radius becomes a variable (diverging beam as substrate is moved out of focus). Hence temperature induced at various points along the scan, varies inversely as the radius of the laser beam.

Including the relation between the induced temperature and the radius of beam in the thermo-kinetic model's functional dependence (Eq. (3)), it can be seen that the fraction of HDT desorbed (ψ) varies in the following functional form:

$$\psi(r) \propto \left(1 - \exp\left(\frac{-1}{r}\right)\right) \quad (4)$$

where, $\psi(r)$ is the amount of HDT desorbed. The functional relationship between the out of focus distance (z) and the radius of the beam (r), according to the theory of divergence of a laser beam, is given by the equation (4)²⁴.

$$r(z) = r_0 \left[1 + \left(\frac{\lambda z}{\pi r_0^2} \right)^2 \right]^{\frac{1}{2}} \quad (5)$$

where, $r(z)$ – 2e-folding radius of the diverged laser beam, r_0 – 2e-folding focal beam spot radius, λ – wavelength of the laser. Combining equations (4) and (5), the desorption as a function of out of focus distance ($\psi(z)$) is given by the equation (6), and plotted in Fig. 2-12 to compare with the experimental data.

$$\psi(z) \propto \left(1 - \exp \left(\frac{-1}{r_0 \left[1 + \left(\frac{\lambda z}{\pi r_0^2} \right)^2 \right]^{\frac{1}{2}}} \right) \right) \quad (6)$$

The variation in oxygen concentration signifying the second SAM molecule concentration is proportional to the amount of primary SAM desorbed. So the theoretical trend for desorption (at a point) along the gradient line, as a function of out of focus distance can be compared with the experimental data obtained for average oxygen intensity (calculated from the fitted curves for oxygen signal from SIMS) variation. Given the uncertainties in the data points, it can be seen that the theoretical trend describes the variation in oxygen concentration as a function of out of focus distance.

2.4 Summary

A new methodology to fabricate surface energy gradients on SAMs using DLP has been developed. The method has been demonstrated by fabricating a wettability gradient using HDT and MHA as contrasting SAMs. It is a simple, non-contact method and can also be easily extended to other systems like chlorosilanes. Furthermore, there is no need for photolithography, either directly or indirectly.

Condensation imaging qualitatively showed the gradients produced. Using quantitative methods of SIMS and modeling, the desorption of HDT is found to be the most sensitive for incident laser intensity ranging between 29.15-6.5 Kw/cm². The threshold laser intensity for desorption of HDT using the 10X Olympus objective was found to be 1.9 Kw/cm². The theoretical trend for the desorption, as a function of out focus distance, has been determined by considering the functional behavior of the governing equations. In general it was found that theoretical trend for desorption, as a function of out of focus distance, represented the experimental data.

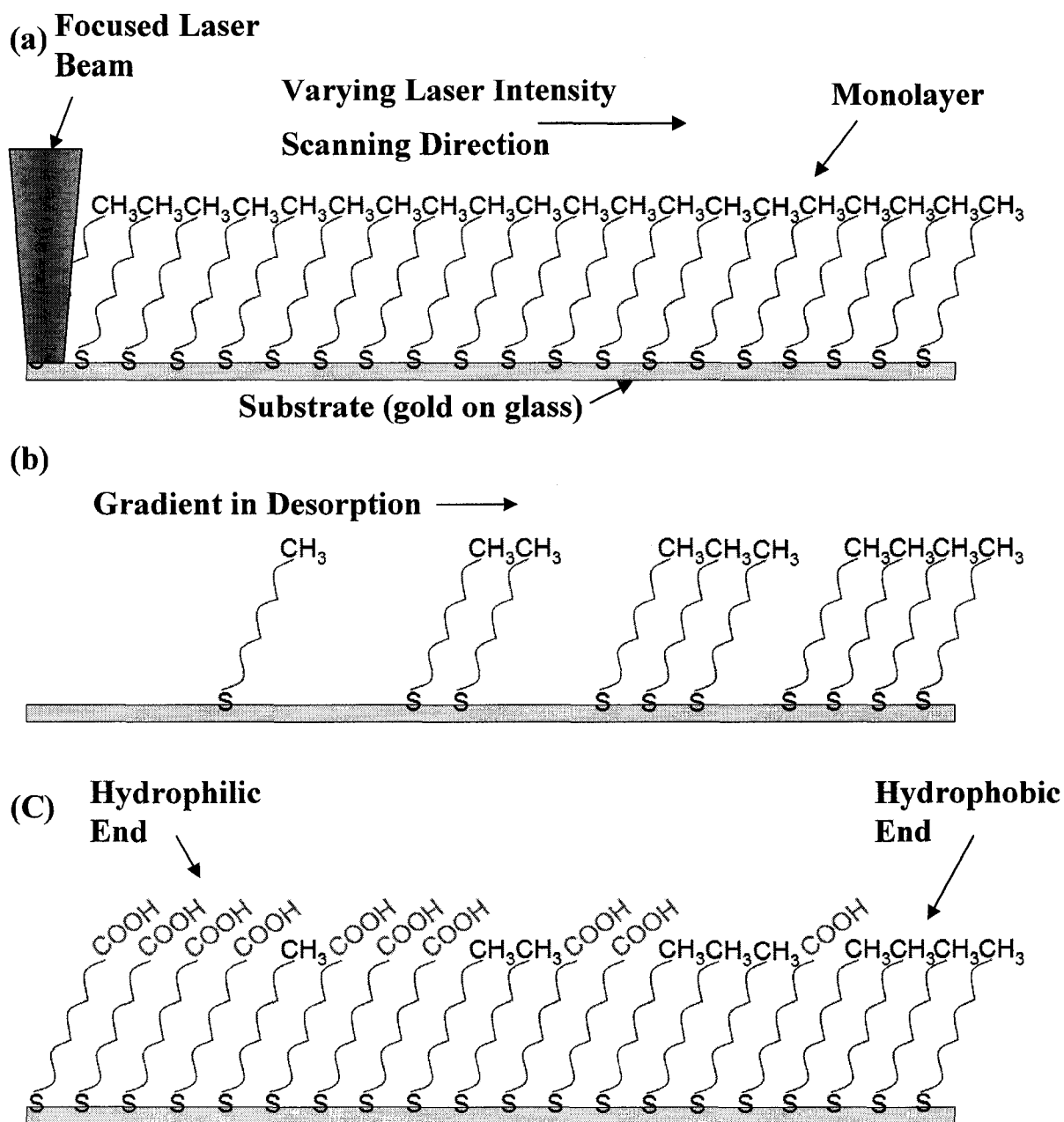


Fig. 2-1: The three steps in production of surface energy gradients using Direct Laser Patterning (DLP) (a) Focused laser beam on homogenous hydrophobic hexadecanethiol SAM, (b) The laser intensity is varied along the scan direction to produce a gradient in desorption (c) Backfilling of the desorption gradient with mercaptohexadecanoic acid - the second SAM. The population of the second SAM molecule (COOH tail group) changes from a maximum at hydrophilic end to zero at the hydrophobic end creating a gradient in surface wetting.

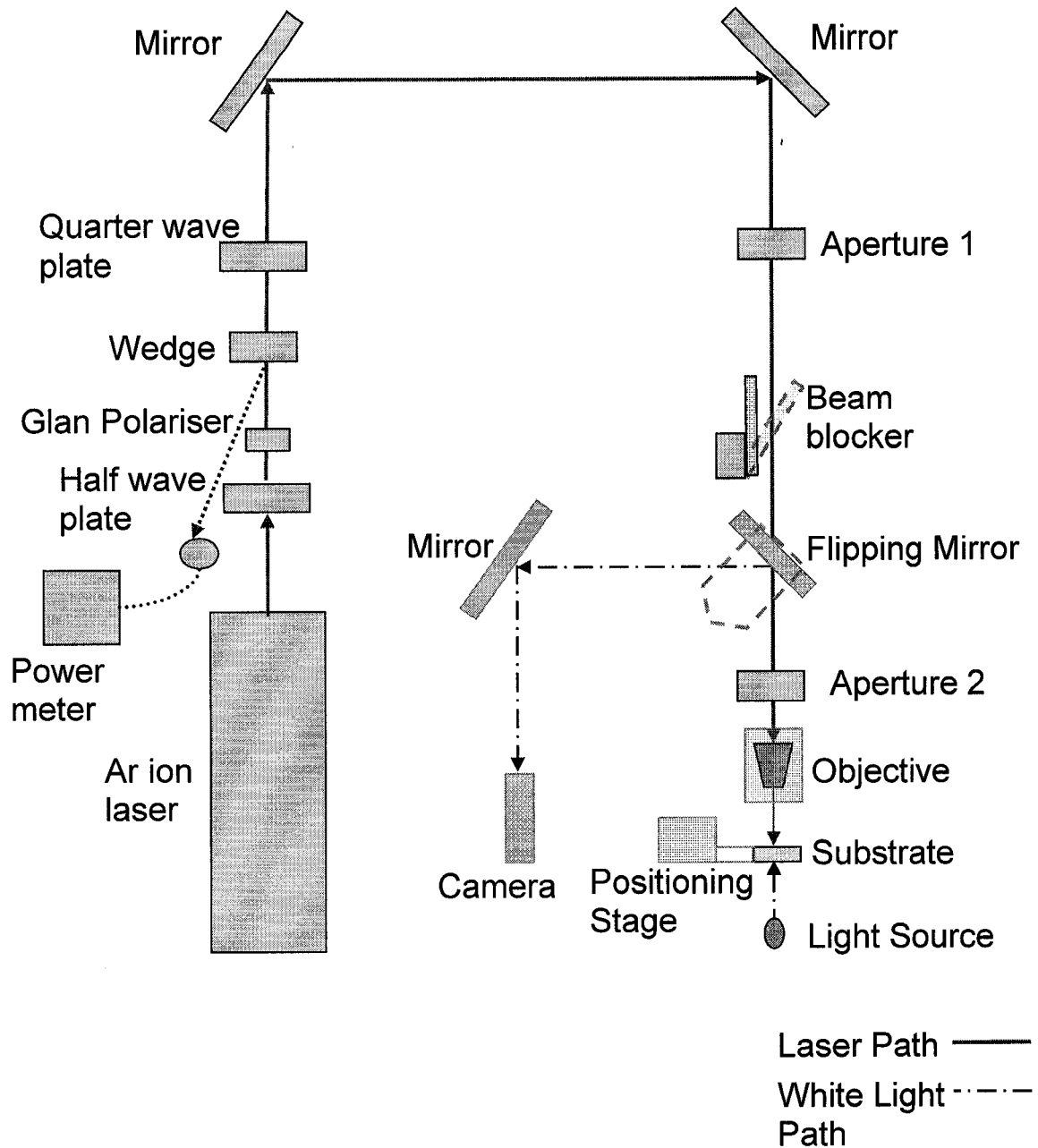


Fig. 2-2: Schematic of the experimental set up for fabrication of surface energy gradients using DLP for self assembled monolayers. Apertures 1 and 2 shown, were used for fine and coarse alignment of laser beam, respectively. The light source shown is used for determining the focal distance of the objective (note that with a 300Å gold layer the samples were semi-transparent).

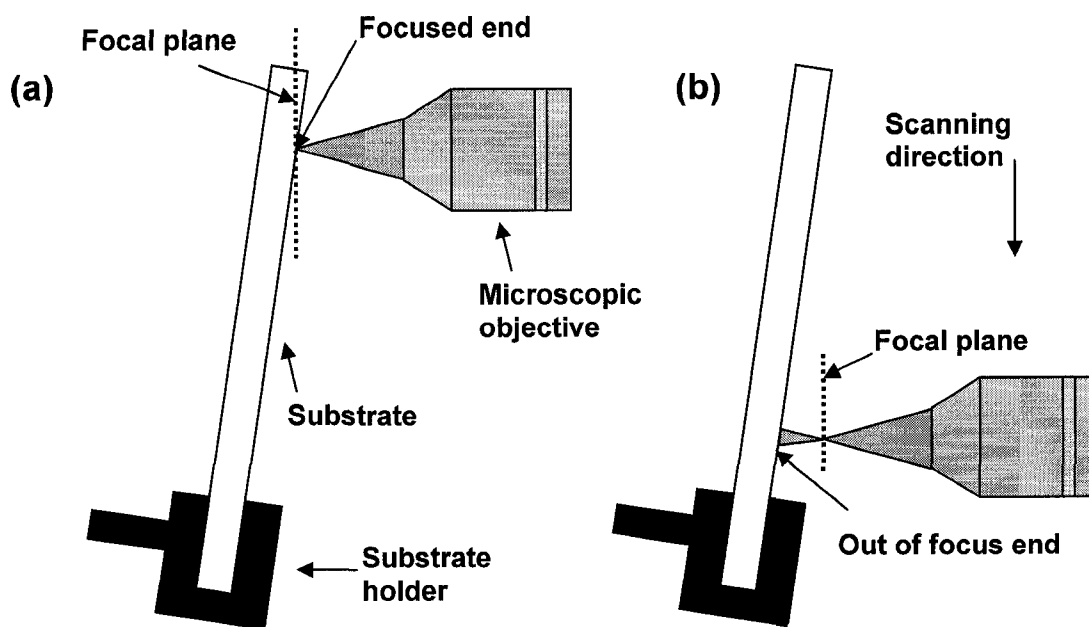


Fig. 2-3: Continuous variation of laser intensity, along the line scan, achieved by keeping the substrate inclined with respect to the focal plane. (a) shows laser beam focused at a point on substrate, this point receives the highest laser intensity and hence correspond to hydrophilic end of the pattern; the hydrophobic molecules will be fully desorbed and back filled with a hydrophilic species. (b) Shows out of focus laser beam at the other end of line scan, the laser intensity drops below the threshold for desorption and hence this end of the pattern is hydrophobic (no desorption of primary SAM).

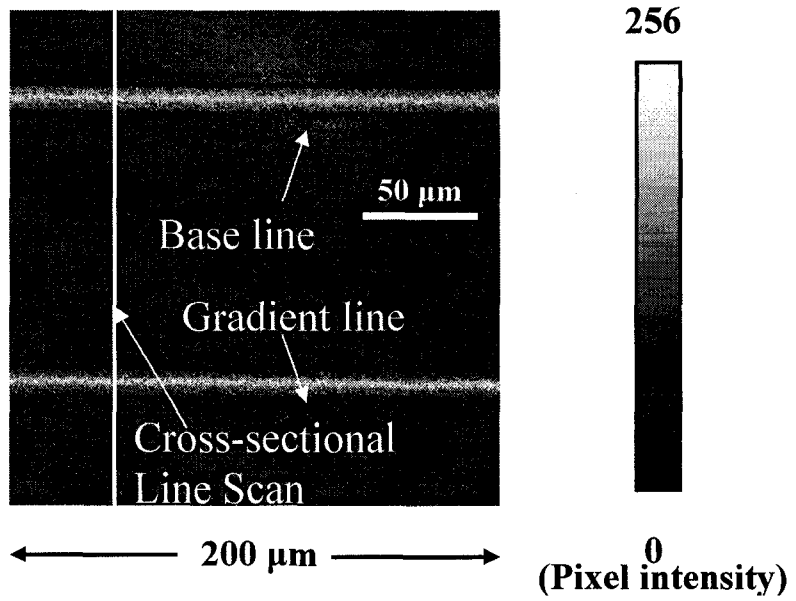


Fig. 2-4: Shows the SIMS image for oxygen ion concentration, at the beginning of the base and gradient lines. The lines represented by lighter colors (higher pixel intensities) correspond to higher oxygen concentration compared to the background. The image also shows the transverse line scans done, using the Ion-image software, to obtain the pixel intensity plot across the line patterns. This procedure was repeated at various locations along the pattern formed.

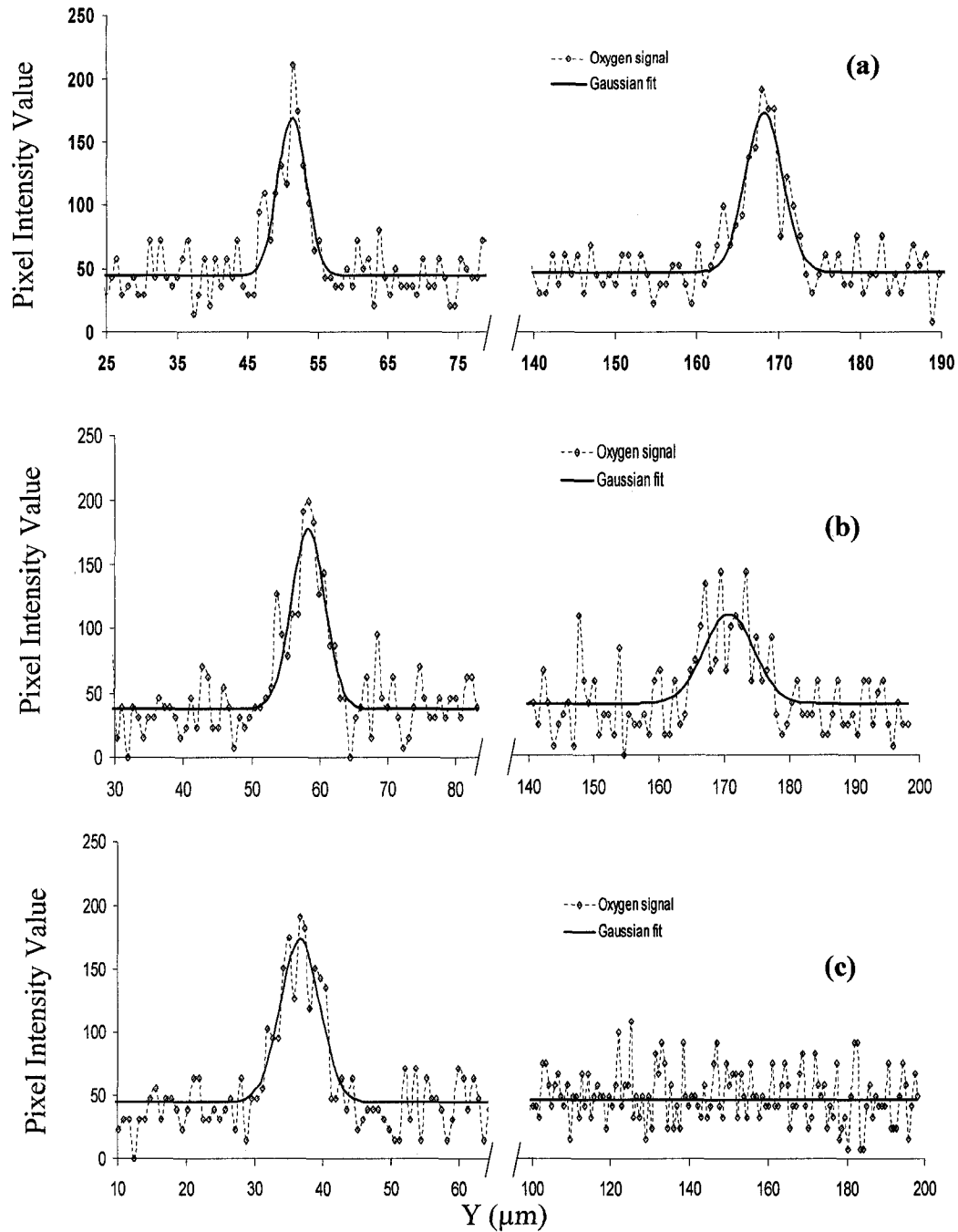


Fig. 2-5: Shows the pixel intensity plot corresponding to the oxygen concentration across the patterns (y-axis) along the base and gradient lines. (a) At the beginning, the base and gradient lines have approximately same oxygen signal, (b) At the middle of the scanned length, the gradient line oxygen signal is lower compared to the base line and (c) At the end of the scan, the gradient line oxygen signal has faded into the background signal. At all the positions the oxygen signal for the base line remained constant given the experimental uncertainty.

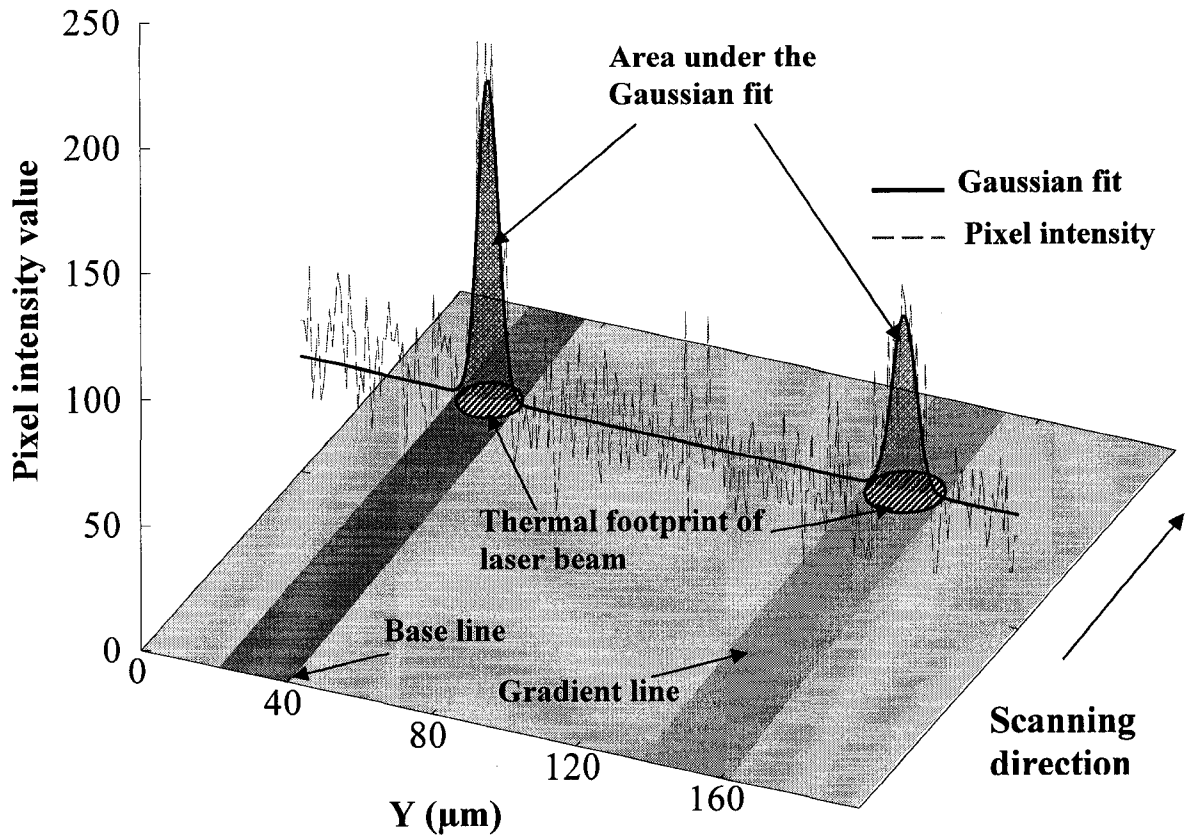


Fig. 2-6: Shows the pixel intensity plot across the patterned lines, a double Gaussian fit (solid heavy line) and the area underneath (hatched area). Hatched areas correspond to the thermal footprint of laser beam. The area under the Gaussian fit (shaded) provides the total pixel intensity corresponding to the total counts of oxygen. The total pixel intensity is then divided by a circular area corresponding to the thermal foot print of the laser beam. The diameter of the thermal foot print of the laser beam corresponds to the full width of the pattern and is calculated based on full width of the Gaussian fit. In comparison to the base line it can be seen that the gradient line has lower value for oxygen signal and a larger laser footprint, hence reduced laser intensity due to a diverged incident laser beam.

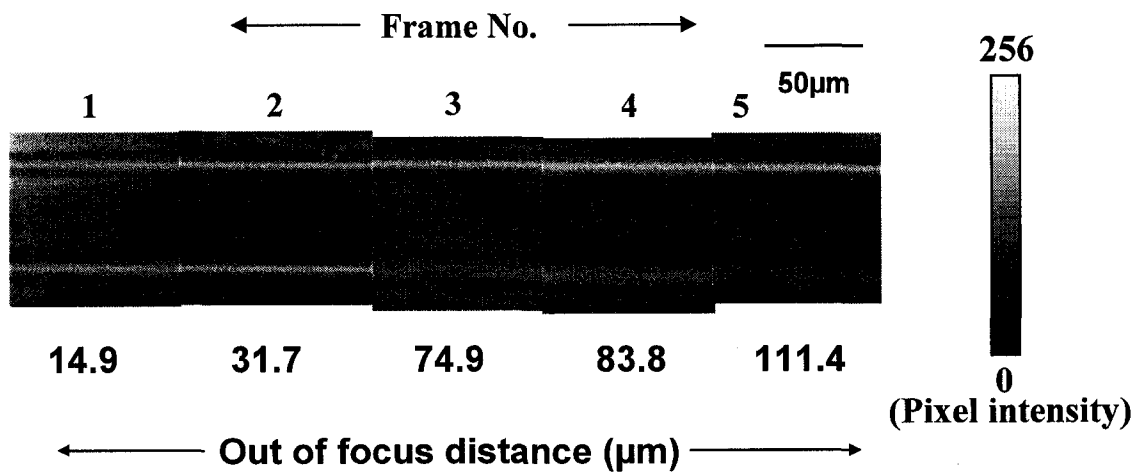


Fig. 2-7: Shows SIMS oxygen ion images from five positions along the laser scan direction. Top line in each frame is the base and the bottom is the gradient. Laser intensity is reduced from left to right for the gradient line. At the beginning of the scan (see frame 1 - leftmost) it can be noted that the gradient and base line have high oxygen concentration at the centre, lesser at the edges and nothing in background, representative of complete backfilling of second SAM at the centre, lesser at the edges and nothing in the background. Further along the scan in frame 3, it can be seen that central high oxygen concentration area vanishes to leave only uniform weaker signal for oxygen, representative of backfilling partial bare regions. The signal for oxygen is seen to consistently go weaker along the laser scan direction (in the subsequent frames) before it finally vanishes into the background, representative of a longitudinal chemical gradient.

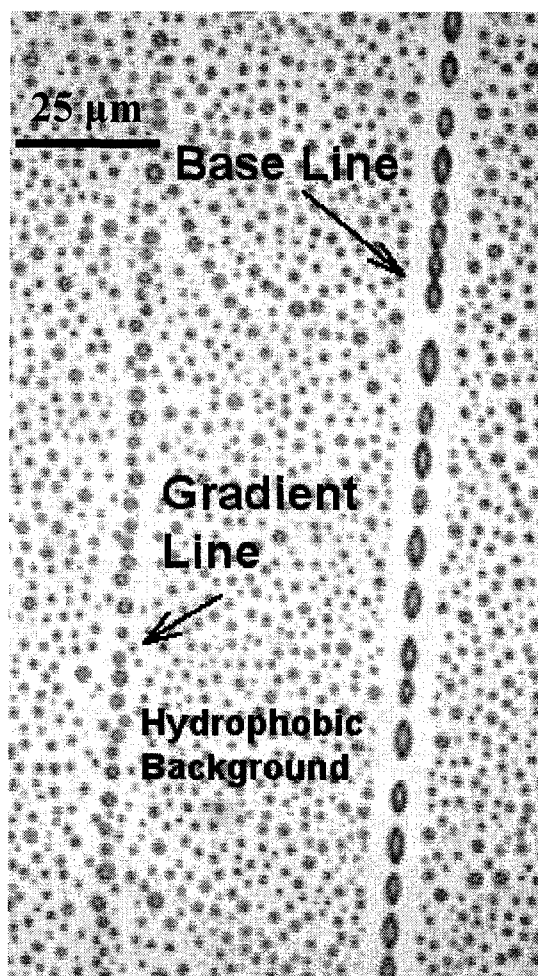


Fig. 2-8: Shows the picture of the condensed water drops on the sample at 10X magnification. The picture is taken approximately at three quarters of the scanned length. The width of both lines are similar. It can be seen that the water droplets wet the gradient and base lines differently. Further, the hydrophobic background corresponding to the hexadecanethiol SAM is seen to be wetted distinctly compared to the patterned lines.

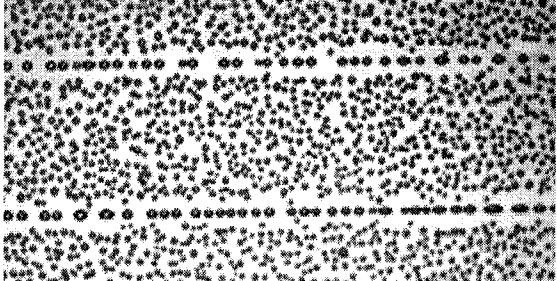
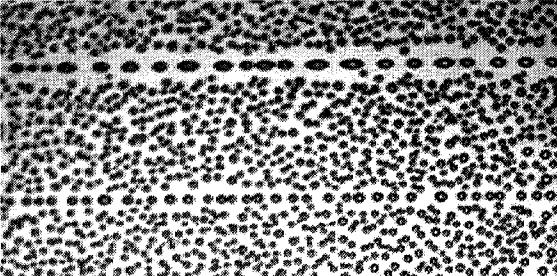
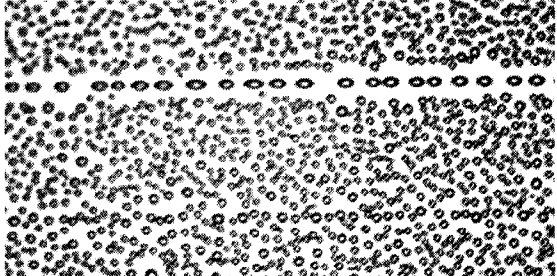
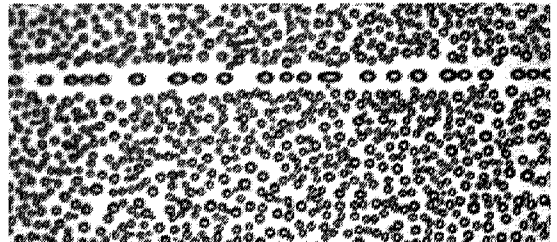
Image at approximate distance from start of the gradient (mm)	Out of focus distance 'Z' (μm)	Condensation image at corresponding position 50 μm —
0	0	
4	80	
6	120	
8	160	

Fig. 2-9: Shows condensation images of the base and gradient lines at various distances from the start point of scan (10X magnification). It can be seen at the start point of scan, the gradient and base line appear consistently wetted. The image at ~ 4 mm from the start point shows the drops in the gradient line have shrunk in size corresponding to a lower wettability. This trend continues and can be seen in the image at ~ 6 mm and finally at ~ 8 mm from the start the gradient line fades into the hydrophobic background. Note that the timing was different for each image

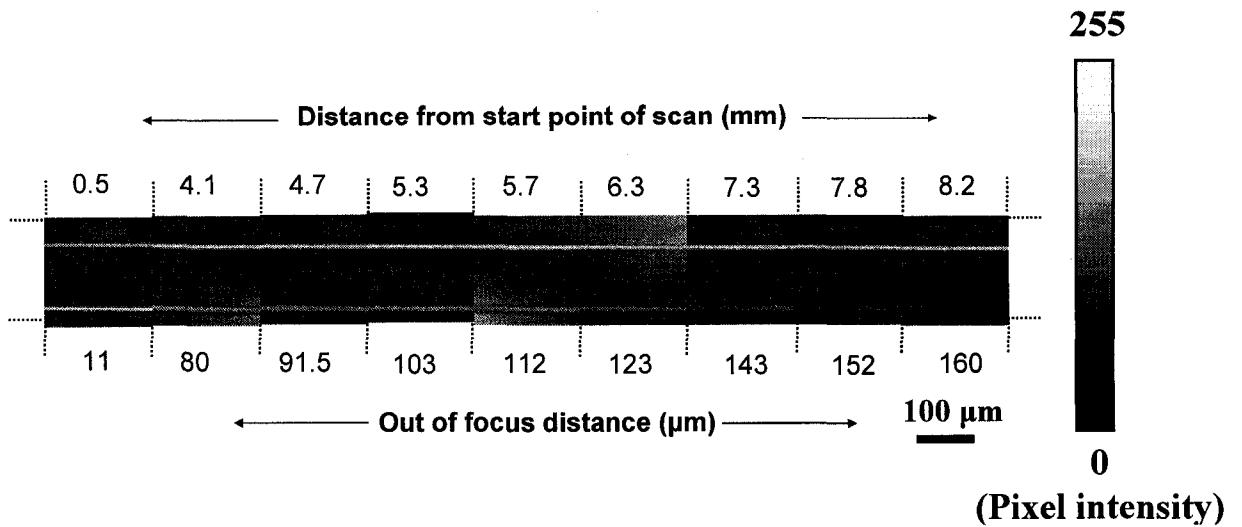


Fig. 2-10: Shows SIMS oxygen ion images of the base (top) and gradient lines (bottom). The images at various distances from the start are juxtaposed to show the relative variation in oxygen concentration. The scale bars shown applies to each of the juxtaposed images. It can be seen that the base line at the top has uniform color (pixel value) representative of the consistent oxygen concentration, whereas the gradient line (bottom) consistently fades and merges into the background at the end thus showing the gradient in chemical concentration.

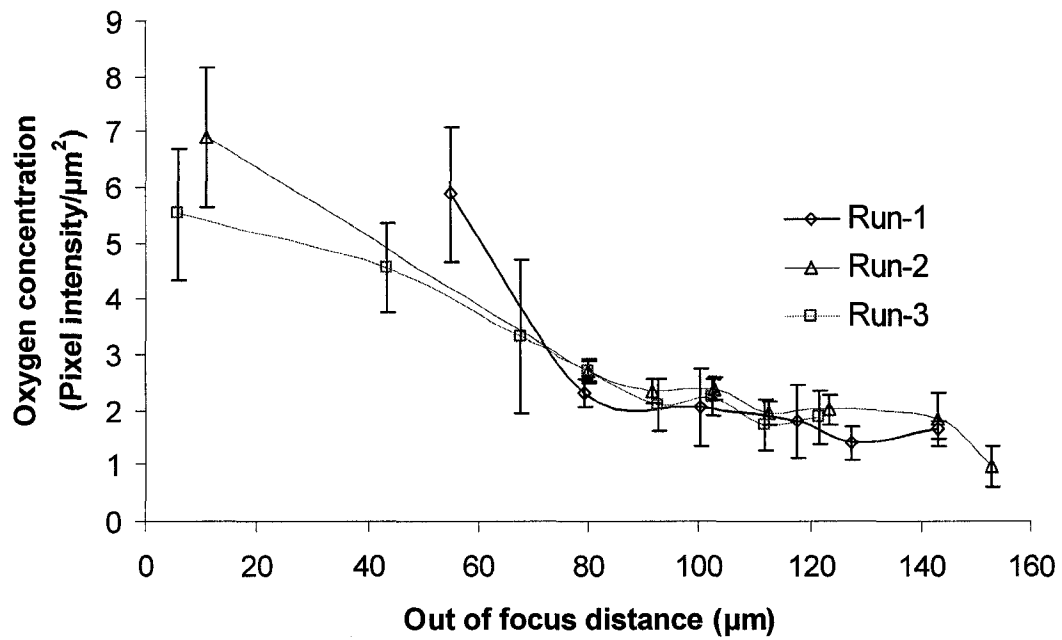


Fig. 2-11: Shows variation of oxygen concentration for three runs of the gradient line, with respect to distance of out of focus of laser beam. Error bars correspond to $\pm 1SD$. The lines joining the data points are to guide the eye only.

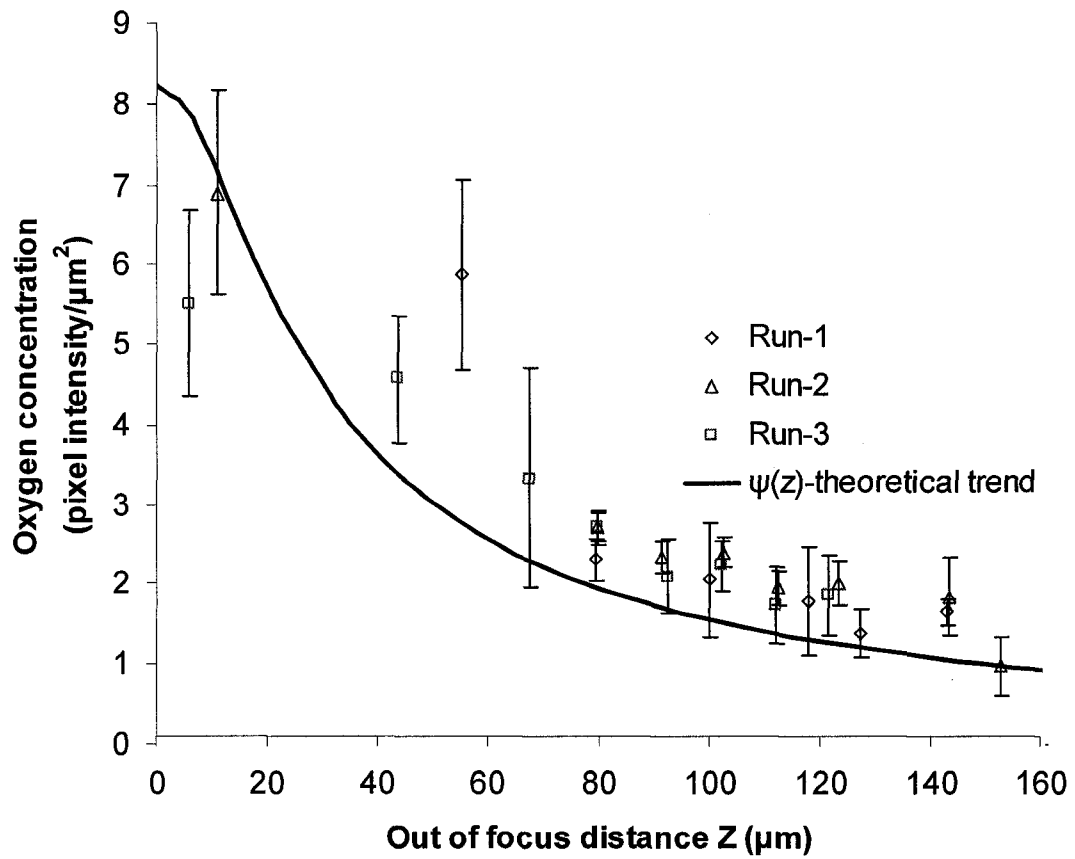


Fig. 2-12: Shows the theoretical trend for desorption as a function of out of focus distance, based on thermo-kinetic model. It can be seen that the theoretical trend follows experimental data, given the uncertainties associated.

2.5 References

- (1) Chaudhury, M. K.; Whitesides, G. M. *Science* **1992**, *256*, 1539-1541.
- (2) Zorba, V.; Persano, L.; Pisignano, D.; Athanassiou, A.; Stratakis, E.; Cingolani, R.; Tzanetakis, P.; Fotakis, C. *Nanotech.* **2006**, *17*, 3234-3238.
- (3) Gunawan, R. C.; Silvestre, J.; Gaskins, H. R.; Kenis, P. J. A.; Leckband, D. E. *Langmuir* **2006**, *22*, 4250-4258.
- (4) Sethuraman, A.; Han, M.; Kane, R. S.; Belfort, G. *Langmuir* **2004**, *20*, 7779-7788.
- (5) Elwing, H.; Welin, S.; Askendal, A.; Nilsson, U.; Lundström, I. *J. Colloid Interface Sci.* **1987**, *119*, 203-210.
- (6) Elwing, H.; Askendal, A.; Lundström, I. *J. Biomed. Mater. Res.* **1987**, *21*, 1023-1028.
- (7) Elwing, H.; Welin, S.; Askendahl, A.; Lundström, I. *J. Colloid Interface Sci.* **1988**, *123*, 306-208.
- (8) Elwing, H.; Askendal, A.; Lundström, I. *J. Colloid Interface Sci.* **1989**, *128*, 296-300.
- (9) Elwing, H.; Goelander, C. *Adv. Colloid Interface Sci.* **1990**, *32*, 317.
- (10) Liedberg, B.; Tengvall, P. *Langmuir* **1995**, *11*, 3821-3827.
- (11) Roberson, S. V.; Fahey, A. J.; Sehgal, A.; Karim, A. *App. Surface Sci.* **2002**, *200*, 150-164.
- (12) Pitt, W. G. *J. Colloid Interface Sci.* **1989**, *133*, 223-227.
- (13) Lee, J. H.; Kim, H. G.; Khang, G. S.; Lee, H. B.; Jhon, M. S. *J. Colloid Interface Sci.* **1992**, *151*, 563-570.
- (14) Ito Y; Heydari M.; Hashimoto A.; Konno T.; Hirasawa A.; Hori S.; Kurita K.; Nakajima A. *Langmuir* **2007**, *23*, 1845-1850.
- (15) Blondiaux, N.; Zurcher, S.; Liley, M.; Spencer, N.D. *Langmuir* **2007**, *23*, 3489-3494
- (16) Shadnam, M. R.; Kirkwood, S. E.; Fedosejevs, R.; Amirfazli, A. *Langmuir* **2004**, *20*, 2667-2676.
- (17) Shadnam, M. R.; Kirkwood, S. E.; Fedosejevs, R.; Amirfazli, A. *J. Phys. Chem. B* **2005**, *109*, 11996-12002.
- (18) Fuierer, R.R.; Carroll, R.L.; Feldheim, D.L.; Gorman, C.B. *Adv. Mat.* **2002**, *14*, 154-157.

- (19) Hartmann, N.; Balgar, T.; Bautista, R.; Franzka, S. *Surface Sci.* **2006**, 600, 4034-4038.
- (20) Kumar, A.; Whitesides, G. M. *Science* **1994**, 263, 60-62.
- (21) Daniel, S.; Chaudhury, M.; Chen, J. *Science* **2001**, 291, 633-636.
- (22) Moody, J. E; Hendel, R. H. *J. Appl. Phys.* **1982**, 53, 4364-4371
- (23) *Fundamental of Photonics*, Saleh, B.E.A. and Teich, M.C., John Wiley & Sons, Inc., U.S.A., **1991**, 83.

Chapter 3 - Fabrication of Multi-Component Chemical/ Surface Energy Gradients of Different Shapes and Lengths

3.1 Introduction

A surface having a continuous spatial variation of surface energy/properties constitutes a surface energy gradient. Energy gradient surfaces transport material directionally in a variety of applications such as: bacteria towards nutrients in chemotaxis¹, cells in the required direction in *in-vitro* studies^{2,3}, guide ganglion cells for axons/nerve growth⁴ etc. Further, energy gradients are also a useful tool for studies, looking at biological interaction of surfaces⁵ (aimed at fabricating bio-compatible surfaces for implants). Apart from their biological applications, energy gradients are also of interest for self-propelling and directing liquid drops⁶⁻⁹ in micro-fluidic and MEMS devices. The wide range of applications has motivated research and development of several methods for fabrication of surface energy gradients¹⁰⁻²¹, a majority of them based on Self Assembled Monolayers (SAM).

A SAM is a single layer of molecules deposited on a substrate from the corresponding solution. A typical example is alkanethiols ($\text{HS}(\text{CH}_2)_n\text{X}$) on gold, where 'X' can be any of CH_3 , COOH , Br etc. SAM surfaces exhibit properties as a function of the tail group of the molecules, for example: in the alkanethiol molecule, if the tail group (X) is Br then the surface is hydrophobic whereas if it is COOH , the surface is hydrophilic. So SAMs can be patterned by selectively removing/replacing the molecules (to locally manipulate surface properties). If removal/patterning is such that the SAM population increases along of scanning direction as shown in Fig. 3-1(a), then the surface exhibits a gradient in

surface energy/ property, this is a single component gradient. When this single SAM gradient is backfilled at the bare regions (of the substrate) with a contrasting SAM molecule i.e. with a tail group, different from the first (see Fig. 3-1(b)), then a two component gradient is produced. If the patterning is repeated and more than two SAM molecules are employed then a multi-component gradient is created. As an example a three component gradient is shown in Fig. 3-1(c), in which a gradient in removal of SAM-1 is backfilled with SAMs 2 and 3. Also, SAMs can be patterned so as to exhibit different surface properties over surface area of a required shape such as trapezium, triangle etc. Such patterns would constitute shape gradients, similar to what has been demonstrated in ref 7 and can be used for applications such as propulsion of liquids also demonstrated in ref 7.

Surface energy gradients have been previously produced on a wide range of length scales, ranging from few nanometers to centimeters¹⁰⁻²¹. A review paper by Ruardy et al.⁵ serves as a comprehensive reference to the earliest methods developed. The earliest methods were mainly based on diffusion and were focused on producing energy gradients of the order of few centimeters – millimeters in length. An energy gradient on a silicon substrate was fabricated by controlled diffusion of alkylsilanes in either liquid^{10,11} or gas⁶ phase. In the liquid phase, diffusion of the SAM molecules (onto the substrate) was controlled such that there was a gradient in deposition of the monolayer. The monolayer deposition (as required) was achieved by using a mixture of low density and high density solvent (with silane as solute) to deposit the monolayer¹⁰. Further by controlling, either the initial concentration of the silane or the flow of high density solvent (using a peristaltic

pump) before mixing of the solvents, gradients of varying steepness were fabricated¹¹. However, there was high contact angle hysteresis and also restrictions in the length and shape of the gradients produced. In the gas diffusion technique, diffusion of the molecules was controlled by placing an evaporating silane source near one end of the substrate. Thus a gradient in deposition of the monolayer was achieved (along the length)⁶. The contact angle hysteresis was found to be relatively less compared to the liquid based diffusion method; however, the other limitations such as restriction in length and shape of gradients were not overcome. Energy gradients were also created on gold surfaces by diffusion of alkanethiols. The diffusion of two different alkanethiols onto a gold strip was controlled using glass filters (placed on either side of a polysaccharide matrix) so as to create an opposing two component concentration gradient¹². The main advantage of this method was that two component gradients were possible, however the other issues discussed with regard to length and shape of gradient remain unaddressed. In all of the methods discussed above, since they were based on diffusion, there was no or little control over the steepness of the gradient and also the gradients were of the order of few millimeters-centimeters. So fabrication of well defined gradient such as in steepness, shape, length and resolution was not possible. While other techniques developed later such as: computer controlled slow immersion of a bare gold substrate in a dilute alkanethiol solution¹³, applying a spatially variable (linear) electrochemical potential across a mercaptoundecanol coated gold film¹⁴ and mechanical manipulation of self assembly of n-octyl trichlorosilane (on silicon) using variably stretched PDMS stamps¹⁵, introduced advantages like the ability to produce two component gradients and

simultaneously have better control over the steepness of the gradients, the issues with regard to producing gradients of arbitrary shapes and resolution were still unaddressed.

Recent advancements in fabrication technology have helped partly address the above remaining issues, through development of techniques based on micro-contact printing^{16,17}, lithography^{9,18-19} and Scanning Tunnel Microscopy (STM)²¹. The simplest of these techniques is based on modified micro-contact printing, micrometer scale gradient of different steepness and shapes were fabricated by varying the contact area/time while printing octadecyltrichlorosilane (OTS) onto silicon¹⁶. This method was simple, two component and gradients of different shapes were also possible. However, since the method was mainly based on diffusion, precise control of surface chemistry was not possible and further the need for new stamps each time for varying the geometry and steepness of gradient surfaces can make it cumbersome. Kraus et al.¹⁷ demonstrated a technique in which a gradient in deposition of hexadecanethiol (HDT) (on gold) was achieved through micro-contact printing using a variable thickness PDMS stamp. The bare regions of gold were then filled with another alkanethiol to create two component gradients. This method is very similar to the previously discussed method except that this is for alkanethiols, so there were similar limitations and additionally only SAMs that could be diffused in PDMS can be used. Methods based on lithography^{9,18-19} used UV radiation through masks to selectively oxidize/photo degrade the monolayer and fabricate patterns. The graded oxidation to produce energy gradients was achieved by exposure of alkanethiols to UV light through a graded photomask and TiO₂ covered glass¹⁸ (the TiO₂ coating functions as a catalyst for oxidation of the alkanethiol). The oxidized monolayer

was then rinsed away and backfilled with an alkanethiol with different tail group to produce a two component gradient. Similarly, alkylsilanes were gradiently photo-degraded in the lithography based methods either by using variable density filters¹⁹ or gradient exposure to UV light (172nm) through a photomask and mesh filters⁹, to produce wettability gradients. All these methods have the flexibility to produce gradients of different length and geometries. However, the need to fabricate different masks each time and the requirement for expensive infrastructure can make these methods cumbersome, inflexible and expensive. Further certain methods¹⁸ required long processing time. A STM based replacement lithography method was developed to create nanometer scaled gradients²¹. This method involved desorbing homogenous dodecanethiolate (in the presence of ferrocenyl-undecanethiolate SAM solution) at selective points, by applying a bias voltage between the STM tip and the monolayer. The voltage and scanning rate was varied to create gradient in desorption which was subsequently backfilled with the ferrocenyl-undecanethiolate monolayer. This method has the versatility of producing gradients of different lengths and geometries and at the same time have precise control over the steepness. However, multi-species gradient capability was not possible and at the same time expensive infrastructure such as STM instrumentation was required. Fabrication of gradient line features using Direct Laser Patterning (DLP) of alkanethiols (on gold), have been previously demonstrated in our work. The incident laser intensity was continually varied along a line scan to produce a gradient in desorption of hexadecanethiol (HDT) SAM on gold. The desorption gradient was then backfilled at the bare regions by mercaptohexadecanoic (MHA) acid SAM to fabricate two component line gradients. The continuous variation in laser intensity along

the scan length was achieved by keeping the sample inclined to the focal plane of the scanning laser beam. This method was capable of producing multi-component gradient lines and gradients of different lengths. However, gradients along curves and other non-linear patterns were difficult to produce, as it required complicated manipulation of the slope of the substrate and there was also broadening of feature width in the gradient lines produced. In this study the aforementioned technique, is advanced to produce gradients of different lengths and geometries that simultaneously allow both - control over the steepness of the gradient and flexibility to produce multi-species gradients.

A multi-component patterned SAM surface has been previously produced using submerged laser ablation (SLAB) method²². However, a gradient in concentration of the multi-components i.e. a surface exhibiting a gradient in different surface properties, is yet to be developed. Such a surface, if possible to fabricate, may be a useful tool in fabrication of various types of 'biochips' that can be used to separate different parts of a cell or migrate different types of cells in different directions. Further, a multi-species gradient can also serve as a multi-combinatorial tool in biological interaction studies and proteome and genome analysis, as it would exhibit a spectrum of different surface properties.

The method explained in this chapter is based on DLP^{23,24} for patterning of SAMs. The proposed method has been demonstrated by fabrication of, first of its kind, multi-component gradients and gradients of different lengths and shapes. The application of DLP to produce surface energy gradients involves three steps (as shown in Fig. 3-2):

formation of a homogenous SAM by solution deposition, followed by selective desorption of the SAM molecules using a focused laser beam. DLP works on the principle of thermal diffusion^{23,24} - the laser energy absorbed by the substrate is thermally conducted to produce localized heating which breaks the Au-S bond and hence desorb the monolayer. So in the proposed method, the laser intensity is continuously varied (leading to variation of surface temperature) along the scan path i.e. a line of required length or a circle etc., to create a gradient in desorption, as shown in Fig. 3-2(b). This desorption gradient is then backfilled with a secondary SAM to create a two component gradient. For a three component gradient, the patterning is continued to create desorption gradient along the required path and backfilling is carried out with a tertiary SAM. The 2 component gradients of different length and shapes have been demonstrated, using HDT (background) and MHA (on patterns) as primary and secondary SAMs, respectively. In addition, bromo undecanethiol (BUD) has been used as the ternary SAM to fabricate the three component gradient. The proposed technique is simple, non-contact and fast. Further does not depend on lithography and by modification of the DLP method demonstrated in [25] can possibly be extended to other systems such as alkylsilanes on silicon.

3.2 Methodology

3.2.1 Sample preparation

The “premium microscopic slides” from Fisher Scientific Co. were used as the substrate. As the glass slides were pre-cleaned, they were used as obtained. Sequential sputtering of a 50Å titanium adhesion layer at a rate of 0.75 Å/sec followed by a 300Å gold layer at a

rate of 0.98 Å/sec was performed on the microscopic slides. On completion of the gold sputtering, the samples were kept immersed in a 1mM ethanolic solution of hexadecanethiol (HDT) (Fluka) for 24 hours, for the primary SAM to form.

3.2.2 Experimental Setup

The block diagram of the set up, used for the experiments, is shown in Fig. 3-3. The laser source used was an air-cooled continuous wave (CW) Argon ion laser (Melles Griot - 543-BS-A03) operating at a wavelength of 488nm. The maximum power output from the laser head was ~90mW. For the purpose of controlling the laser power downstream in the optical train, a Half Wave Plate (HWP) - Glan polarizer combination was used. The HWP was mounted on a computer controlled rotation stage (Newport - PR50CC) so that there was automated laser power control, downstream of the Glan polarizer. An optical wedge was used to sample the beam (~4%) for online power measurement. The quarter wave plate was used to change the polarization of the reflected laser beam (from the sample) so as to avoid destructive interference with the incident one. The mirrors were used for directing the laser beam onto the sample. The apertures in the setup were used for the purpose of aligning the laser beam before patterning. A computer controlled beam blocker was used for the purpose of blocking the laser beam when patterning was required to be paused. A 4X microscopic objective from Olympus (UPlan FI) was used for focusing the laser beam. The objective was mounted on a micrometer driven translational stage. The sample holder was attached to a computer controlled translational stage (Newport - ILS50CC), put in a two-axis configuration. The focal point of the objective was determined by forming an image of the sample in the CCD camera, using a

white light source, as shown in Fig. 3-3. In order to account for the difference in wavelength, the focal distance obtained was corrected by an offset to obtain the focal point of the objective for the laser beam. As the objective lens has a series of propriety lens inside its casing, the required correction factor was experimentally determined to be +742 μm for the setup, as configured.

3.2.3 Experimental Methodology

In the proposed method (based on DLP), it is required to continually vary the laser intensity (power/unit area) during patterning, to create surface energy gradients (on SAMs). This can be achieved by continuous manipulation of either the beam spot area or the laser power. In this chapter, the latter approach of manipulating the laser power, holding the beam radius constant is adopted. The laser power is manipulated using the HWP – Glan polarizer combination (see Fig. 3-3). The intensity of the laser beam transmitted through the polarizer depends on the azimuth angle of the HWP and is given by the Malus law²⁶:

$$I = I_0 \cos^2(2\theta) \quad (1)$$

where, I is the laser intensity transmitted, I_0 is the incident laser intensity and θ is the azimuth angle of the HWP. So, by appropriately rotating the HWP during patterning, the laser power can be continually attenuated from an initial value to a minimum (for a constant beam spot radius). The minimum is determined by the threshold laser intensity for which there is no desorption of HDT. The patterning process was automated using a computer program written in Labview (National Instruments Inc.) with pre-programmed inputs of the desorption threshold and laser power equation i.e. Eq.(2) as a function of the

azimuth angle of the HWP. Based on prior preliminary experiments, the threshold intensity for HDT desorption (using the 4X objective) was determined to be ~ 24.1 kW/cm². The laser power variation as a function of azimuth angle of HWP was determined experimentally and can be described by the equation given below:

$$P = 0.0412[\cos(4\theta - 6.589) + 1] \quad (2)$$

In addition to these two inputs i.e. the desorption threshold and the laser power equation (Eq.(2)), inputs such as length of the scan path, its shape, velocity of scanning beam and the initial power value were provided by a user. With such information the stages can be controlled as required, to fabricate the required gradient in a particular shape. Also, by varying the rate of power attenuation i.e. the velocity of HWP rotation, gradients of different lengths/steepness were produced. The patterned samples were then rinsed with ethanol and dried in a stream of nitrogen before immersion into a 1mM solution of 16-mercaptohexadecanoic acid (MHA) (Sigma Aldrich) for 2 minutes to backfill the bare or partially bare gold regions. For the three component gradient, after creating the two component gradient as detailed above, patterning was continued as required, following which a 1-bromoundecanethiol SAM was deposited in the newly patterned areas by solution deposition (2 minutes dipping). The samples were rinsed with ethanol and dried with nitrogen each time after patterning and deposition of a monolayer. This was done to rinse away any physisorbed materials on the sample. The samples processed were stored in a chamber filled with nitrogen until further analysis was conducted. For the three component gradient, Secondary Ion Mass Spectroscopy (SIMS) imaging was used to capture the spatial variation in concentration of different SAM molecules.

In order to select a laser power for patterning that was well below the threshold for damage to gold, a series of lines were patterned on a sample using powers ranging from 100-15mW at the source (laser) and imaged using a Scanning Electron Microscope (SEM). The SEM image of the lines is shown in Fig. 3-4. It can be seen that the lines patterned with powers greater than 70mW (the rightmost three lines in Fig. 3-4) have a white central core, signifying damage of gold. So, in order to be well below the damage threshold and at the same time have a power range to produce gradients, laser beam with an initial power of ~40mW, after HWP-Glan polarizer, was selected for patterning.

The laser beam was focused using a 4X objective (Olympus UPLAN FI) onto the sample (HDT SAM on gold supported by a glass substrate). Before patterning, the sample was adjusted using a tilt stage so that it was perpendicular to the scanning laser beam. Hence there was no laser intensity variation due to divergence of the laser beam. The initial laser intensity was found to be 97.43 kW/cm^2 corresponding to a laser power of ~40mW and beam radius of $3.615 \mu\text{m}$.

The Labview program combined with user defined inputs such as initial laser power (~40mW) and velocity of scanning ($200 \mu\text{m/sec}$) was used to produce gradients of three different lengths (3, 6 and 12 mm). The difference in steepness/length was achieved by varying the velocity of the HWP rotation stage. The required velocity (of the HWP stage) was calculated based on the length of the gradient required and the HDT desorption threshold. As an example: for a 3 mm long gradient, the total time of patterning is 15 sec (calculated based on a constant velocity of $200 \mu\text{m/sec}$ for the translational stages). So

within this duration it is required to move the HWP +12.36 degrees (calculated based on equation (1)), from the initial position, in order to vary the laser power from the initial value to the desorption threshold (along the scan path). Hence the required velocity of HWP stage is calculated as 0.824 degrees/sec. The velocity required for different lengths was calculated as explained above and patterning carried out accordingly. The same procedure was followed (by the program), to create gradients of different shapes. Another set of gradient lines with the same parameters were produced on a different sample and characterized to verify repeatability of the process. The gradient lines hence fabricated, were characterized using Secondary Ion Mass Spectroscopy (SIMS) spectral analysis.

3.3 Results and Discussion

The patterned gradient lines were visible to the naked eye, when the sample was rinsed with ethanol (due to the difference in wetting between the patterns and background). However, without any probe liquid the patterns were invisible, to the naked eye and as well as under an optical microscope. So, the patterned gradient lines were imaged using SEM. The images revealed the patterns through a contrast difference (See Fig. 3-5) due to the difference in the tail group interactions with the incoming electron beam. The patterned lines were darker compared to the background. Similar contrast difference has been observed previously^{23,24} and Lopez et al.²⁷ have reported that the contrast in SEM images of patterned SAM surfaces (consisting of different alkanethiols on gold) is sensitive to the structure and composition of the SAMs. So in the given case, due to the composition difference between the patterned lines (MHA) and the background (HDT), the SEM images distinctly revealed the gradient lines (See Fig. 3-5). Also, the contrast

difference fading along the line into the background signifies a decrease of MHA concentration along the patterned gradient lines. Further, it can be noted that the gradient lines are of different lengths (3, 6 and 12 mm), so the steepness of surface energy/MHA composition in the gradient line has been successfully varied.

The mechanism of the explained method can be understood by taking a closer look at the SEM pictures of the 6mm gradient shown in Fig. 3-6. It can be observed that the gradient line at the beginning of patterning is represented by a dark central region flanked by two narrow less dark regions in a light background. This observed profile in MHA concentration, transverse to the direction of scan signifies: full/complete desorption of HDT at the centre, partial at the edges and nil in the background. This can be interpreted as production of a chemical gradient similar to what has been achieved via UV technique²⁸. As the laser intensity is constantly decreased along the length, it is seen that the full desorption region narrows down and at certain point disappears to leave only partially desorbed regions (see frame 3 in Fig.3-6). This point at which the full desorption area vanishes is where the laser intensity falls below the threshold for full desorption. The narrowing full desorption region from the start of the gradient till the full desorption threshold point, signifies a longitudinal trapezium shaped gradient (similar to the gradients demonstrated in [7]). After the threshold for full desorption is reached, there is constant decrease in the amount of partially desorbed HDT until patterning ceases or the threshold intensity for any desorption is reached. In this later stage, a surface energy gradient with fairly uniform chemical concentration of species in the traverse direction to the scanning path is formed. As such, a longitudinal chemical gradient is created. To sum

up, the mechanism of the patterning yields three kinds of gradients in the patterned lines, namely: (1) a micrometer/nanometer scale sharp lateral energy gradient across the patterns during the initial stages of scanning; (2) a millimeter scale longitudinal shape gradient (before the threshold for full desorption is reached), and (3) a millimeter scale longitudinal partial desorption gradient (after the threshold for full desorption is reached). Figure 3-7 shows the schematic of the three types of gradients formed. As such, depending on the application, the laser power can be tuned to produce any or all of the chemical gradients needed. For example, when it is required to fabricate a micrometer or nanometer scale sharp lateral gradients or millimeter scale shape gradients, a laser power range above the threshold for full desorption can be selected whereas if a millimeter scale surface energy gradient is required then patterning can be carried out, using a laser power range below the threshold for full desorption. Though the different gradients explained have not been fabricated individually, the laser power range that can be used to produce each of them (using the 4x objective) has been established. Based on the 3, 6 and 12 mm gradient lines fabricated, the threshold laser intensity for full desorption and any desorption (using the 4X objective) has been established at 37.26 kW/cm^2 and 24.1 kW/cm^2 , respectively. So when the incident laser intensity is varied from $37.26\text{-}24.1 \text{ kW/cm}^2$ (for the given system), a millimeter scale surface energy gradient is created. Whereas when the incident laser intensity range is selected above 37.26 kW/cm^2 (for the given system), a millimeter scale shape gradient and micrometer scale sharp lateral gradients are fabricated.

To verify whether the dark central region observed in the SEM images of the patterned lines correspond to full MHA coverage, a control experiment was performed. It involved SEM imaging of a sample, coated completely with MHA on one part and HDT on the other. The pixel values extracted from the image for the MHA, normalized with respect to the HDT pixel value was found to be 103 ± 27 at 95 % confidence level. This is comparable to the normalized (with respect to the HDT back ground) pixel intensity value of 109 ± 13 (at 95 % confidence level) obtained for the dark central region in the SEM images of the gradients produced. So the central dark region corresponds to complete coverage of MHA corresponding to the full desorption of HDT.

The width of the fabricated gradient lines was observed to consistently reduce, along the length. In order to capture this pattern width variation, the width of the pattern was measured (from the SEM images using Image-J software) at various positions along the gradient lines. The procedure for measuring the pattern width from SEM images using Image-J software (National Institutes of Health) has been explained in detail in the appendices section (A1-5). The pattern widths measured for the three gradient lines (3, 6, and 12 mm gradients) plotted as a function of the scanned length is shown in Fig. 3-8. It can be seen that, for all the gradient lines, the pattern of variation is approximately linear. Further, it can also be seen that the rate of variation is different for the three gradient lines i.e. the slope increases as the length decreases. This behavior is expected as pattern width is dependent on the incident power^{23,24} and the rate of power variation is different for 3, 6 and 12 mm gradients. The pattern width of the gradient lines at the full desorption threshold point is indicated in Fig. 3-8. It can be seen that the pattern width variation is

approximately linear both before and after this point. It can also be noted that the pattern width is same ($\sim 10 \mu\text{m}$) for all the three gradient lines, at this point. Further, it can be seen that the full desorption threshold point is reached at different lengths for the 3, 6 and 12 mm gradients which again signifies the difference in the rate of MHA variation for the different gradient lines. It is interesting to note that this method of laser intensity variation i.e. manipulation of laser power (along the scanned length) yields gradient lines of narrowing width whereas continuous manipulation of laser beam radius i.e. 'Out of focus' method (see chapter 2) yields gradient lines with an increasing width. So, if need be, gradient lines of constant width can be fabricated by combining both the methods.

The gradient lines were also characterized by Secondary Ion Mass Spectroscopy (SIMS). The SIMS oxygen ion signal was expected to weaken along the gradient line, corresponding to a decrease in MHA concentration. To capture this, SIMS spectral analysis was performed at various positions covering a $40\mu\text{m} \times 40\mu\text{m}$ area, along the gradients. The total count of oxygen ions at each position was determined, using a SIMS Ga ion beam $0.6 \mu\text{m}$ in diameter and set at a power level of 25 KeV. The total oxygen ion count was found by integrating the area under the peak obtained for oxygen and subtracting the counts for background (done by Ion-Spec. software). To see the relative variation of MHA concentration along the gradients, the total oxygen counts for each analyzed position of the three gradient lines are plotted as a function of length of the scanned line in Fig. 3-9. It can be seen that the rate of oxygen concentration variation increases with decrease in length of the gradient signifying the change in steepness of the gradient produced. Also, the general trend observed in the pattern of oxygen

concentration variation is found to be approximately linear and consistent for the three gradients produced. The results obtained were repeated by a set of replicated gradient lines on a different sample, yielding similar observations.

The general trend observed in the SIMS experimental results can be explained by considering the equations of the thermo-kinetic model²⁴ given below:

$$c(x, y) = c_0(x, y) \exp\left(-\int_{t_0}^{t_1} \frac{K_B T(x, y, t)}{h} \exp\left(-\frac{\Delta G}{RT(x, y, t)}\right) dt\right) \quad (3)$$

where, c – concentration of SAM at a point, c_0 – initial concentration at a given point, K_B is Boltzmann constant, h – Planck's constant, ΔG – Gibbs free energy for activation, R – universal gas constant, t – time and T – temperature distribution. Based on a previous study, i.e. ref [24], the temperature distribution can be modeled using the following equation:

$$T = T_0 + \frac{PA\sqrt{2}}{kr\pi^{\frac{3}{2}}} \int_0^{\infty} \frac{1}{(U^2 + 1)} \exp\left\{-2\left(\frac{(X + VU^2)^2 + Y^2}{(U^2 + 1)}\right)\right\} dU \quad (4)$$

where, T_0 – room temperature, k – thermal conductivity of glass, A – absorptivity of the sample, r – 2e-folding beam radius and X , Y , V and U are dimensionless numbers. They are defined as $X = 2x/r$, $Y = 2y/r$, $V = vr/8D$ and $U = (8Dt/r^2)^{1/2}$, where, v – velocity of patterning, D – thermal diffusivity, t is time and x , y are co-ordinates with x being the scanning direction.

It should be noted that equations (3) and (4) describe a quasi-static thermo-kinetic model that provides the SAM concentration at a point, after laser beam irradiation. So by

deriving the functional dependence of SAM concentration at a point from equations (3) and (4) and incorporating the functional variation of the parameters (along the gradient) affecting SAM concentration, an approximate theoretical functional relation describing the dynamic patterning process can be determined. To derive the functional dependence of SAM concentration, considering equation (3), it can be seen that the temperature is the only variable in the integrand of the equation (3). Hence the integral, is the time integral of temperature at a point. Taking the initial concentration of HDT SAM as 1 corresponding to a 100% coverage, the SAM concentration after irradiation varies in the following functional form:

$$c \propto \exp(-T) \quad (5)$$

The amount of HDT desorbed, i.e. equal to the amount of MHA backfilled (ψ) can be obtained, by subtracting equation (5) from the initial SAM concentration (i.e.1). As such, ψ can be found as:

$$\psi \propto (1 - \exp(-T)) \quad (6)$$

The variation of temperature at a point, along the scanned length needs to be incorporated in equation (6) in order to obtain the functional trend of ψ . So, considering equation (4) for the given case i.e. varying power along the scanned length, it can be seen that the temperature at a point is a function of the power alone. The integrand in the equation (4) is dimensionless and all other parameters such as beam radius (r), thermal conductivity (k), absorption (A) and room temperature (T_0) are constant for the given case. So incorporating the temperature-laser power relation in equation (6), one will have:

$$\psi \propto (1 - \exp(-P)) \quad (7)$$

But the power is varied as a function of the HWP azimuth angle and is given by the equation (2). The final functional relation obtained by combining equations (7) and (2) is as given below:

$$\psi \propto \left(1 - \exp\left(-0.0412[\cos(4\theta - 6.589) + 1]\right)\right) \quad (8)$$

where, $\theta = (\theta_{initial} + i_{increment})$; $\theta_{initial}$ is the HWP azimuth angle corresponding to the initial laser power, and $i_{increment}$ is the relative angular movement of the HWP during patterning. The term $\theta_{initial}$ is a constant however $i_{increment}$ is a variable along the length of the gradient and is obtained by multiplying the appropriate HWP velocity (for 3, 6 and 12 mm gradient) with the length l (at which ψ is required) and then dividing it by the patterning velocity (200 μ m/sec). Unknown co-efficients a and b were then introduced in this theoretical trend, as shown in equation (9) in order to obtain a best fit to the experimental data i.e. SIMS oxygen concentration variation obtained along the length of the gradient lines.

$$\psi = \left(a - b \exp\left(-0.0412 \left[\cos\left(4 \left(\theta_{initial} + \frac{HWP_{velocity} \times l}{patterning\ velocity} \right) - 6.589 \right) + 1 \right] \right) \right) \quad (9)$$

Using Matlab (curve fitting toolbox), equation (9) was fitted to the SIMS experimental data for the 3, 6 and 12 mm gradient lines, as shown in Fig. 3-10. The co-efficients a and b for the fits for 12, 6 and 3 mm gradient lines were found to be 1.27E+7, 1.28E+7, 1.18E+7, 1.19E+7, 8.85E+6 and 8.91E+6, respectively. The R^2 value of the fit was found to be to be close to unity. This signifies that the simplified parametric trend given by equation (9) closely represents the experimental data.

Further, to compare the trend of the theoretical model i.e. Eq. (8) with the experimental data, a scaling factor in the form of a scalar co-efficient ‘a’ was introduced in Eq. (8) as shown below:

$$\psi = a \left(1 - \exp \left(-0.0412 \left[\cos \left(4 \left(\theta_{initial} + \frac{HWP_{velocity} \times l}{patterning\ velocity} \right) - 6.589 \right) + 1 \right] \right) \right) \quad (10)$$

Equation (10) was then fitted to the experimental data (using Matlab toolbox) as shown in Fig. 3-11. The co-efficient ‘a’ was found to be 8.96E+6, 7.52E+6 and 6.93E+6 for the 3, 6 and 12 mm gradient, respectively. The correlation factors obtained were not close to unity as the parametric model however this theoretical model represented by Eq. (10) was found to follow the experimental data, acceptably.

As a demonstration of the capability to produce gradients of different shapes, a “U of A” shaped energy gradient was fabricated. The SEM image of the pattern is shown in Fig. 3-12 (a). It can be seen that for character ‘U’, starting from the bottom center, the pattern starts to become darker on either arm of ‘U’ and continues till the tip of the arms i.e. meaning surface energy variation from low (at the bottom center) to high at the ends of the ‘U’ shape. Similarly, for character ‘o’, it can be seen that starting from the bottom center, the pattern slowly becomes darker (on either side) until the diametrically opposite point i.e. the top of the letter ‘o’. The surface energy variation in other characters such as ‘f’ and ‘A’ can be understood by following the direction in which the different scanned paths fade. Also, the gradient in surface energy/wettability of the ‘UofA’ pattern has been captured using a condensation image shown in Fig. 3-12(b). In Fig. 3-12(b) it can be seen that condensate drop structure is at bottom of figures ‘U’ and ‘o’ are similar to the HDT

background, as the chemistries are similar whereas at the hydrophilic end of these characters the drop condensate structure are distinct from the background.

For the three component gradient, a circle pattern with a gradient in desorption of HDT (top-bottom) was created and backfilled with MHA SAM. After rinsing with ethanol and drying the sample in nitrogen, patterning was continued outside the circle pattern to create a gradient line (inline with the diameter of semi circle) on HDT. This line was backfilled with BUD. The gradient lines were pattern so that the end of the line was crossing the circle. The patterns hence produced were characterized using SIMS imaging. The SIMS images were produced for oxygen and bromine (79 and 81) are shown in Fig. 3-13. It can be seen that the oxygen is concentrated only on the circle, further the oxygen concentration is seen to decrease from top to bottom of the circle signifying a chemical gradient in MHA along the circle. The bromine is found to be deposited along the gradient line patterned and a gradient in concentration of the bromine signal is also seen along the line. However, a weak signal for bromine is also seen along the circle. This is probably due to the deposition of BUD in the defective sites of MHA. This problem can possibly be avoided by using a SAM like ferrocenyl undecanethiolate which has been observed to avoid adventitious replacement at defective sites of dodecanethiolate SAM²¹. Nevertheless, the proposed method has been demonstrated to produce: first of the kind, 3 SAM species gradient in arbitrary geometries. Further, the pattern created i.e. a circle with a mixed monolayer of MHA and BUD and BUD on the line with HDT as background may potentially broaden the spectrum of applications.

3.4 Conclusions

A novel DLP based methodology to fabricate chemical/surface energy gradients of different shapes and length using alkanethiol SAMs, has been developed. The method has demonstrated capabilities to produce three SAM species gradients. The proposed method is simple, non-contact, does not require lithography or a mask for patterning.

The gradient lines and shapes have been clearly revealed by SEM images. Also, using the SEM images the mechanism of the explained method has been established. It has been observed that by way of the mechanism three different kinds of gradients namely: (1) a micrometer scale sharp lateral energy gradient across the patterns during the initial stages of scanning; (2) a millimeter scale longitudinal shape gradient and (3) a millimeter scale longitudinal partial desorption gradient are created as parts of the fabricated gradient lines. So, depending upon the application the suitable laser power range can be selected to create any or all of the gradients. The limits for the creation of either of three types of the above mentioned gradients i.e. the laser intensity thresholds for full desorption and any desorption have been established at 37.26 kW/cm^2 and 24.1 kW/cm^2 , respectively for the given system i.e. 4X Olympus objective. The variation in the SIMS oxygen signal along the gradient line showed the corresponding variation in MHA concentration for the gradient lines produced. The theoretical trend has been determined by considering functional dependence of the governing equations. Also, the trend was fitted to the SIMS experimental data and was found to have good correlation factor. Finally, multi-

component gradient has been demonstrated by fabricating a three SAM gradient using HDT, MHA and BUD.

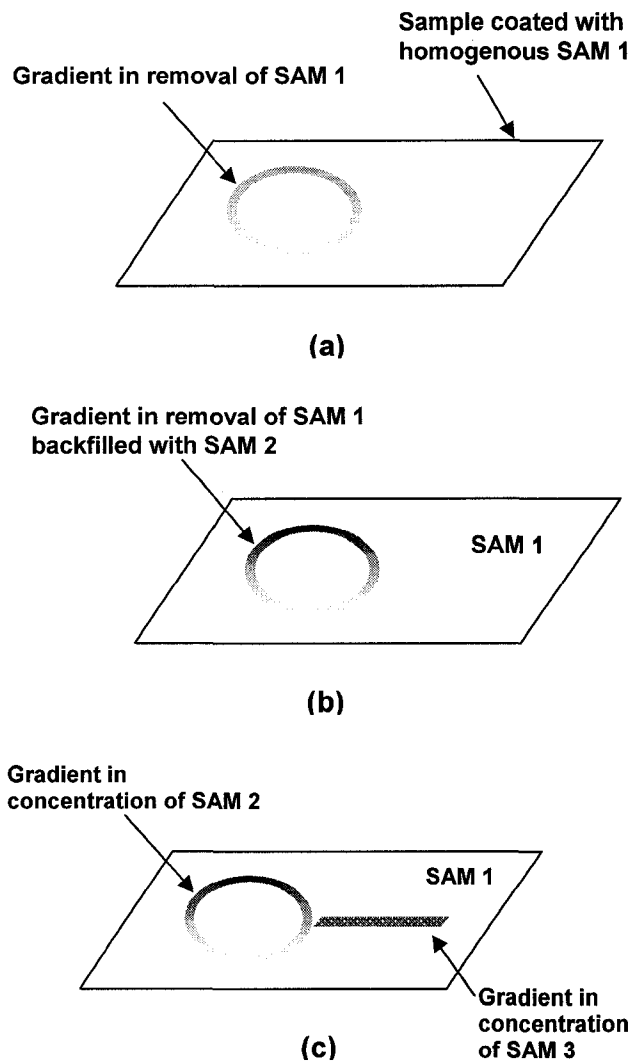


Fig. 3-1: Shows single, double and triple component SAM gradients. (a) Shows a single component gradient formed by gradient in removal of SAM 1 (b) shows a two component concentration gradient created by filling the bare regions of the substrate, in the single component gradient with SAM 2. (c) Shows a three component gradient fabricated by creating a spatial gradient in population of SAM's 1, 2 and 3 in different directions.

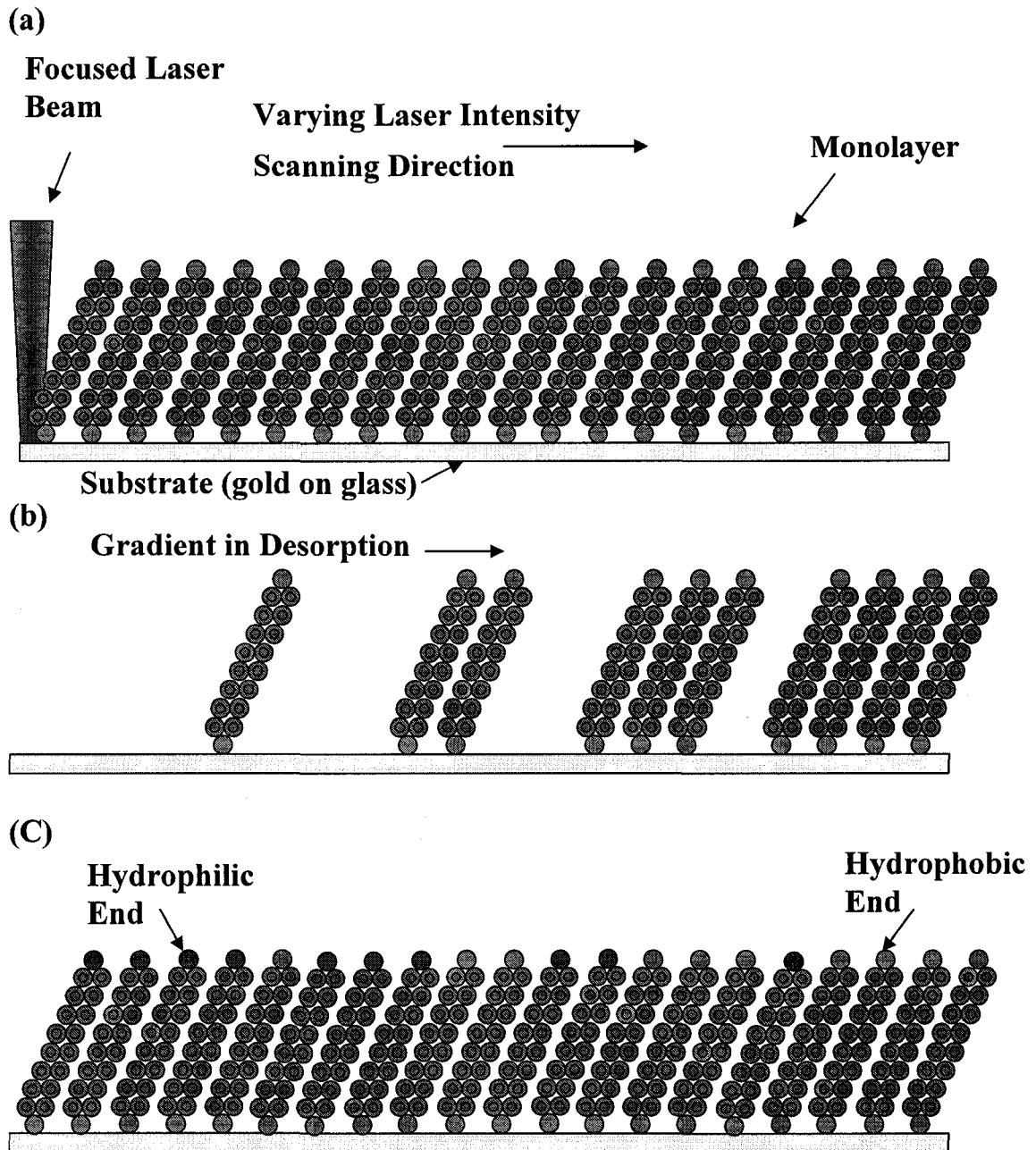


Fig. 3-2: Illustrates the three steps involved in patterning of surface energy gradients using DLP. (a) Focus laser beam onto a homogenous SAM (HDT) on the substrate, (b) Vary the laser intensity continuously i.e. the laser power along the scan direction in the given case, to create a single component gradient, (c) Backfill the bare and partially bare regions with a different alkanethiol to create a two component gradient. Repeat steps (b) and (c) to create three or more component gradients.

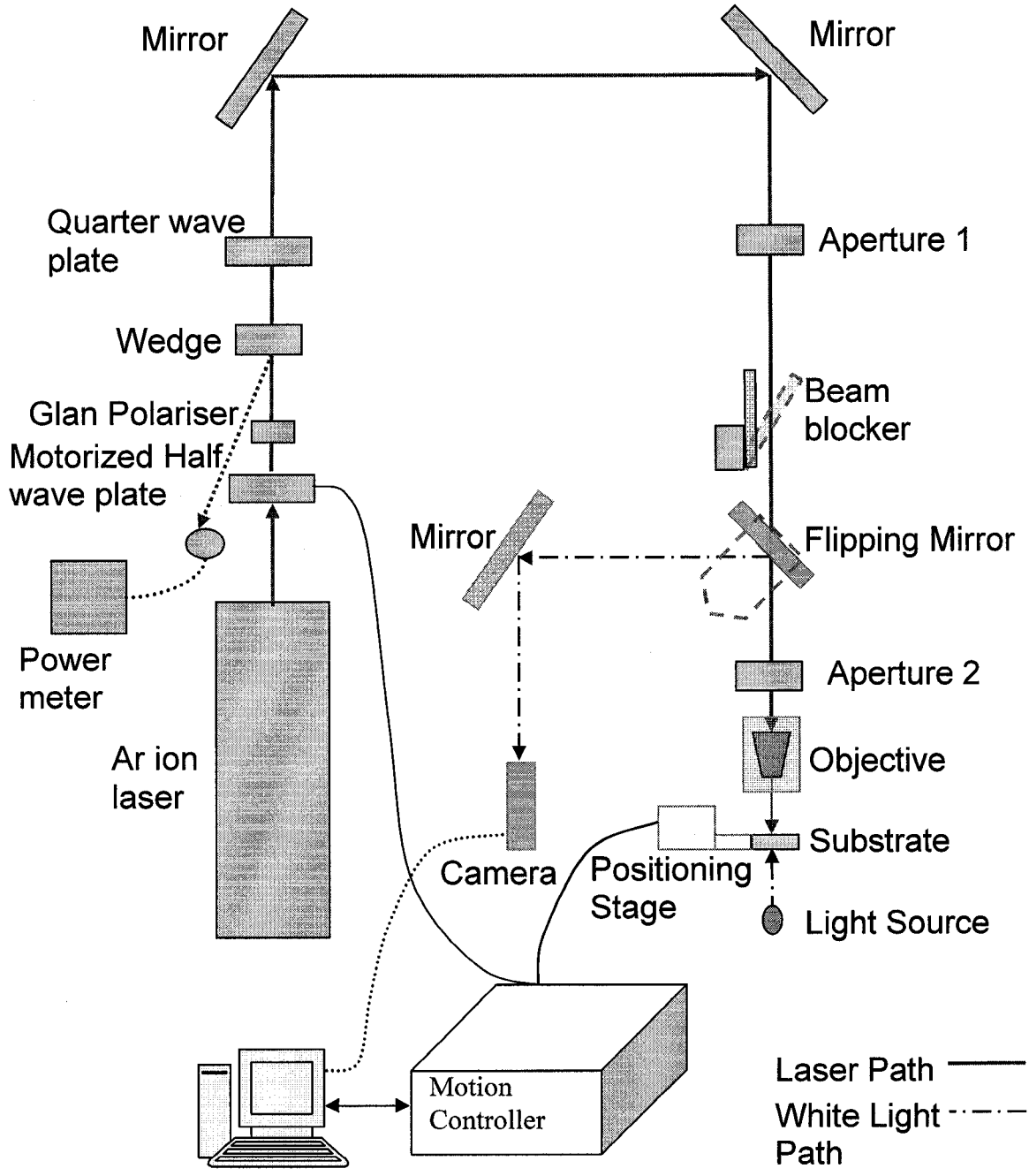


Fig. 3-3: Shows the schematic of the experimental setup used. The half wave plate was mounted on a rotation stage and controlled in tandem with the translational stages to produce gradients of different lengths and shapes. Note that the white light source was used to form an image of the sample (semitransparent) in the CCD for determining the focal point of the objective.

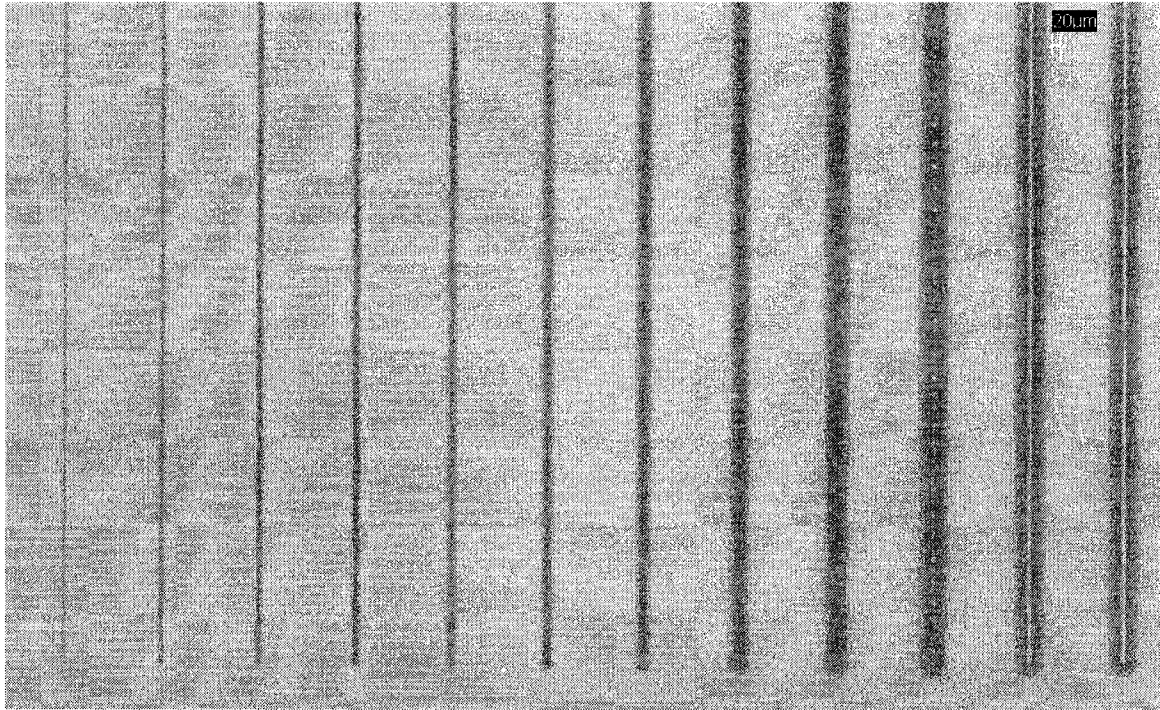


Fig. 3-4: Shows lines patterned at decreasing powers from the right to left. The rightmost patterned with 100 mW, then subsequent lines to the left were patterned at decrements of 10 mW until the 7th one (40mW). Thereafter lines to the left are patterned in decrements of 5 mW, with the last one (leftmost) at 15 mW. Note - white central core in the 3 rightmost lines signify damage of gold.

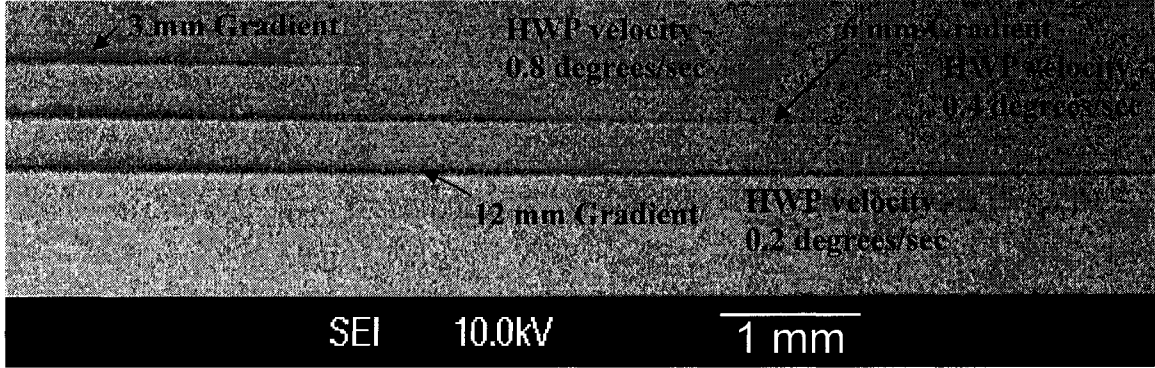


Fig. 3-5: Shows SEM image of the different length gradient lines patterned. The difference in steepness was achieved by varying the laser power along the scan. The lines fading into the background signify a gradient in MHA composition along the length.

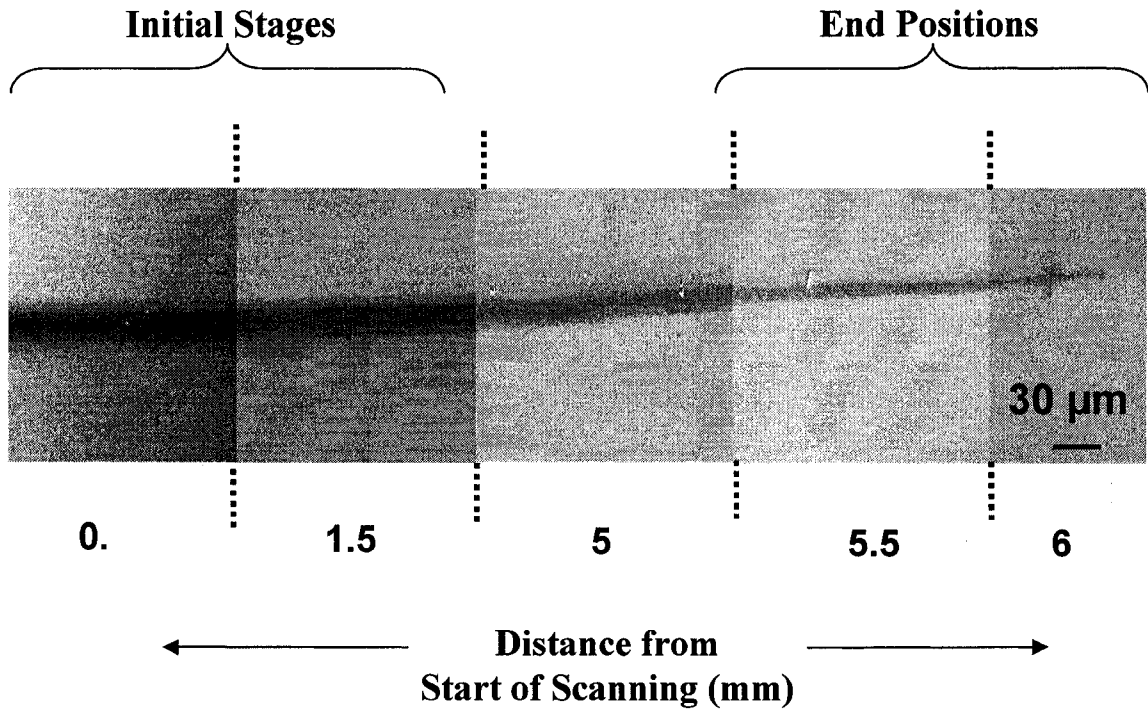


Fig. 3-6: Shows juxtaped SEM images of the 6mm gradient taken at various positions along the length. It can be seen that at the initial stages of scanning (frame 1) the lines have a central dark region, flanked by two less dark regions in a light background – representative of full MHA coverage at the centre, lesser at the edges and nil in the background. Further along the scan as the laser power is reduced and when it is below the threshold for full desorption, it can be seen that there is no full desorption (see frame 3). The amount of partial desorption decreases from thereon before it finally fades into the background in frame 5.

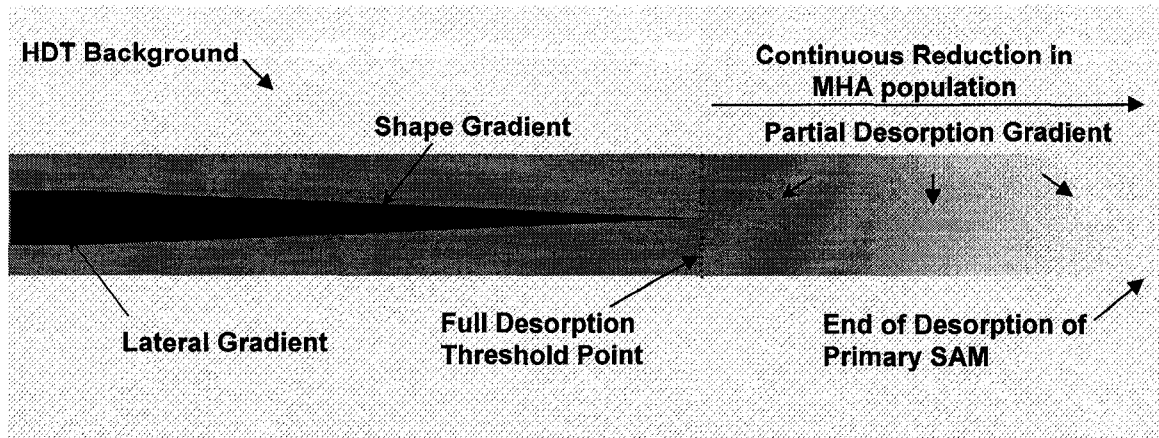


Fig. 3-7: The schematic illustrates the different gradients created in the patterned lines. The position of the dotted line is where the threshold for full desorption is reached. Until this point two types of gradients are created: (1) a longitudinal, millimeter scale, shape gradient due to the narrowing full desorption regime, (2) a lateral micrometer scale sharp energy gradient, from the center line till the HDT background. After the full desorption threshold, only partial desorption occurs and from hereon, until patterning ceases, the amount of partial desorption consistently reduces to create a partial desorption gradient.

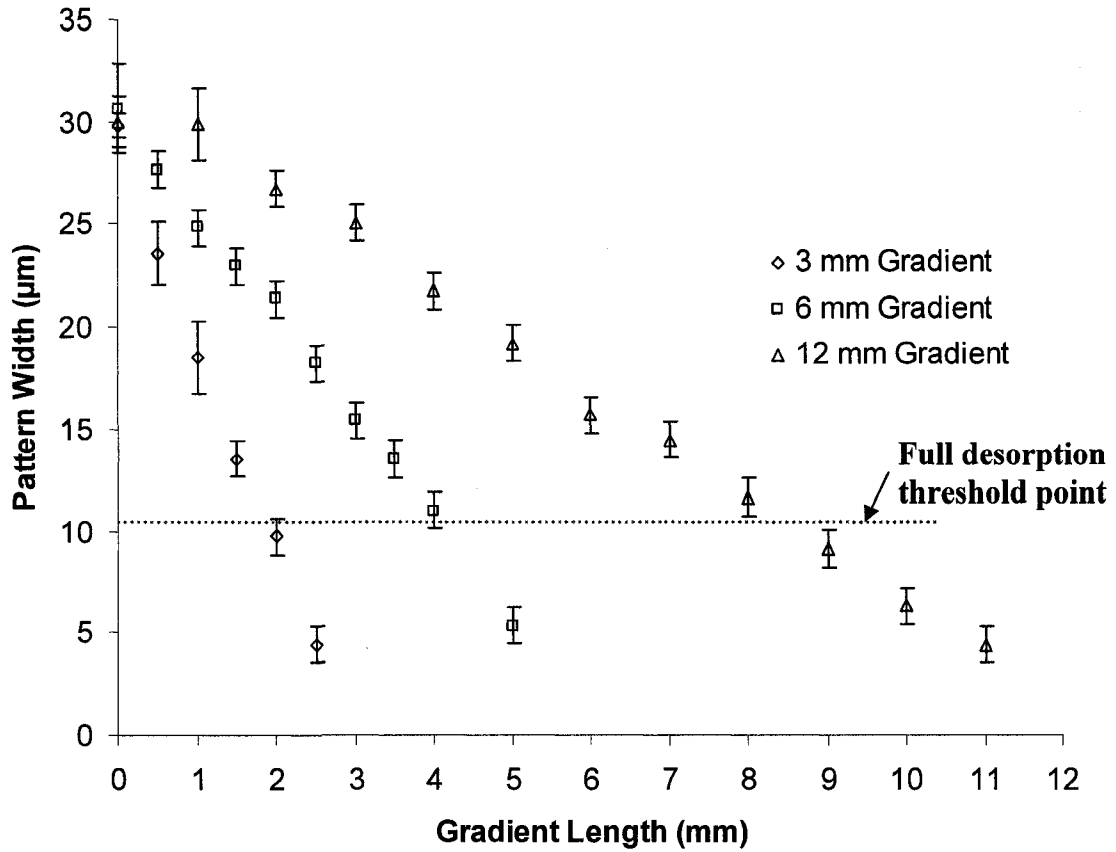


Fig. 3-8: Shows the pattern width variation for the 3, 6 and 12 mm gradient lines along their length. The pattern width was measured from the SEM images taken along the gradient line. The pattern of variation is found to be approximately linear and similar for all the gradient lines produced. Also, the rate of variation is observed to be different for different length gradients. Further from the SEM images the approximate point where the full desorption threshold is reached is indicated by a dotted line in the graph. At this point, all the gradient lines are found to have an approximate width of 10µm. Also, it can be noted that this point is reached at different lengths for the 3, 6 and 12 mm gradient lines. This signifies the difference in steepness of the gradient lines. Note that the pattern width values reported correspond to average of three values measured and the error bars correspond to $\pm 2SD$.

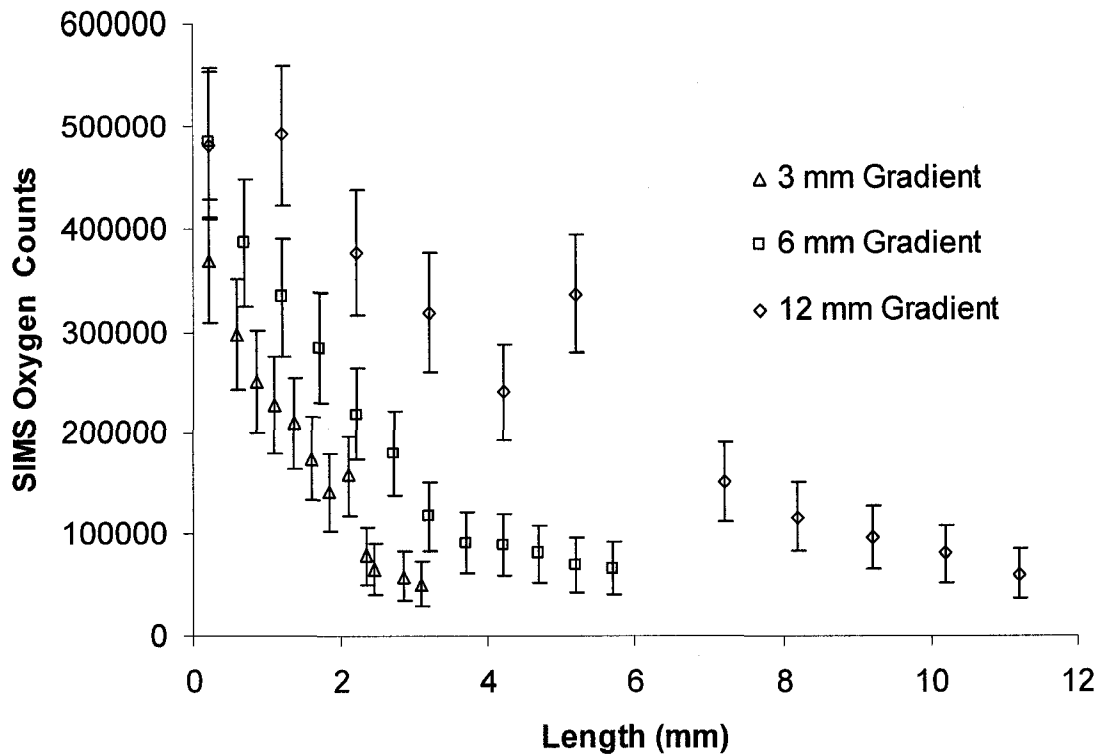


Fig. 3-9: Shows the SIMS oxygen count variation for the three gradient lines produced. The difference in rate of variation in oxygen counts for the gradient lines signifies the difference in the steepness of the MHA concentration/surface energy. Note the error bars correspond to 95% confidence level of the total counts for oxygen (given by Ion Spec. software). Note that the SIMS analysis area was consistent for all the locations and was larger than the total line width.

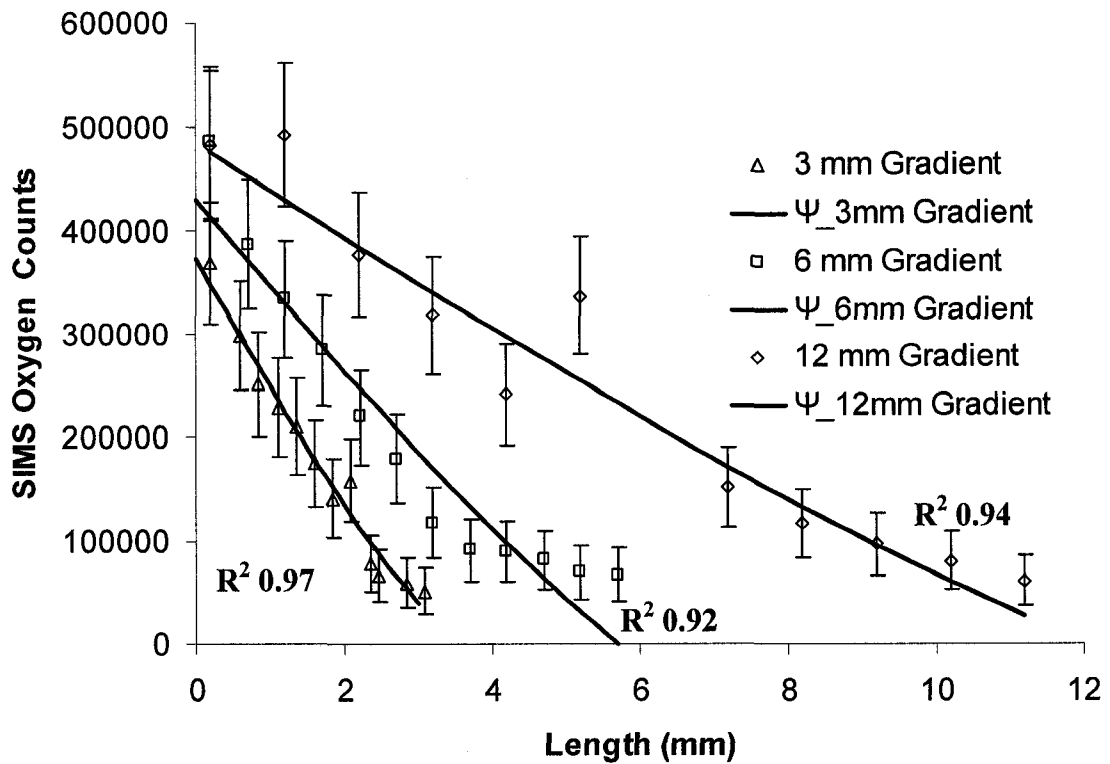


Fig. 3-10: Shows the simplified parametric model fitted to the SIMS experimental data obtained for the gradient lines. It can be seen that the fitted trends closely follow the oxygen count variation along the gradient lines. Note that the error bars correspond to 95% confidence level of the total counts for oxygen (given by Ion Spec. software).

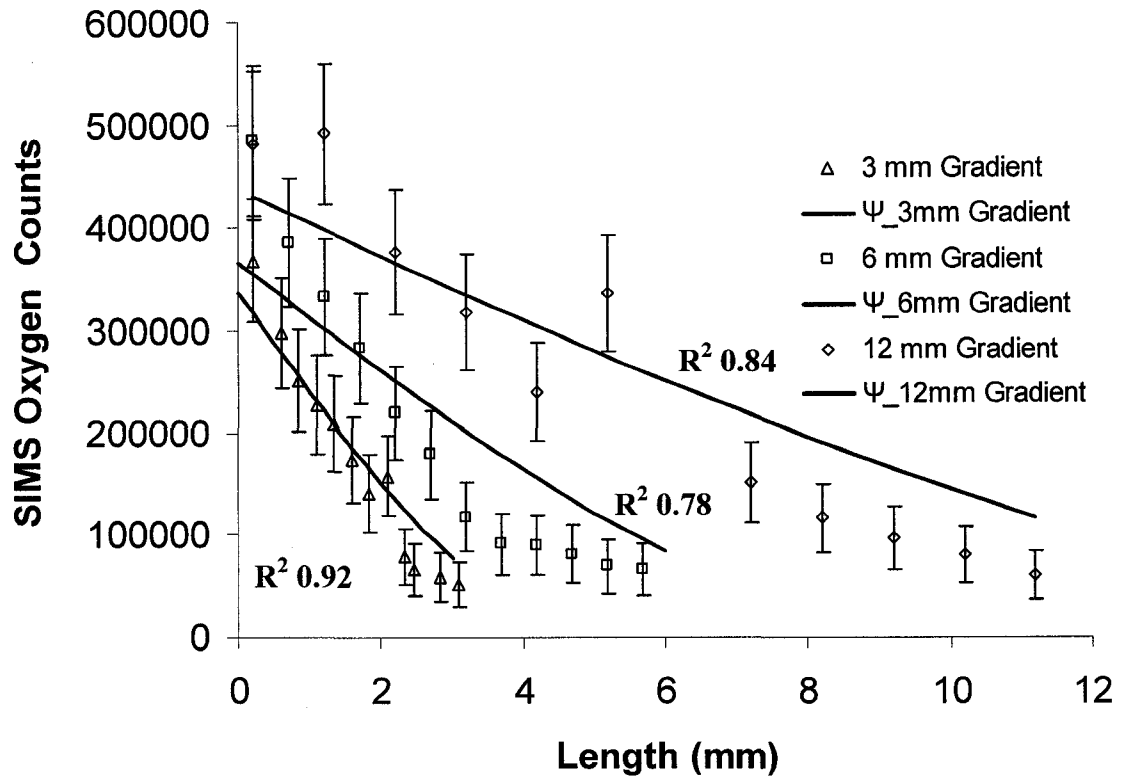
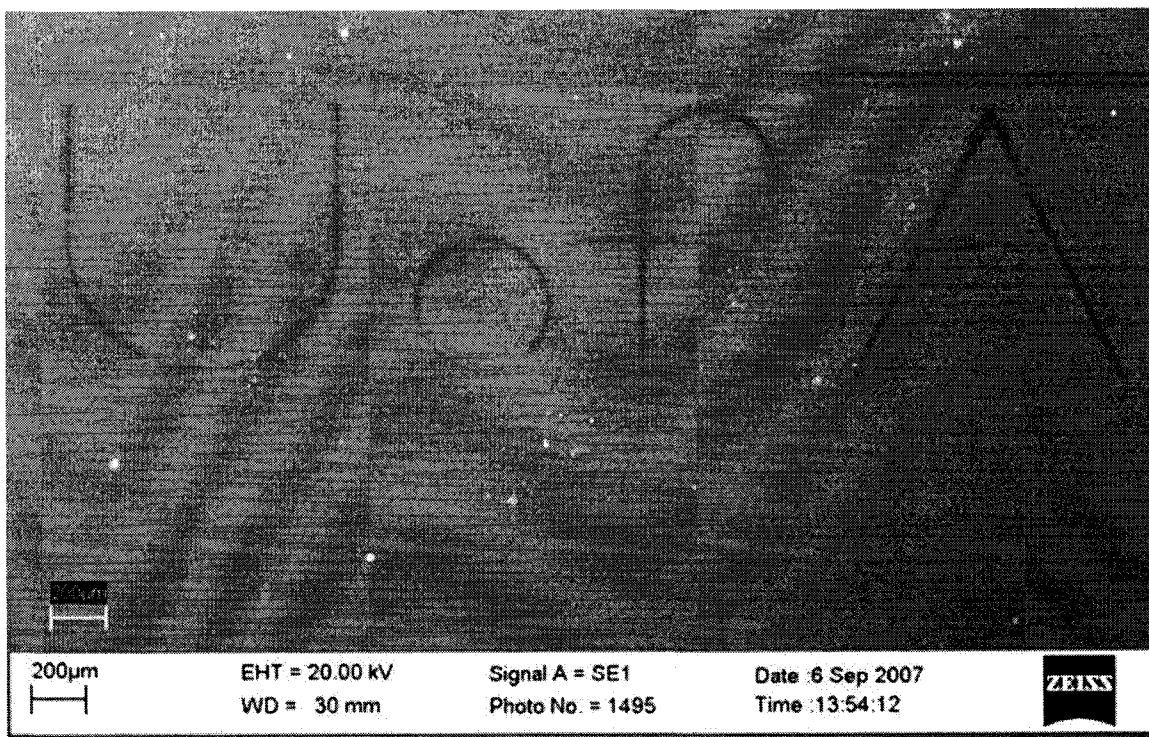
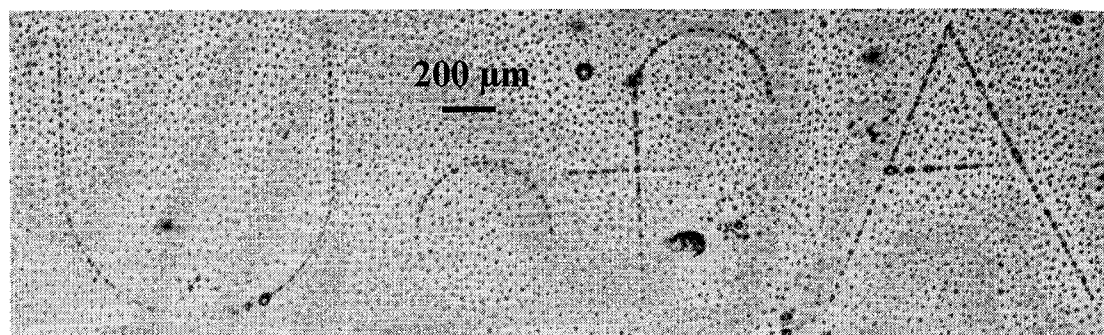


Fig. 3-11: Shows the trend of the theoretical model fitted to the SIMS experimental data obtained for the gradient lines. It can be seen that the fitted trends follow the oxygen count variation along the gradient lines. Also, the difference in the rate of oxygen count/MHA variation for the different lengths of the gradient line is captured. Note that the error bars correspond to 95% confidence level of the total counts for oxygen (given by Ion Spec. software).



(a)



(b)

Fig. 3-12: (a) Shows the SEM image of the “UofA” gradient pattern created. It can be seen that all the letters of the created pattern fade from top to bottom and left to right (in the dashed of characters ‘f’ and ‘A’), signifying a MHA gradient in the specified directions (note that the background is HDT). (b) Shows the corresponding condensation image of the pattern. Note that the small drops formed on the HDT monolayer in the background is due to over exposure to condensation. Also the erratic big drops in the condensation image and white regions in the SEM image correspond to some particles adhered to the surface.

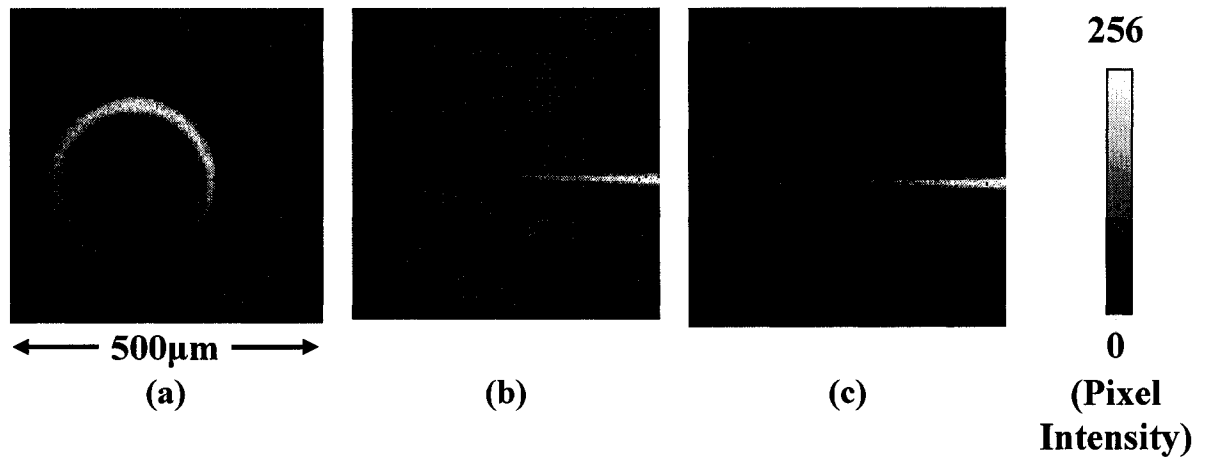


Fig. 3-13: Shows the SIMS secondary ion images for (a) oxygen, (b) bromine-79 and (c) bromine-81 for the three species gradient produced. Note that all the mappings were simultaneously done over a 500x500µm area and the provided pixel intensity scale bar is applicable to all the images. (a) shows the patterned circle as regions of higher oxygen concentration (lighter areas) compared to the HDT background (darker areas) due to the backfilled MHA. Also it can be seen that there is gradient in oxygen concentration in the circle (top to bottom) signifying a chemical gradient i.e. of MHA in the specified direction. (b) and (c) show the patterned gradient as regions of higher concentration of bromine (lighter areas) in a HDT background (darker regions), due to the backfilled BUD. A gradient in concentration of bromine along the lines can also be noted. Further a weak signal for bromine is also seen along the circle perhaps indicating BUD deposited at sites of deficient MHA packing.

3.5 References

- (1) Dekker, L. V.; Segal, A. W. *Science* **2000**, 287, 982-985.
- (2) Gunawan, R. C.; Silvestre, J.; Gaskins, H. R.; Kenis, P. J. A.; Leckband, D. E. *Langmuir* **2006**, 22, 4250-4258.
- (3) Kumar, G.; Ho, C.; Co, C. In *In Geometric control of directional cell migration*; 05AIChE: 2005 AIChE Annual Meeting and Fall Showcase; NY, United States: Cincinnati, OH, United States, 2005; p 4268.
- (4) Song, H. J.; Poo, M. M. *Curr. Biol.* **1999**, 9, 355-363.
- (5) Ruardy, T. G.; Schakenraad, J. M.; van der Mei, H.C.; Busscher, H. J. *Surface Science Report* **1997**, 29, 1-30.
- (6) Chaudhury, M. K.; Whitesides, G. M. *Science* **1992**, 256, 1539-1541.
- (7) Zhang, J.; Han, Y. *Langmuir* **2007**, 23, 6136-6141.
- (8) Daniel, S.; Chaudhury, M.; Chen, J. *Science* **2001**, 291, 633-636.
- (9) Ito Y; Heydari M.; Hashimoto A.; Konno T.; Hirasawa A.; Hori S.; Kurita K.; Nakajima A. *Langmuir* **2007**, 23, 1845-1850.
- (10) Elwing, H.; Askendal, A.; Lundstrom, I. *J. Biomed. Mater. Res.* **1987**, 21, 1023-1028.
- (11) Golander, C. G.; Caldwell, K.; Lin, Y. S.; *Colloid Surf.* **1989**, 42, 165-172.
- (12) Liedberg, B.; Tengvall, P. *Langmuir* **1995**, 11, 3821-3827.
- (13) Morgenthaler, S.; Lee, S.; Zurcher, S.; Spencer, N. D. *Langmuir* **2003**, 19, 10459-10462.
- (14) Plummer, S. T.; Wang, Q.; Bohn, P. W.; Stockton, R.; Schwartz, M. A. *Langmuir* **2003**, 19, 7528-7536.
- (15) Efimenko, K.; Genzer, J. *Adv Mater* **2001**, 13, 1560-1563.

- (16) Song, F.; Cai, Y.; Newby, B. Z. *Appl. Surf. Sci.* **2006**, *253*, 2393-2398.
- (17) Kraus, T.; Stutz, R.; Balmer, T. E.; Schmid, H.; Malaquin, L.; Spencer, N. D.; Wolf, H. *Langmuir* **2005**, *21*, 7796-7804.
- (18) Blondiaux, N.; Zurcher, S.; Liley, M.; Spencer, N. D. *Langmuir* **2007**, *23*, 3489-3494.
- (19) Roberson, S. V.; Fahey, A. J.; Sehgal, A.; Karim, A. *App. Surface Sci.* **2002**, *200*, 150-164.
- (20) Meyyappan, S; Shadnam, M. R.; Amirfazli, A. (submitted work) *Langmuir*
- (21) Fuierer, R. R.; Carroll, R. L.; Feldheim, D. L.; Gorman, C. B. *Adv Mater* **2002**, *14*, 154-157.
- (22) Rhinow, D.; Hampp, N. A. *Adv Mater* **2007**, *19*, 1967-1972.
- (23) Shadnam, M. R.; Kirkwood, S. E.; Fedosejevs, R.; Amirfazli, A. *Langmuir* **2004**, *20*, 2667-2676.
- (24) Shadnam, M. R.; Kirkwood, S. E.; Fedosejevs, R.; Amirfazli, A. *J. Phys. Chem. B* **2005**, *109*, 11996-12002.
- (25) Hartmann, N.; Balgar, T.; Bautista, R.; Franzka, S. *Surface Sci.* **2006**, *600*, 4034-4038
- (26) Variable attenuator for lasers.
[http://www.newport.com/file_store/Optics and Mechanics/AppsNote26.pdf](http://www.newport.com/file_store/Optics_and_Mechanics/AppsNote26.pdf)
(November 2007)
- (27) Lopez, G.; Biebuyck, H.; Whitesides, G. *Langmuir* **1993**, *9*, 1513-1516.
- (28) Burgos, P.; Geoghegan, M.; Leggett, G. J. Preparation of surface energy gradients on the submicron scale by photooxidation. In *Proceedings of 234th American Chemical Society National Meeting & Exposition Proceedings*, Boston, U.S.A, August 19-23 2007; American Chemical Society: Washington DC, U.S.A, 2007.

Chapter 4 – Summary, Conclusions and Future Work

4.1 Summary and Conclusions

Direct Laser Patterning (DLP) of Self Assembled Monolayers (SAM) has been successfully extended to produce surface energy gradients. In the proposed methodologies, the incident laser intensity has been continually varied to create surface energy gradients. The laser intensity has been varied by continuous manipulation of either the laser beam radius on the sample, or the laser power. The first approach i.e. the continuous manipulation of laser beam radius was achieved by means of a simple method called ‘out of focus’ method in which the sample (hexadecanethiol (HDT) SAM on a gold film supported by a glass substrate) was kept inclined to the focal plane of the scanning laser beam. The laser power was continuously manipulated in the second approach i.e. the ‘laser power method’ by means of computer controlled rotation of a Half Wave Plate (HWP), placed before a Glan polarizer. Gradient line features using HDT and mercaptohexadecanoic (MHA) as first and second SAM were produced by both approaches. Also, in the second approach, the speed of HWP rotation was varied to fabricate gradients 3, 6 and 12mm long. Further, energy gradients (in required directions) along different shapes such as ‘UofA’ were produced, by appropriately controlling the laser power. Using the second approach, for the first time, a three component SAM concentration gradient has been demonstrated (along arbitrary shapes) with HDT, MHA and bromoundecanethiol (BUD) SAMs. Both the methodologies have common advantages of being fast, non-contact and flexible (in terms of varying the parameters of the gradients). Also there was no need of expensive infrastructure like lithography or Scanning tunnel Microscopy (STM). Also, the mechanism of the ‘laser power’ method is

found to incorporate three kinds of gradients, namely: (1) a micrometer scale sharp lateral energy gradient across the patterns during the initial stages of scanning; (2) a millimeter scale longitudinal shape gradient and (3) a millimeter scale longitudinal partial desorption gradient in the patterned lines. So, depending upon the application the suitable laser power range can be selected to create any or all of the gradients.

The gradient line features produced using the two methods were characterized using secondary ion mass spectroscopy (SIMS). SIMS was used to capture trend in variation of MHA concentration along the gradient lines. The trend was observed to be non-linear for the gradient lines produced using the 'out of focus' method whereas approximately linear for the 'laser power method'. The observed trends in experimental data (for both the methods) were also reconfirmed by the corresponding theoretical trend functions derived. The theoretical trend in variation of the HDT desorption was derived by considering the functional dependence of the equations of thermo-kinetic model. The variation in laser beam radius (for the out of focus method) and the laser power variation (for the laser power method) was then incorporated in the functional dependence of HDT desorption in order to obtain the corresponding theoretical trends for each case. The two component gradients created along 'UofA' shape was imaged using Secondary Electron Microscopy. The fading of the characters in different directions signifies a MHA concentration gradient in that direction. The spatial multi-component gradient fabricated using HDT, MHA and BUD was characterized using SIMS imaging. The signal for MHA and BUD, used as secondary and trinary SAMs weakened along the different patterns created (crossing each other) to result in arbitrary shape multi-component gradient. Finally, to

sum up, two novel methodologies (based on DLP of SAMs) have been developed to fabricate micrometer scaled surface energy gradients. The ‘out of focus’ method is simple and can be used to create surface energy gradients along lines. However gradients of different shapes are not easily possible. The ‘laser power’ method on the other hand is quite flexible in terms of producing gradients of different shapes and multi-component gradients but requires computer control. So the developed methods are different from each other and depending on the need, any one can be selected.

4.2 Future Work

There are many directions in which this project work can be continued. One of the immediate possibilities of extension would be to create gradients on other systems such as alkylsilanes on silicon (by modification of the laser patterning demonstrated in [1]). At the application level, the single component gradients produced (using the methodologies) can be etched to see what kind of channel is created. The channel fabricated i.e. possibly a channel with a physical micro-gradient in depth may be useful in applications fields such as Microelectromechanical Systems (MEMS) and microfluidics. On the other hand, the two component wettability gradients produced, can be optimized with regards to the steepness/rate of surface property variation so that one can try and move liquid drops using the gradient features. Such a gradient with optimized steepness can prove useful in micro-fluidic/MEMS applications, where controlled volume of liquids need to be conveyed. In a similar fashion, studies can be carried out to optimize the steepness for various other biological applications such as directed cell migration etc.

Since DLP and application of DLP to produce surface energy gradients in relatively new, there are many areas of improvement and unanswered questions with the application DLP to produce surface energy gradients that can also define scope of future work. For example: due to the profile of the laser beam a lateral gradient is created in the features produced, this can be possibly be avoided by patterning with a laser beam having a top-hat profile. Also due to the mechanism of the 'laser power' method it has been observed three different kinds of gradients i.e. a sharp lateral gradient, a millimeter scale shape gradient and a millimeter scale surface energy gradients are created in the patterned features. So individual patterning of each of the above said gradients can be tried by selecting the appropriate laser intensity range based on thresholds limits (established for the given system). Another area of possible improvement would be to develop a comprehensive theoretical model to represent the dynamic situation of patterning gradients. This kind of theoretical model would help in obtaining the absolute accurate values of desorption (along the gradient) and hence would better represent the experimental data, as compared to the theoretical trend function derived from the quasi-static equations. The three component gradient demonstrated using one of the methodologies developed is another area where there are some unanswered questions. For example: the cause for the weak bromine signal along the circle needs to be further investigated, in the context of possible reasons of why this is happening. Alternatively, the experiments can be repeated using a SAMs like ferrocenyl undecanethiolate and dodecanethiolate as in ref 2 so as to avoid replacement of the primary SAM and hence create non-defective three component gradients.

4.3 Reference

- (1) Hartmann, N.; Balgar, T.; Bautista, R.; Franzka, S. *Surface Sci.* **2006**, 600, 4034-4038
- (2) Fuierer, R. R.; Carroll, R. L.; Feldheim, D. L.; Gorman, C. B. *Adv Mater* **2002**, 14, 154-157.

Appendix 1 – Details of Experimental Procedures

A1-1 Cleaning of Glassware

The glassware used for the experiments were initially cleaned using soap solution, to remove any visible dirt. Following this the glassware were thoroughly rinsed with water and kept under chromosulfuric acid (a mixture of concentrated sulfuric acid and chromium oxide) for 12 hours. This was to remove any organic contaminants present. The glassware were then removed from the chromosulfuric acid and thoroughly rinsed with deionized water, followed by 100% ethanol and let to dry under a heat lamp.

A1-2 Calibration of Laser Power

The incident laser power was measured using a Gentec power meter, placed ~15cm past the focusing objective/lens (so as not to damage the sensor). Additionally, a semiconductor power meter (Thorlabs) measured sum of both front and back reflections from a wedge (see Fig. A1-1). The laser power was set at fixed level and after ~10 min when the fluctuations in the laser power have gone down, the power readings from both the meters was recorded. This process was repeated for a series of laser power within the entire range (maximum to zero) to create the calibration table (see Table A1-1). After calibration, the online power measured was used as reference to calculate the incident laser power. Note that the calibration needs to be repeated, each time the alignment of the Thorlabs power head is changed.

A1-3 Focusing of the laser beam

The focus of the objective lenses both 4X and 10X (used in the experiments) were initially determined by forming an image of a scratch made on the sample, in a CCD camera as shown in Fig. A1-2. The white light source used, was firmly held behind the semi-transparent sample using a post. The objective mounted on the translational stage, was moved back and forth to form a sharp image of the scratch. The focus hence obtained (using white light) was corrected by a factor to account for wavelength difference between the laser beam and the white light used.

The required correction factor offset (for determining the focal point of the objective for the laser) and the focal beam spot radius were determined experimentally. The beam radius at the white light focus of the objective was determined by means of a knife edge experiment¹. Following this, the objective was offset (by a known value from the white light focal point) and knife edge experiment carried out to determine the radius at that beam plane. The beam radius obtained was found to be smaller than the radius obtained at the white light focal point. So, the offset (positive in this case) was in the right direction. As along the beam propagation direction, the laser beam radius is expected to decrease towards and reach the minimum at the focal point and then increase again. According to theory, this trend is hyperbolic². So, a series of knife edge experiments were carried out (to determine the beam radii) at subsequent beam planes along the propagation direction and a hyperbolic curve was fitted to the data. The co-efficient of this hyperbolic fit provided the difference between the laser beam and white light focal plane of the objective (required correction offset for the objective) and also the focal

beam spot radius. As an example the procedure followed for characterizing the 4X Olympus objective is detailed below.

The white light focal point of the 4X objective (obtained by focusing at the scratch made on the sample) was found to be at 44.568 mm position of the translational stage (on which the objective is mounted). Note that this is a relative position and the mentioned absolute value serves only as a reference to calculate the offset. At this point, a knife edge held in between the objective lens and the power meter was traversed in steps along the X-axis, and the laser power measured. The variation in laser power obtained is shown in Fig. A1-4. This curve was then differentiated to obtain the laser beam intensity profile (see Fig. A1-4). A Gaussian curve (corresponding to TEM_{0,0} mode of laser), also shown in Fig. A1-4 was fitted to this data, using Matlab (curve fitting toolbox) to obtain the beam radius. The objective was then progressively moved towards the sample in steps of 100 μm and at each step the knife edge experiment was repeated. It was observed that the beam radius consistently reduced until 45.268mm whereas after that at 45.368mm started increasing. Hence the objective's focus for the laser beam was somewhere between 45.268 and 45.368 mm. In order to obtain the divergence of the beam after the focal plane and be able to fit a curve, knife edge measurements were carried out in 3 planes (200μm apart) after 45.368 mm position. The radii hence measured along the beam propagation, are plotted as a function of the objective's position; see Fig. A1-5. A hyperbolic curve was fitted to the data, as shown in Fig. A1-5. The coefficients of this fit provided the beam radius and the exact focal point of the laser beam as 3.6 μm and 45.310 mm, respectively. So the difference between the white light focal point (44.568)

and the focal point of the laser beam (45.310) gave the correction factor required as +742 μm .

A1-4 Keeping the sample inclined using the tilt stage

The different approaches for fabricating gradient lines i.e. varying the beam spot area for a fixed laser power or varying the laser power for a fixed beam radius have different requirements i.e. the sample needs to be kept inclined or perpendicular to the scanning laser beam, respectively. This is achieved by determining the focus, at two scratches made along the edges of the sample as shown in Fig. A1-3 (front view). Depending upon the values obtained i.e. the initial position of the sample the tilt stage was adjusted so as to make it flat or further inclined, depending on the requirement.

The explained procedure can be understood by following this example. Two scratches 16.15 mm apart were made on a sample. The focus values i.e. the microscopic objective's position based on translational stage readings, at both scratches (left and right –as seen from the monolayer/gold film side of the substrate) were found to be 44.4 and 44.37mm, respectively. This indicated the substrate was out of focus by 0.03 mm in the left with respect to the right side (see Fig. A1-3). Based on the distance between the scratches, the angle of inclination of the sample to the focal plane was calculated to be 0.1064 degrees. So, the sample was inclined by this calculated angle in the opposite direction (using a tilt stage), to make it perpendicular to the scanning laser beam. The same procedure was followed to keep the sample inclined at a required angle. Note that after setting the tilt stage, the focus at the scratches was verified before patterning.

A1-5 Programming of the stages

The translational stages (ILS-100-CC from Newport inc.) in X-Y configuration and the Half Wave Plate (HWP) rotation stage (PR-50-CC from Newport inc.) were all programmed using Labview (National Instruments Inc.). All these stages and additionally the beam blocker (connected the computers serial port) needed to be controlled in tandem to produce continuous variation in laser intensity, as required. So two programs one aimed at producing gradients along lines and the other for gradients along different shapes were written. Both the programs are discussed in detail with regard to the usage and principles of programming.

The program for making gradient lines is 'gradient_make-latest.vi'. This can be found in the following folder: 'c:\Documents and settings\sm39\desktop\labview-vis' in the computer that is assigned for the laser set up. The front panel of the program as the user would see is given in Fig. A1-6. The front panel has number of displays and a button for initiating the patterning. The first step is to initiate patterning by clicking that button and then the user is prompted for inputs, through a dialog box also shown in Fig. A1-6. The user is required to provide various inputs such as: starting power value required for the gradient, length of gradient required, velocity of patterning, distance required between the gradient lines i.e. the distance required to be moved in the y-direction, distance between scratches and distance from edge of the sample to the beginning of the gradient. Based on these inputs, the program controls the various stages and the beam blocker to fabricate the required gradient.

The execution of the program can be understood by following the flowchart shown in Fig. A1-7. First, the HWP is rotated by the required angle so that the required laser power is reached. The angle by which the rotation is calculated by the program calculated based on the preprogrammed laser power equation which is a function of the azimuth of the HWP. Then the time available for patterning is calculated based on the velocity of patterning i.e. the speed of the X-axis stage and the required length of the gradient. The velocity of rotation of HWP is then computed based on the angle of HWP rotation required to reach the desorption threshold (pre-programmed) and the time available for patterning. The velocity of the rotation stage is changed accordingly and then the x-axis stage is moved by the required distance so that the point where the patterning needs to be started is reached. Now the beam blocker is opened and both the x-axis stage and the rotation stage are operated simultaneously so that the laser power is varied along the straight line scan, as required.

The principle of the program used for patterning gradients along different shapes is very similar to the 'gradient maker' program except that the laser intensity was varied along an arbitrary shape. The front panel of this program is shown in Fig. A1-8. The pattern button in the front panel, needs to be pressed for initiating the patterning. Following this the user is prompted to enter the various parameters such as: starting power value, length of the gradient, velocity of patterning and name of the text file which contains the commands for moving the X-Y stages. The text file is prepared based on arbitrary shape required. More on moving the stages in the required shape, preparation of the text file and the path where it needs to be stored can be found in the Newport manual⁴. Given all these inputs

combined with the preprogrammed inputs such as threshold for start of desorption and the laser power equation (as a function of azimuth angle of HWP), the stages were controlled as required to fabricate the gradient in the required shape. Also a program that can be used to pattern binary lines with out varying the laser power was written. This works in a similar fashion as the 'gradient maker' except that the laser power is held constant along the scanned path. This program is 'pattern-latestd.vi' and can be found in the folder as the 'gradient maker'. Note that for moving the stages temporarily i.e. while focusing the website hosted by the controller at the <http://129.128.138.9> and further file transfer was achieved through Filezilla software, using the address <ftp://129.128.138.9>.

A1-6 Measuring pattern width

The widths of the gradient lines fabricated were measured from the SEM images using the Image-J software. First, a straight line was drawn on the scale bar of the SEM image and the length of this line was measured (using Image-J). Similarly, a straight line representative of the total width (covering the partial and full desorption areas as shown in Fig. A1-9) of the patterned gradient line was drawn and the length subsequently measured. The pattern width was then calculated based on the lengths of the two lines and the value of the scale bar. For example, the width of the gradient line in the SEM picture shown in Fig. A1-9 was measured by drawing lines 'A' and 'B' also shown in Fig. A1-9. The length of line 'A' which is representative of the scale was measured to be 1.1 inches and length of line 'B' representative of the line width was measured to be 0.24 inches. So the line width of the gradient line was calculated by taking the ratio of the measured lengths of the line 'B' to 'A' i.e. $(0.24/1.1)$ and then multiplying by the scale

bar value of 100 μm . In the given case, the width of the gradient line was calculated to be 21.8 μm . This process was repeated for a couple of times and the average of the widths obtained was taken as the final value.

Table A1-1: Calibration data for laser power measured during patterning (Thorlabs) versus the total incident laser power measure by Gentec power meter. The Gentec power meter provides output in mV which can be converted to power using the formula given below.

S. No.	Thorlabs Power (mW)	Gentec Power (mV)
1	10.4	10.5
2	10	10.12
3	9	9.13
4	8	8.13
5	7	7.17
6	6	6.1
7	5	5.11
8	4	4.1
9	3	3.14
10	2	2.12
11	1	1.05
12	0	0.02

The incident laser power is calculated from the Gentec reading using the following formula³:

$$P = \frac{(V_{measured} - V_{zero})}{S_{1064nm}} M_{\lambda}$$

Where P is the total power, $V_{measured}$ is voltage measured using the voltmeter attached to Gentec power head, V_{zero} is the voltage measure when the laser beam is not incident or blocked, S_{1064nm} is the calibration sensitivity as provided by Gentec and M_{λ} is the multiplier used to convert the 1064nm power to the power at the desired wavelength.

As an example, for 7mW in thorlabs:

$$\text{The total incident power on sample} = \left(\frac{7.17 - 0.02}{114.16} \right) \times 0.957 = 59.94mW$$

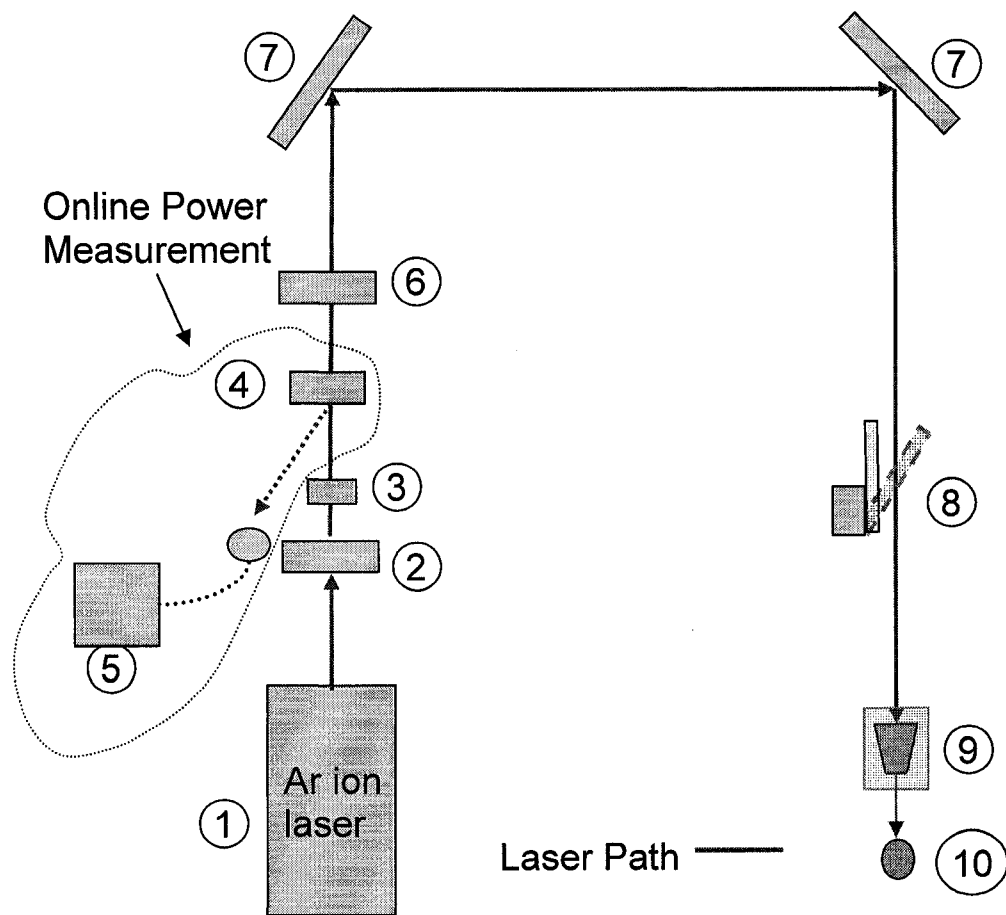


Fig. A1-1: Shows the set up for calibration of laser power. The laser beam (488nm wavelength) from the Ar-ion laser head (1) passes through a half wave plate (2) and Glan polarizer (3) combination, which is used to control the laser power downstream. Then ~4% of the beam is sampled using an optical wedge (4), to aid online power measurement using Thorlabs power meter (5). The beam then passes through a quarter wave plate (6), bounces off the mirrors (7) and finally is steered to the focusing objective lens (9). In between the mirror and the objective there is beam blocker (8) used to temporarily block the beam, if required. The Gentec power meter (10) placed after the objective measures the total incident laser power on sample. The online power measured includes both the front and back reflections from a wedge. This power is calibrated using the Gentec power as a standard and serves as a reference to calculate the total incident laser power.

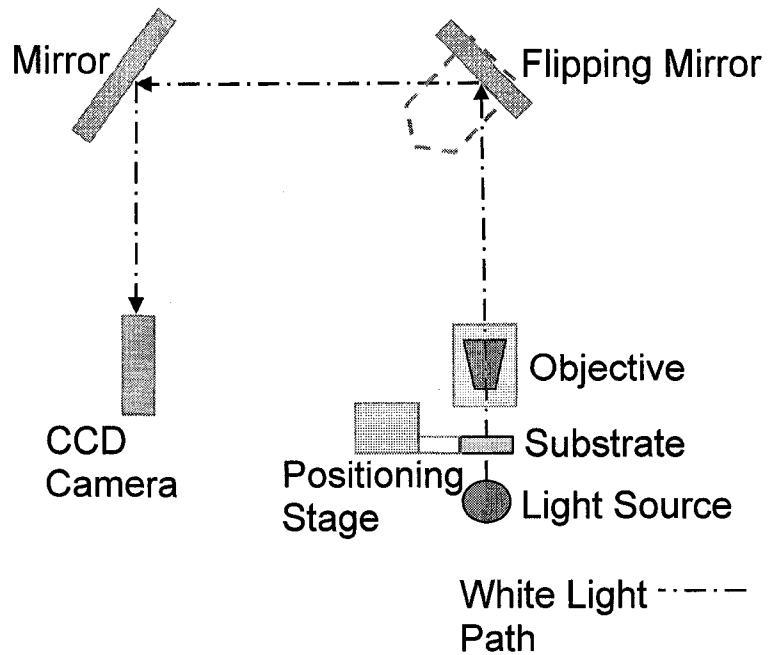


Fig. A1-2: Shows the set up used for determining the focus of the objective using white light. The scratch made on the sample, illuminated from behind the thin gold film coated sample which was semitransparent is used as the subject of focus. The objective is moved back and forth so that a sharp image is formed in the CCD camera.

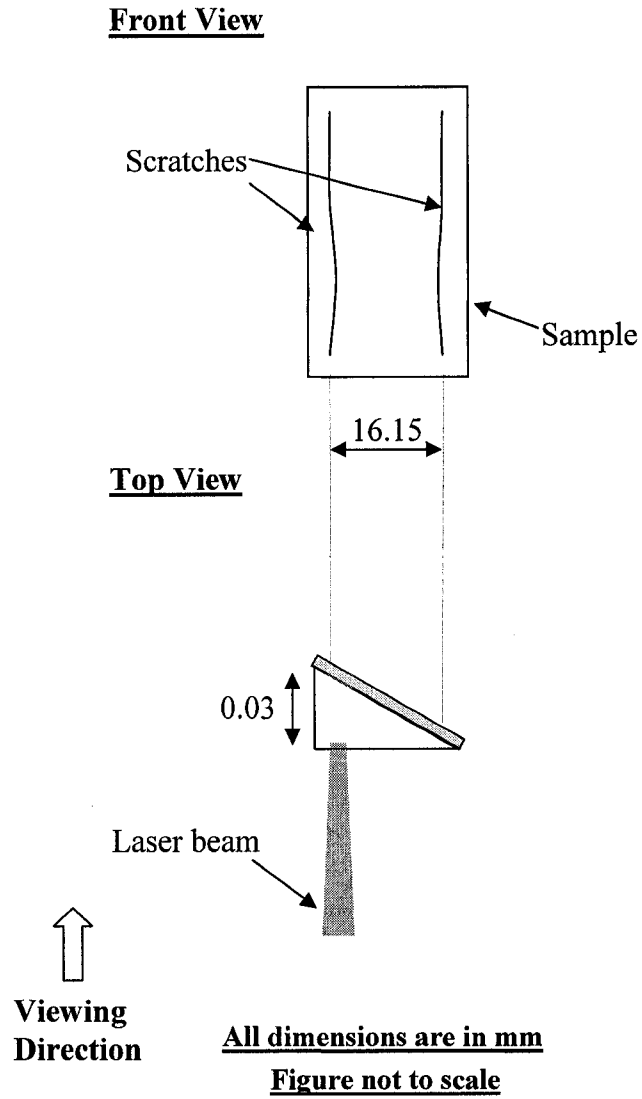


Fig. A1-3: Shows the top and front view when the sample out of focus by 0.03 mm at one end compared to the other. The distance between the scratches is 16.15 mm, so the angle is calculated to be 0.1064 degrees.

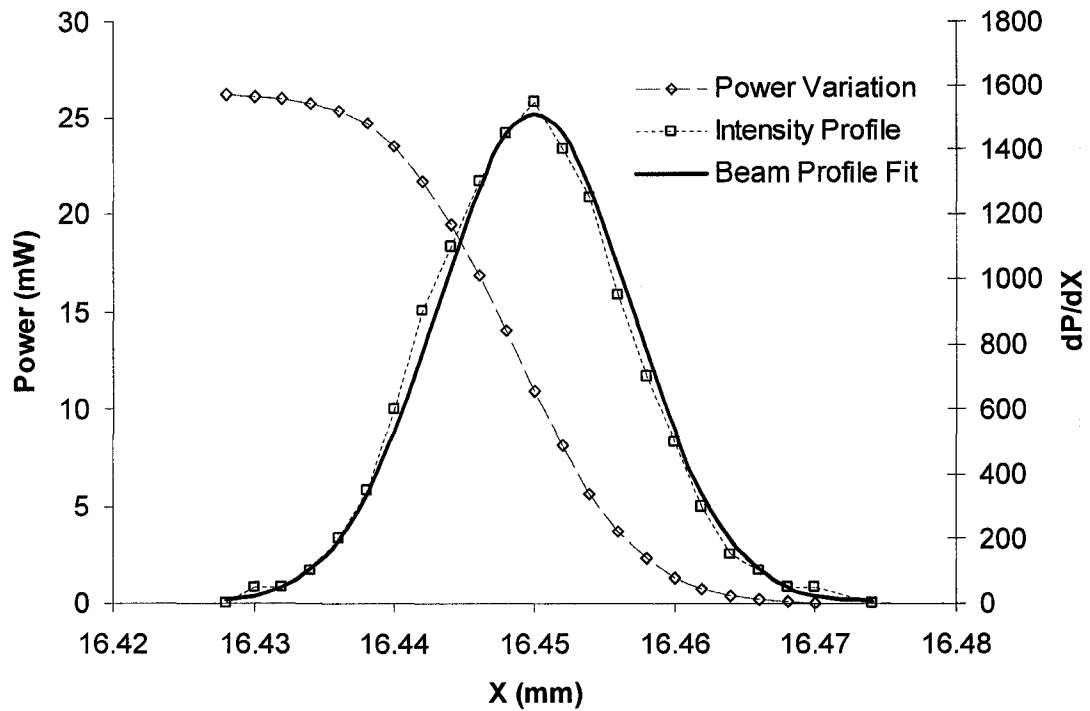


Fig. A1-4: Shows the laser power variation (represented by diamond open symbols) measured as the knife edge is traversed in steps along the X-axis. The data is then differentiated so as to obtain dP/dX . The power differential along the X-axis provides the laser beam intensity profile (represented by square open symbols) in that direction. A Gaussian curve is then fitted (represented by continuous thick line) to the intensity profile using Matlab (curve fitting toolbox) to obtain the laser beam radius.

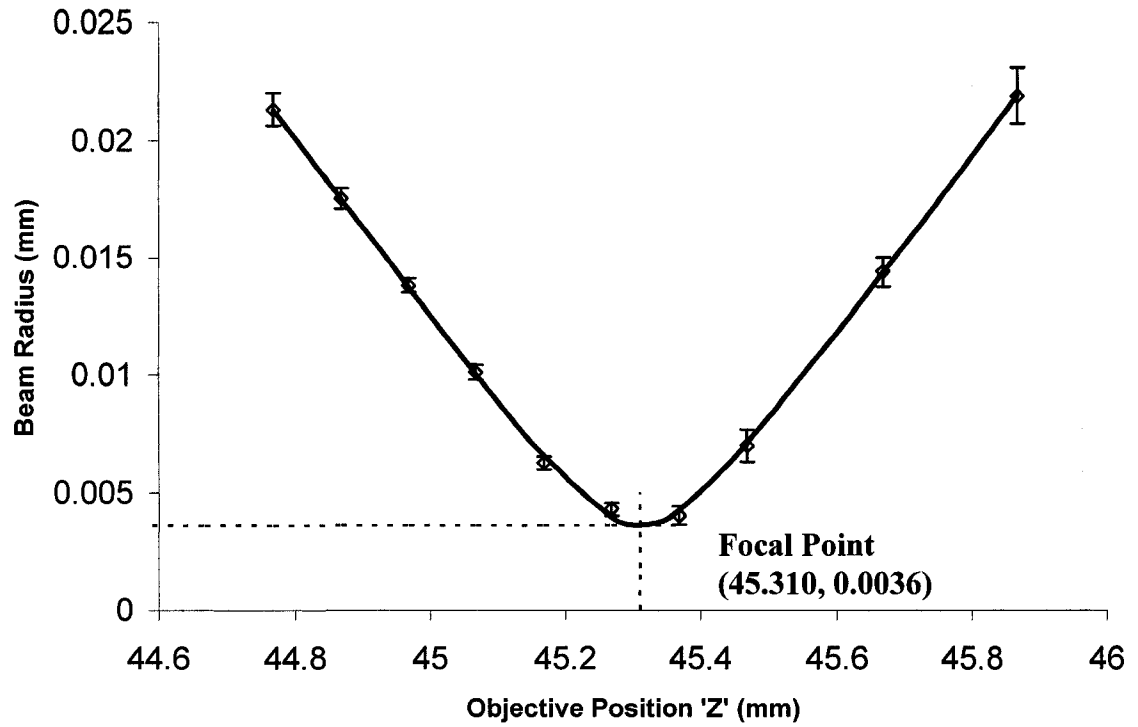


Fig. A1-5: Shows the beam radii along the beam propagation direction. The error bars of the beam radii correspond to 95% confidence limits given by curve fitting toolbox of Matlab. According to the fit, the minimum beam radius decreases to a minimum of 3.6 μm when the objective is at 45.310 mm. This is the focal point of the objective for the laser.

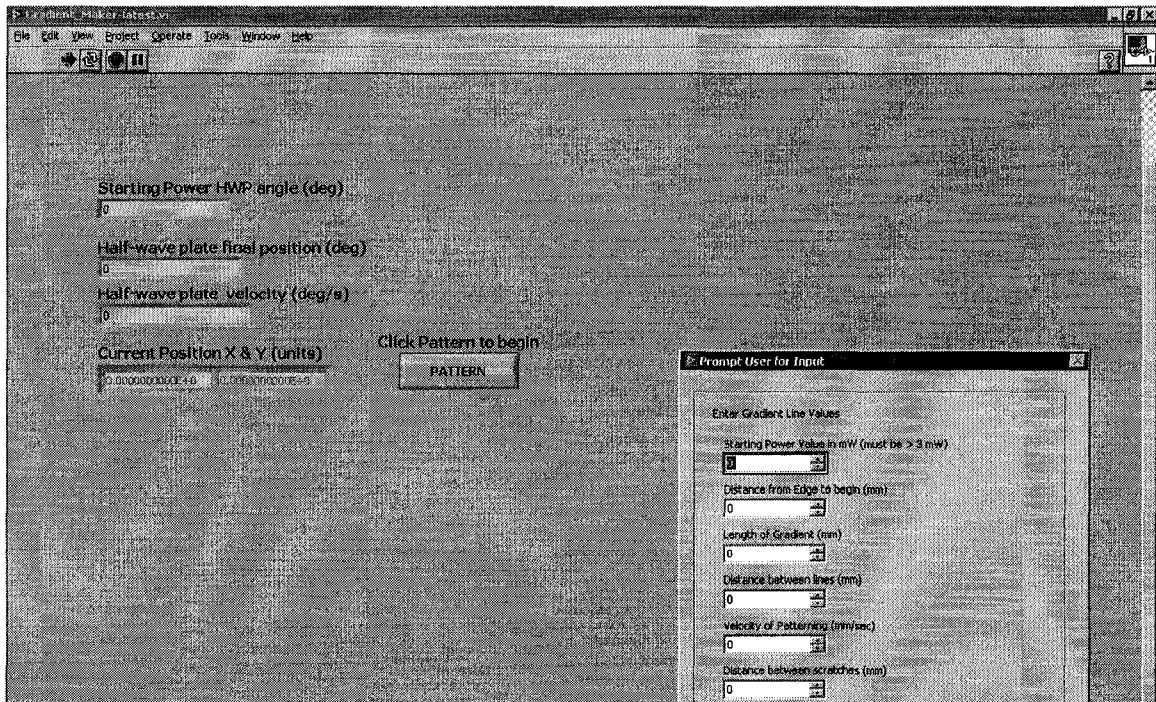


Fig. A1-6: Shows front panel of the gradient maker program. The dialog box seen in the right is shown when the pattern button is initiated. The dialog box prompts the user for various inputs required for fabrication of the gradient lines. The other objects in the front panel are used to display data related to the patterned gradient line.

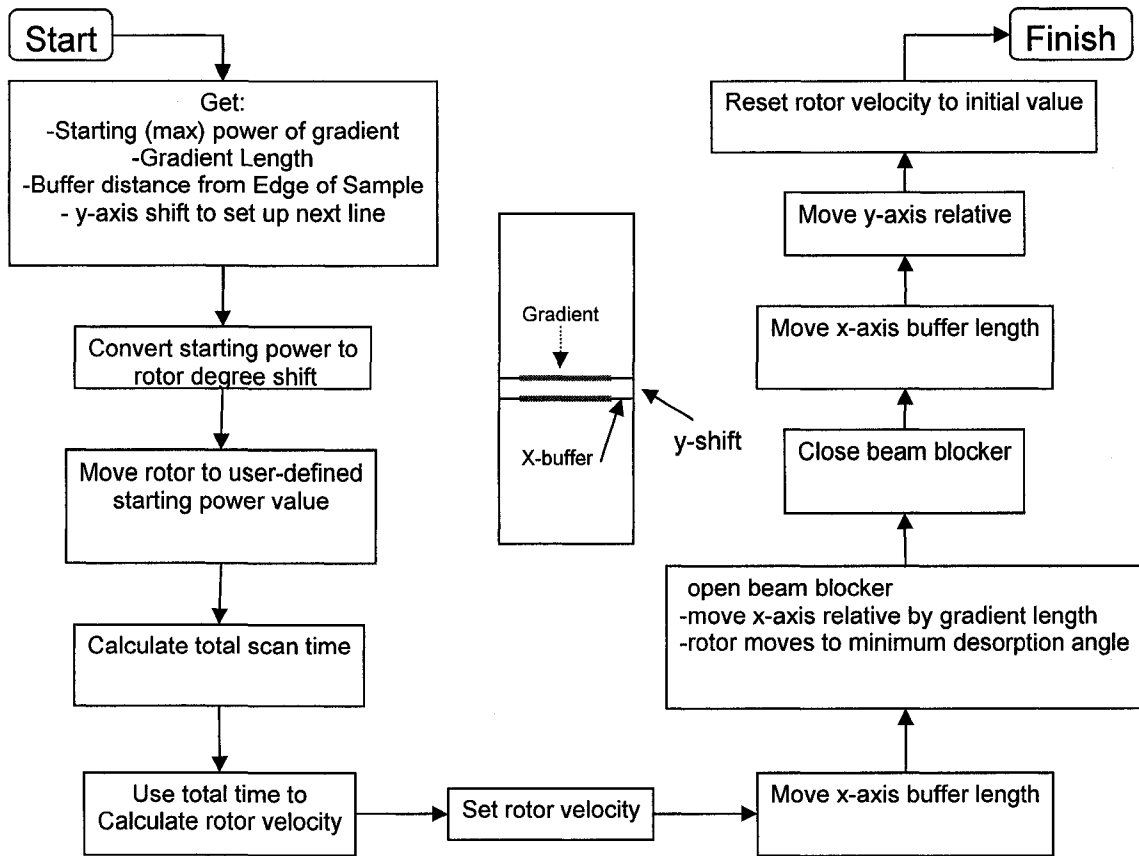


Fig. A1-7: Shows the flow chart of the gradient maker program. In between the flow chart a schematic representing the gradient lines on the sample is shown. Picture courtesy – J. Bacque.

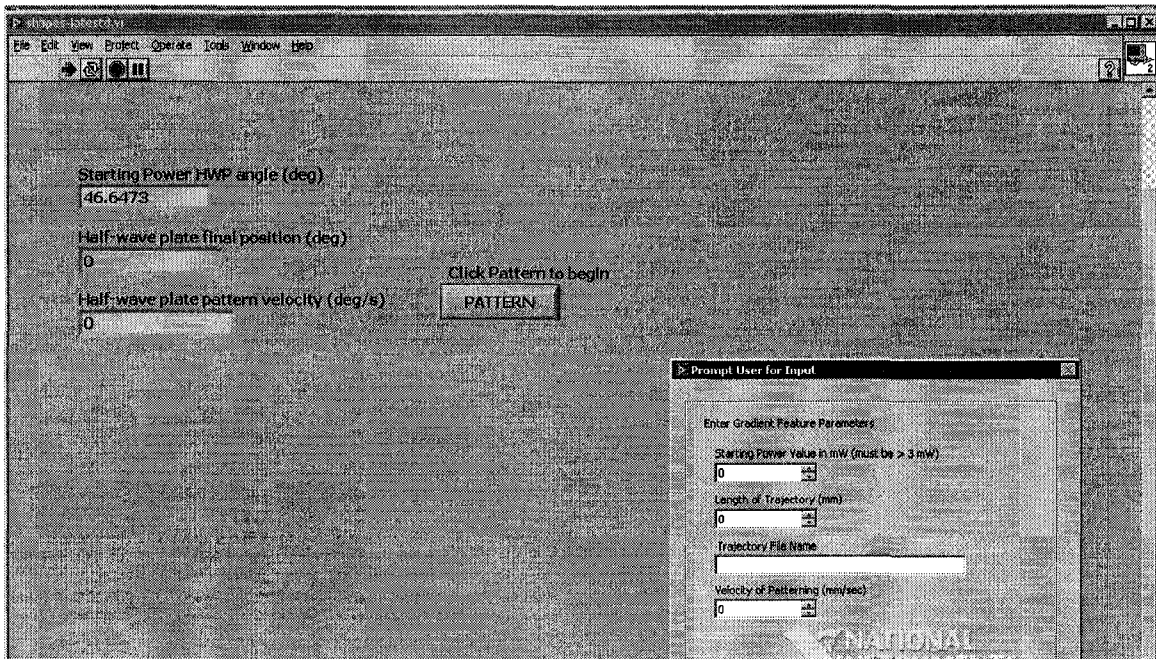


Fig. A1-8: Shows the front panel of the program used to fabricate gradients along arbitrary shapes. When patterning is initiated the dialog box shown on the right prompts user for inputs, required for patterning the gradients.

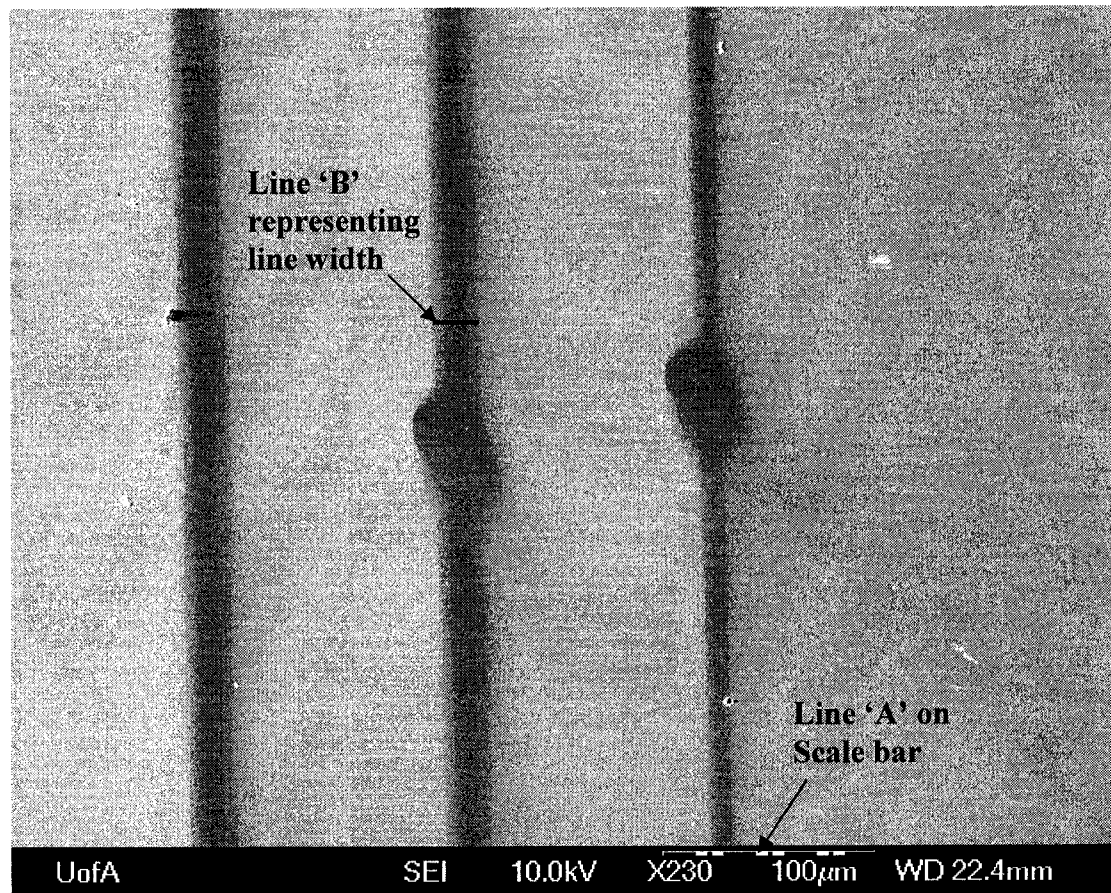


Fig. A1-9: Shows SEM picture of the patterned gradient lines and the straight lines drawn using Image-J for measuring the line width. Line 'A' shown in the picture is drawn representative of the scale bar and line 'B' is drawn representative of the width of the patterned gradient. Based on the lengths of 'A' and 'B' and the value of the scale bar the pattern width is calculated. Note that the start and end points of the lines representing the total line width were picked visually.

A1-5 References

- (1) Mauck, M. *Appl. Opt.* **1979**, 18, 599-600.
- (2) *Fundamental of Photonics*, Saleh, B.E.A. and Teich, M.C., John Wiley & Sons, Inc., U.S.A., **1991**, 83.
- (3) Kirkwood S. E.; Raso D.; 'Calibration Verification of the Gentec PS-310WB Power Meter with Adapter' – technical report.
- (4) XPS Motion Controller User's Manual and Motion tutorial, pages 72-76.

Appendix 2 – Other Experimental Results

The Fig. A2-1 shown in the next page are pictures taken at different time frames, during condensation of water on a fabricated pattern (which is a line that is tangent to a circle). The pattern was fabricated using the ‘laser power manipulation method’ explained in Chapter 3. The pattern has an energy gradient along the circle such that the region where the circle touches the line is more hydrophobic than the opposite side. Also, the lines are hydrophobic when they touch the circle). So, ideally the final pattern would look like an omega “ Ω ” in condensation imaging, due to the wettability gradient in fabricated pattern. The region of interest is indicated by a box in all the frames of Fig. A2-1.

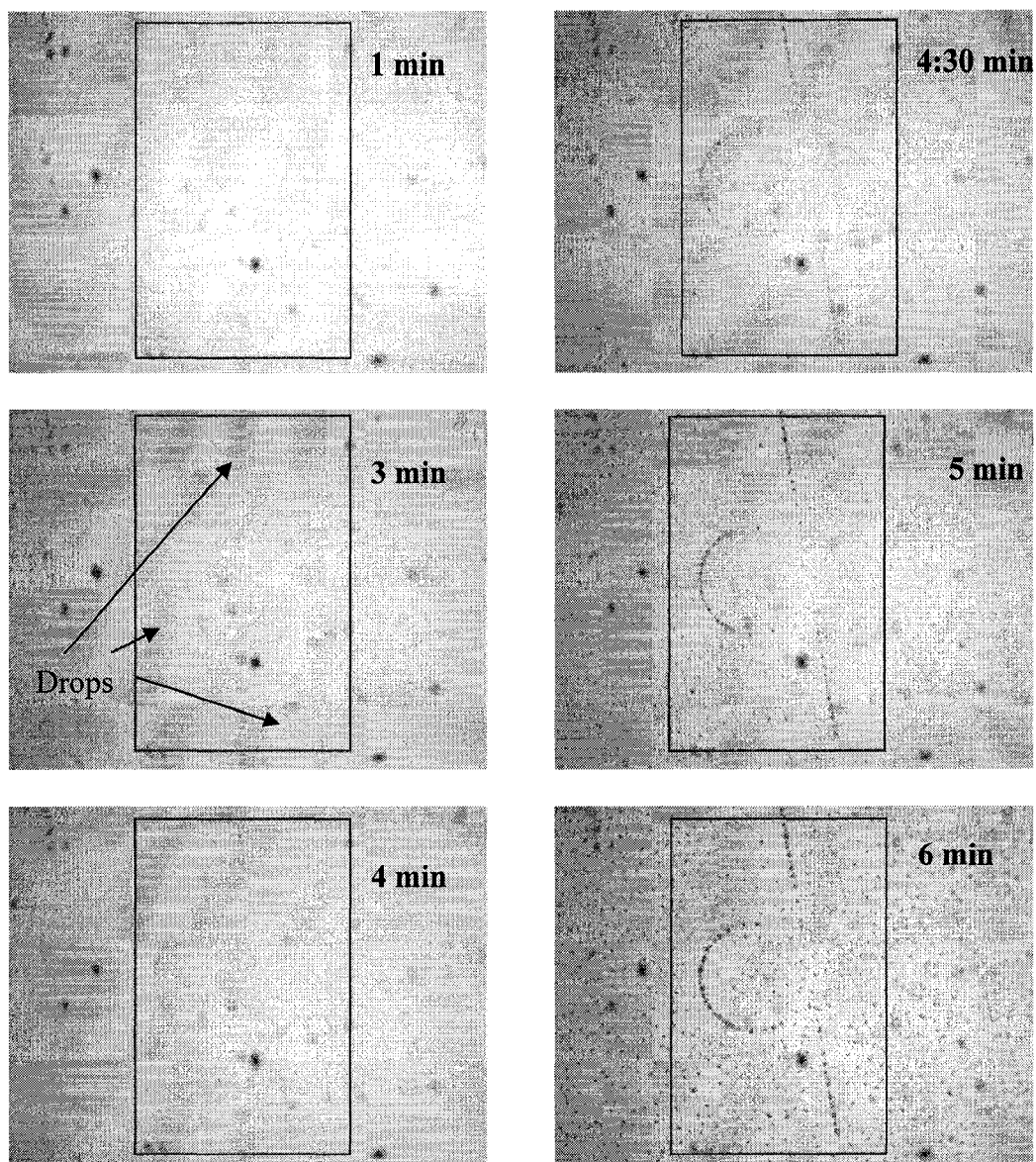


Fig. A2-1: Shows sequential pictures taken during the condensation of water drops on the sample. The black dots seen consistently on all frames are due to dust. At about 3-4 min drops can be seen to start condensing on the most hydrophilic regions of the “Ω” shaped patterns. In the subsequent pictures it is seen that these drops grow along the gradient revealing the same. At about 5 min drops are also seen to condense in the primary monolayer (background).

In order to capture the variation in the mercaptohexadecanoic acid (MHA) molecule, Secondary Ion Mass Spectroscopy (SIMS) spectral analysis was carried out at various positions, along the length of the gradient lines. The total count of oxygen ions corresponding to the COOH tail group of the MHA molecule was acquired at each position. The oxygen concentration variation hence obtained for the second set of 3, 6 and 12 mm is plotted as a function of the length of the gradient lines in Fig. A2-2. Also, the theoretical trend function for the amount of hexadecanethiol (HDT) desorbed has been fitted to the SIMS experimental data.

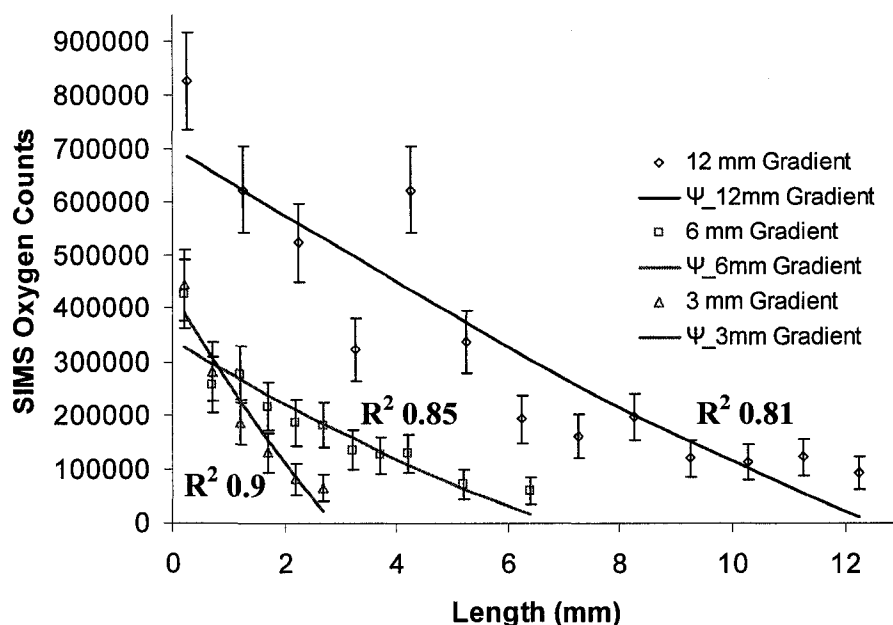


Fig. A2-2: Shows the SIMS oxygen concentration variation for the second set of gradient lines. The total counts of oxygen ions obtained at various positions along the three different gradient lines are represented by open symbols and the error bars correspond to 95% confidence level (given by Ion-spec. software). It can be seen that the rate of oxygen concentration is different for the 3, 6 and 12 mm gradient lines signifying the difference in steepness. The simplified parametric model (represented by continuous thick lines) has been fitted to the experimental data. The trends were found to follow the experimental data, similar to what has been observed for the first set of gradients.